CHALMERS
UNIVERSITY OF TECHNOLOGY

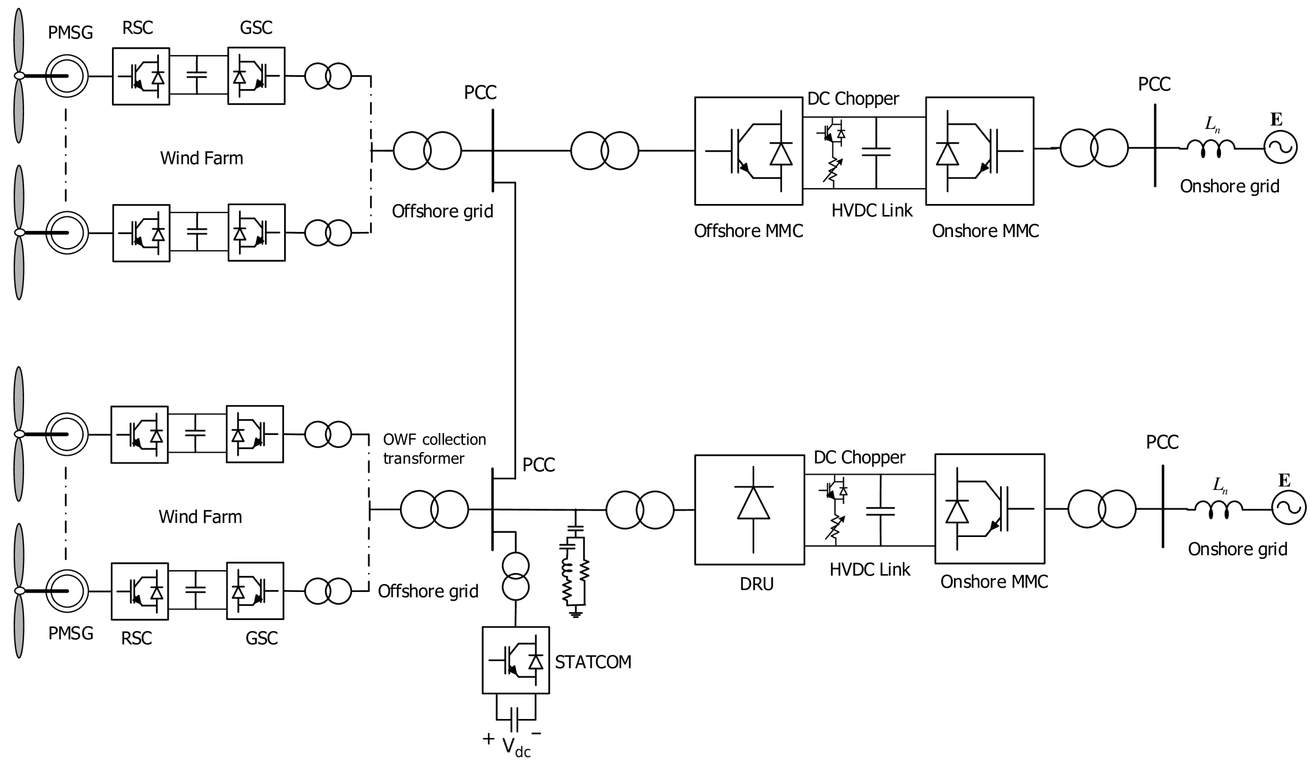

Comparison of AC and DC Offshore Wind Farm Systems using Grid-Forming Control of Grid-Connected Voltage-Source Converters

Master's thesis in Electric Power Engineering

VIJAY SREENIVAS

DEPARTMENT OF ELECTRICAL ENGINEERING
CHALMERS UNIVERSITY OF TECHNOLOGY
Gothenburg, Sweden 2021
www.chalmers.se

MASTER'S THESIS 2021

Comparison of AC and DC Offshore Wind Farm Systems using Grid-Forming Control of Grid-Connected Voltage-Source Converters

VIJAY SREENIVAS

Department of Electrical Engineering
Division of Electric Power Engineering
CHALMERS UNIVERSITY OF TECHNOLOGY
Gothenburg, Sweden 2021

Comparison of AC and DC Offshore Wind Farm Systems using Grid-Forming Control of Grid-Connected Voltage-Source Converters

Supervisor: Dr. Lidong Zhang, Hitachi ABB Power Grids Research
Examiner: Prof. Massimo Bongiorno, Department of Electrical Engineering

Master's Thesis 2021
Department of Electrical Engineering
Division of Electric Power Engineering
Chalmers University of Technology
SE-412 96 Gothenburg
Telephone +46 31 772 1000

Typeset in LaTeX
Printed by Chalmers Reproservice
Gothenburg, Sweden 2021

Comparison of AC and DC Offshore Wind Farm Systems using Grid-Forming Control of Grid-Connected Voltage-Source Converters
VIJAY SREENIVAS
Department of Electrical Engineering
Chalmers University of Technology

Abstract

The electricity grid is hastily expanding, and it is anticipated that the global energy demand will increase up to 40% by 2050 compared to today. Offshore Wind Farms (OWFs) will play a vital role and grow significantly in the coming years in the attempt to meet the decarbonization goals in several countries and will contribute a huge share to the 'Carbon-Neutral 2050' goal set by the European Union (EU). Wind energy harnessing has become the largest form of power generation capacity in Europe. OWF's have paved the way for generating and transmitting bulk green energy and huge investments are being carried over.

Nearly 20 GW of offshore wind capacity has been installed in the EU in 2018 and the current policies support robust growth aiming to multiply offshore wind capacity by four over the next decade. Alongside Europe, China and the US have taken strides forward on offshore wind power generation. Guangdong province is planning to install 30 GW offshore wind along its coastal area by 2030. Offshore wind development has also started in the US targeting 30 GW along the Atlantic coast by 2035. Recently, NYISO and ISO-NE announced 2.4 GW and 3 GW power purchase agreements. There are several solutions available for connecting the offshore wind farm to the main grid. First, the traditional Alternating Current (AC) transmission. The major drawback of this solution is the high losses related to the long-distance cable. Thus, this solution is only feasible for short-distanced OWF or intermediate reactive power compensation devices have to be installed. Second, Voltage-Source Converter (VSC) based High-Voltage Direct-Current (HVDC) transmission. This is the most promising solution for such applications. A number of VSC-HVDC offshore wind projects have been applied worldwide. Third, Line-Commutated Converter (LCC) based HVDC transmission or diode-based DC connection. Compared to the VSC technology, the traditional LCC is less costly but usually requires a local Static Synchronous Compensator (STATCOM) to support the wind farm.

The goal of the project is to compare the AC and DC solutions to effectively interconnect the OWF to the main grid with robust performance, least possible losses and cost. Power-Synchronization Control (PSC) strategy will be implemented as the grid-forming control scheme for the grid-connected VSCs. PSC can be applied to a VSC-HVDC converter station, a STATCOM, and even to a wind power generator directly. The entire control scheme should consider the coordination of the various devices in the wind farm, as well as fault ride-through in the overall system.

Keywords: Grid-forming control, Power-synchronization control, Modular multilevel converter, STATCOM, Offshore wind farm, HVDC, weak AC systems

Acknowledgements

I received a lot of support and guidance from many people throughout my thesis work. Therefore I would like to express my sincere gratitude to them. I would first like to thank Hitachi ABB Power Grids Research for giving me the opportunity to carry out my thesis in the most interesting field of the interconnection of offshore wind farms with grid-forming control which is currently a hot topic.

I would like to express my deepest gratitude to my supervisor, Dr. Lidong Zhang, Principal Scientist at Hitachi ABB PGR, whose expertise was invaluable in guiding and supporting me technically throughout this project. It has been an honor working with him. I want to also thank Dr. Michele Luvisotto, Digital Power Systems Research Team Manager at Hitachi ABB PGR for providing constant support to ensure my thesis is being carried out smoothly during the COVID-19 pandemic situation. I also appreciate all of the help I have received from my colleagues at Hitachi ABB PGR during this time.

I would like to thank Prof. Massimo Bongiorno who initially inspired and motivated me to carry out my thesis in this particular field, and also for being my supervisor and examiner at Chalmers. I also thank him for extending his support and stepping up during the times when required.

Finally, I want to thank my family and friends for their unwavering support during the course of my thesis.

Vijay Sreenivas, Gothenburg, August 2021

Contents

List of Figures **xiii**

List of Tables **xvii**

1 Introduction **1**
1.1 Background and motivation 1
1.2 Project scope and contribution of the thesis 2
1.3 Thesis Outline 3

2 Theory **5**
2.1 The war of currents - DC versus AC transmission 5
2.2 High-Voltage Direct-Current transmission 8
2.2.1 LCC-HVDC 8
2.2.2 VSC-HVDC 11
2.3 Application of Flexible AC Transmission Systems 18
2.3.1 Power Quality 19
2.4 Types of Grid-connected Wind Turbine Generators 21
2.5 Challenges in interconnecting Offshore Wind Farms 24
2.6 Strength of the Grid 24
2.7 Grid-Following versus Grid-Forming Control 25
2.8 Power-Synchronization Control 27
2.8.1 Power-Synchronization Control of Grid-connected VSCs 28
2.9 MMC Control and Design 31
2.9.1 Lower level controls 32
2.9.2 Selection of Number of Submodules and Redundant Submodules 33
2.9.3 DC Capacitor sizing of Submodules 33
2.9.4 Selection of Arm Inductance 34

3 Verification and Validation of Power-Synchronization Control **35**
3.1 System description and modeling 35
3.2 Step tests for Active power control and DC link voltage control . . . 35
3.3 Low-Voltage Fault Ride-Through Analysis 36

4 Test System 1: Back-to-Back MMC-HVDC **39**
4.1 System description and modeling 39
4.2 Interconnection of Offshore Wind Farm into AC grids 40

4.2.1 LVFRT Analysis (active power transfer from Offshore to Onshore) . . . 40
4.2.2 LVFRT Analysis (active power transfer from Onshore to Offshore) . . . 40
4.3 Island mode operation studies . . . 43
4.3.1 Frequency droop control . . . 43
4.3.2 Island system exporting active power from OWF to the onshore grid. . . . 44
4.3.3 Island system feeding the offshore load . . . 44
4.3.4 Passive mode operation . . . 47
4.4 Summary . . . 48

5 Test System 2: DRU-HVDC 49
5.1 System description and modeling . . . 49
5.2 Interconnection of Offshore Wind Farm into AC grids . . . 50
5.2.1 LVFRT Analysis at Offshore grid . . . 51
5.2.2 LVFRT Analysis at Onshore grid . . . 52
5.3 Step test for DC link voltage control of STATCOM . . . 53
5.4 Island mode operation studies . . . 53
5.4.1 Island system exporting active power from OWF to the onshore grid . . . 54
5.4.2 Island mode operation feeding the offshore load . . . 57
5.5 STATCOM sizing . . . 58
5.6 Summary . . . 59

6 Test System 3: STATCOM-HVAC 61
6.1 System description and modeling . . . 61
6.2 Island mode operation and LVFRT studies without STATCOM . . . 62
6.3 STATCOM sizing . . . 62
6.4 Island mode operation and LVFRT studies with a STATCOM . . . 63
6.5 Island mode operation and LVFRT studies with two STATCOMs . . . 65
6.6 Summary . . . 68

7 Results with OWF GFM-PSC of Test system 1 and 2 69
7.1 Test system 1 with OWF GFM-PSC . . . 69
7.2 Test system 2 with OWF GFM-PSC . . . 71

8 Conclusions and Future Work 75
8.1 Conclusions . . . 75
8.2 Future Work . . . 76

9 Ethics and Sustainability 79
9.1 Code of Ethics . . . 79
9.1.1 Code 1 . . . 79
9.1.2 Code 5 . . . 79
9.1.3 Code 7 . . . 80
9.2 Sustainability . . . 80

9.2.1 Goal 7 80
9.2.2 Goal 13 80
9.2.3 Goal 15 81

Bibliography **83**

A Appendix 1 **I**
A.1 Implementation of $\alpha\beta$ and dq transformations I
A.1.1 abc-$\alpha\beta$ transformation I
A.1.2 $\alpha\beta$-dq transformation II

B Appendix 2 **III**
B.1 Technical Data of the MMC-HVDC system III
B.2 Technical Data of the DRU-HVDC system IV
B.3 Technical Data of the STATCOM (1200 MVA)-HVAC system V
B.4 Technical Data of the STATCOM (600 MVA)-HVAC system VI

List of Figures

2.1 HVDC vs HVAC transmission cost comparison. 7
2.2 Graetz bridge for LCC-HVDC system. 9
2.3 12-pulse LCC [17]. 9
2.4 Capacitor-Commutated Converter. 11
2.5 Two-level voltage source converter. 12
2.6 Three-level neutral-point-clamped voltage source converter. 13
2.7 Three-phase MMC with half-bridge submodules [28]. 14
2.8 Half-bridge commutation cells. 15
2.9 Capacitor Balancing Algorithm [18]. 15
2.10 P-Q diagram for a typical VSC-HVDC converter [26]. 16
2.11 Type 1 WTG 21
2.12 Type 2 WTG 22
2.13 Type 3 WTG 22
2.14 Type 4 WTG 23
2.15 Generic structure of a grid-following control 26
2.16 Generic structure of a grid-forming control 26
2.17 Synchronization mechanism between SMs in an ac system 27
2.18 Overall control scheme with Power-Synchronization Control 29
2.19 Bumpless-transfer angle synchronization scheme [26]. 30
2.20 Anti-windup scheme for alternating voltage controller [26]. 31
2.21 PS-PWM technique [51]. 32
2.22 Circulating Current Suppression Control in dq frame. 33

3.1 Back-to-Back MMC-HVDC interconnected to two AC grids. 35
3.2 Active power control for SCR = 1. 36
3.3 Cascaded DC-Link and Active-Power Control. 37
3.4 (a) Three-phase MMC terminal voltages. (b) Active power of the MMC-HVDC link. (c) PSL and PLL synchronization angle. (d) MMC valve current. (e) d component of the MMC voltage reference. (f) Total capacitor voltages of upper and lower arms (zoomed). 38

4.1 Back-to-Back MMC-HVDC interconnected to an offshore wind farm. 39
4.2 LVFRT capability of the MMC-HVDC link during three-phase AC system faults at offshore and onshore grids while transferring active power from OWF to the onshore grid. 41

4.3 LVFRT capability of the MMC-HVDC link during three-phase AC system faults at offshore and onshore grids while transferring active power from the onshore grid to the offshore grid. 42
4.4 A typical island system. 43
4.5 Frequency droop controller. 44
4.6 LVFRT capability of the MMC-HVDC link during island mode operation. 45
4.7 LVFRT capability of the MMC-HVDC link during island mode operation, feeding the offshore load. 46
4.8 LVFRT capability of the MMC-HVDC link during passive mode operation. 47

5.1 DRU-HVDC interconnected to an offshore wind farm. 49
5.2 LVFRT capability of the DRU-HVDC link during three-phase AC system fault at the offshore grid. 50
5.3 LVFRT capability of the DRU-HVDC link during three-phase AC system fault at the onshore grid. 51
5.4 DC link control of STATCOM. 52
5.5 A typical island system. 53
5.6 LVFRT (offshore) capability of the DRU-HVDC link during island mode operation. 54
5.7 (a) Active and reactive power from OWF. (b) Active and reactive power from STATCOM. (c) Frequency of the offshore grid. 55
5.8 LVFRT (onshore) capability of the DRU-HVDC link during island mode operation. 56
5.9 (a) Active and reactive power from OWF. (b) Active and reactive power from STATCOM. (c) Frequency of the offshore grid. 57
5.10 (a) Active and reactive power from OWF. (b) Active and reactive power from STATCOM. (c) Frequency of the offshore grid. (d) PCC voltage of the offshore grid. 58

6.1 STATCOM-HVAC link interconnected to an offshore wind farm. . . . 61
6.2 HVAC link interconnected to an offshore wind farm. 62
6.3 LVFRT capability of the HVAC link during island mode operation. . 63
6.4 Upper plot: DC-link voltage of the WTG. Lower plot: Three-phase AC voltages of the WTG. 64
6.5 LVFRT capability of the STATCOM-HVAC link during island mode operation. 65
6.6 (a) Active and reactive power from OWF. (b) Active and reactive power from STATCOM. (c) Frequency of the offshore grid. 66
6.7 Two-STATCOM-HVAC link interconnected to an offshore wind farm. 66
6.8 LVFRT capability of the Two-STATCOM-HVAC link during island mode operation. 67
6.9 (a) Active and reactive power from OWF. (b) Active and reactive power from STATCOM. (c) Frequency of the offshore grid. 67

7.1 Back-to-Back MMC-HVDC interconnected to an offshore wind farm. 69

7.2 LVFRT capability of the MMC-HVDC link during island mode operation. . . . 70
7.3 Upper plot: DC-link voltage of the WTG. Lower plot: Three-phase AC voltages of the WTG. . . . 71
7.4 DRU-HVDC interconnected to an offshore wind farm. . . . 71
7.5 LVFRT capability of the DRU-HVDC link during island mode operation. . . . 72
7.6 Upper plot: DC-link voltage of the WTG. Lower plot: Three-phase AC voltages of the WTG. . . . 72

A.1 Reference frame transformations. (a) abc frame to a rotating vector in the stationary $\alpha\beta$ frame. (b) Stationary $\alpha\beta$ frame to synchronous dq frame. . . . II

List of Tables

2.1 Half-bridge switching states. 14
2.2 Capacitor voltage balancing criteria. 15
2.3 FACTS devices and functions. 20
2.4 SCR and strength of the grid 25
2.5 Strong grid vs Weak grid 25

5.1 STATCOM sizing 59

6.1 STATCOM sizing 63

B.1 Technical data of the MMC-HVDC system. AC: per unit based on 200 MVA and 183 kV. DC: per unit based on 200 MW and 150 kV. . III
B.2 Technical data of the DRU-HVDC system. IV
B.3 Technical data of the STATCOM (1200 MVA)-HVAC system. V
B.4 Technical data of the STATCOM (600 MVA)-HVAC system. VI

Nomenclature

AC Alternating Current

AVC Alternating Voltage control

BESS Battery Energy Storage System

CCC Capacitor-Commutated Converter

CCSC Circulating Current Suppression Control

CLC Current-Limitation Controller

CSC Current-Source Converter

D-STATCOM Distribution Static Compensator

DC Direct Current

DFIG Doubly-Fed Induction Generator

DRU Diode-Rectifier Unit

DVC Direct Voltage Control

DVR Dynamic Voltage Restorer

EC European Commission

EU European Union

FACTS Flexible Alternating-Current Transmission System

GFC Grid-Forming Converter

GFL Grid-Following

GFL-VCC Grid-Following-Vector Current Control

GFM Grid-Forming

GFM-PSC Grid-Forming-Power-Synchronization Control

GHG Greenhouse Gas

GSC Grid Side Converter

GTO Gate Turn-off Thyristor

GW Gigawatt

HVAC High-Voltage Alternating-Current

HVDC High-Voltage Direct-Current

IEEE Institute of Electrical and Electronics Engineers

IG Induction Generator

IGBT Insulated-Gate Bipolar Transistor

IM Induction Machine

ISO-NE ISO New England

LCC Line-Commutated Converter

LVFRT Low-Voltage Fault-Ride-Through

MMC Modular Multilevel Converter

MVA Mega Volt-Ampere

MVAr Mega Volt-Ampere Reactive

MW Megawatt

NPC Neutral Point-Clamped

NYISO New York Independent System Operator

OWF Offshore Wind Farm

OWS Offshore Wind System

p.u. per unit

PCC Point of Common Coupling

PEC Power Electronic Converter

pf Power Factor

PI Proportional Integral

PLL Phase-Locked Loop

PMSG Permanent Magnet Synchronous Generator

PS-PWM Phase-Shifted Pulse-Width Modulation

PSC Power-Synchronization Control

PSL Power-Synchronization Loop

PWM Pulse-Width Modulation

RES Renewable Energy Sources

RPC Reactive Power Compensation

RSC Rotor Side Converter

SCIG Squirrel-Cage Induction Generator

SCR Short-Circuit Ratio

SDG Sustainable Development Goal

SM Submodule

SM Synchronous Machine

SSSC Static Synchronous Series Compensator

STATCOM Static Synchronous Compensator

STS Static Transfer Switch

SVC Static VAR compensator

TCR Thyristor Controlled Reactor

TCSC Thyristor Controlled Series Compensation

THD Total Harmonic Distortion

TOV Temporary Overvoltage

TSC Thyristor Switched Capacitor

VCC Vector Current Control

VRES Large-Scale Variable Renewable Energy Sources

VRR Variable Rotor Resistance

VSC Voltage-Source Converter

VVC Voltage Vector Control

WRIG Wound Rotor Induction Generator

WT Wind Turbine

WTG Wind Turbine Generator

1

Introduction

This chapter describes the background and motivation of the thesis. The project's goal and scope, as well as the thesis's key scientific contributions are presented. Finally, the outline of the thesis is presented.

1.1 Background and motivation

The growing concern about climate change due to the emission of greenhouse gases (GHGs) especially carbon dioxide (CO_2) has led to the 'Green Transition' by integrating large-scale Renewable Energy Sources (RES) into power system networks. Integrating more RES into the generation mix would be a key tool to realize the global transition towards net-zero emission. The electricity grid is hastily expanding, and it is anticipated that the global energy demand will increase up to 40% by 2050 compared to today. OWFs will play a vital role and grow significantly in the coming years in the attempt to meet the decarbonization goals in several countries and will contribute a huge share to the 'Carbon-Neutral 2050' goal set by the EU.

The European Commission (EC) has set up the 'European Green Deal' policy to become the first climate-neutral continent. The ultimate goal of the EC is to be on par with the 'Paris Agreement' objective to keep the global temperature increase to well below 2°C and pursue efforts to keep it to 1.5°C [1]. The EU aims to be climate-neutral by 2050 with net-zero greenhouse gas emissions and to achieve this goal, the EC has unveiled the EU Strategy on Offshore Renewable Energy [1]. The strategy targets to increase Europe's offshore wind capacity from its current level of 12 GW to 60 GW by 2030, and 300 GW by 2050.

It is estimated that nearly 800 billion Euros will be required to execute this ambitious long-term plan. Huge investments are also being carried out in research and development to further advance the technology and to address the challenges in employing offshore wind farms. To achieve this, cost-effective OWF system designs with improved reliability and efficiency should be realized with the integration of advanced power-electronics and digital solutions.

Europe being a world leader in offshore wind technology can become a powerhouse for its global development by harnessing all the potential of offshore wind. Offshore wind generates sustainable energy that competes with and sometimes is cheaper than the existing fossil fuel-based power plants [1]. OWFs have the ability to generate more energy at a more consistent pace than their onshore counterparts due to greater and more consistent wind speeds.

The major concern of today is that as large-scale Variable RES (VRES) such as wind and solar power are being integrated into the existing AC grid by decommissioning the existing fossil fuel-based power plants (e.g. coal or natural gas-powered thermal power plants, nuclear power plants, etc.), this induces stability issues to the AC system network [2]. The VRES is an intermittent source of energy that is unpredictable and un-controllable as opposed to the traditional controlled source with synchronous machines. As the existing synchronous machines are being removed from the AC grid, the voltage and frequency stability are lost causing supply-demand power imbalance. To combat this major problem, Grid-Forming Converters (GFCs) are being deployed so that the performance of a synchronous machine can be replicated.

A GFC is a power electronic-based high power converter that behaves as a voltage source, capable of generating and controlling the required voltage magnitude and frequency of the grid. GFCs can operate AC grids with or without rotating machines. GFCs can imitate the properties of a synchronous machine such as droop-based load-sharing, synthetic inertial-emulation, synchronized and stand-alone operation (e.g. island mode), and black-start behavior [3]. Flexible Alternating-Current Transmission Systems (FACTS) and High-Voltage Direct-Current (HVDC) are power electronic-based devices that are mainly used to regulate the bus voltage and enhance the active power transfer capability of the power system. These devices eliminate the bottlenecks in the transmission lines and improve the reliability of the power system with a high share of RES penetration [4], [5].

Due to large-scale penetrations of RES, especially OWFs, into exiting AC power system, requires a massive new transmission network that would enable new power transfer corridors, especially in mature networks such as in Europe, North America, and China to accommodate the increased development of renewable generation. This scenario has led to the development of state-of-the-art VSC-HVDC transmission systems. VSC-HVDC systems have been successfully deployed to interconnect large OWFs, not only because they are less expensive and more efficient than AC transmission systems, but also because of the benefits of VSC-HVDC technology, such as independent control of active and reactive power, black-start capability, and support for weak AC systems [6], [7]. Such large-scale RES integrations employing VSC-HVDC are significantly growing in the North Sea region, China and US.

Therefore, the ultimate solution to solve all the major problems (e.g. grid disturbances and faults, blackouts, stability issues, etc.) in interconnecting a weak grid like the OWFs is to employ a grid-forming control strategy integrated with the FACTS and HVDC devices to pave way for 100% RES in the future.

1.2 Project scope and contribution of the thesis

The objectives of the thesis are:

1. The main goal of the thesis is to present three different system topologies that could be used to effectively inter-connect the OWF to the main AC grid.
2. Test system 1 will be modeled by interconnecting an OWF to a back-to-back Modular Multilevel Converter (MMC)-HVDC system. The MMCs will be modeled and designed using the PSC strategy. The performance of the entire system will be verified by investigating low-voltage fault-ride-through

(LVFRT) capability on both offshore and onshore grids during island operation.
3. Test system 2 will be modeled by interconnecting an OWF to a Diode-Rectifier Unit (DRU)-HVDC system. The performance of the entire system will be verified by LVFRT analysis during island operation.
4. Test system 3 will be modeled by interconnecting an OWF to a STATCOM-HVAC transmission line. The performance of the entire system will be verified by LVFRT analysis during island operation.
5. The entire modeling and designing of the systems are conducted by time simulations using PSCAD/EMTDC software. Any kind of experimental work is out of the scope of the thesis.
6. Detailed modeling of the cables is not included in the scope, however, for test system 3 the HVAC transmission line is modeled using pi-sections with adequate cable data from Nexans.

1.3 Thesis Outline

The Master's thesis is divided into six chapters.

Chapter 1: Adequate background knowledge is given to better understand the current trends and development in offshore wind technology, and its effect while integrating it into the AC system.

Chapter 2: The underlying theory behind DC and AC transmission, types of High-Voltage Direct-Current transmission, application of Flexible AC Transmission Systems, types of wind turbine generators, challenges in interconnecting offshore wind farms, strength of the grid, Grid-Following versus Grid-Forming Control, and Power-Synchronization Control are briefly explained.

Chapter 3: Testing and Verification of Power-Synchronization Control on a weak AC system using a back-to-back MMC-HVDC system is performed.

Chapter 4: System studies of test system 1 where an OWF is interconnected to the main AC grid with a back-to-back MMC-HVDC system. The MMCs are equipped with grid-forming-power-synchronization control (GFM-PSC).

Chapter 5: System studies of test system 2 where an OWF is interconnected to the main AC grid with a DRU-HVDC system. As the DRUs are uncontrollable, a STATCOM is placed at the offshore grid to provide the necessary voltage support during island mode operation. The onshore MMC and the offshore STATCOM utilizes GFM-PSC.

Chapter 6: System studies of test system 3 where an OWF is interconnected to the main AC grid with a STATCOM-HVAC system. This is a complete AC solution where the OWF is integrated with GFM-PSC. The STATCOM is equipped with GFM-PSC.

Chapter 7: The effect of replacing vector current control in the wind turbine converters by power-synchronization control in test systems 1 and 2 are investigated.

Chapter 8: Summarizes the thesis by comparing all three test systems and provides suggestions for future work.

Chapter 9: Discusses the ethical and sustainability aspects of the project.

2
Theory

This chapter gives a brief explanation of the fundamental theory that is applied in the thesis. In section 2.1, DC versus AC transmission system is compared. In section 2.2, two major HVDC technologies, i.e., HVDC transmission using Line-commutated converter (LCC-HVDC) and forced-commutated voltage-source converters (VSC-HVDC) are described. In section 2.3, the application of FACTS is briefed. In section 2.4, different types of wind turbine generators that are available today are discussed. In section 2.5, the challenges in interconnecting OWFs are highlighted. In section 2.6, the strength of the grid is discussed. In section 2.7, Grid-Following and Grid-Forming Control strategies are explained. In section 2.8, an overview of the Power-Synchronization Control strategy is given with other control loops used in VSC-HVDC.

2.1 The war of currents - DC versus AC transmission

The history of electric power systems originated with Direct-Current (DC) transmission and the first electric generator was a DC machine. Thomas Edison constructed the first power system using DC transmission at a low voltage level in 1882.

DC worked well with incandescent lamps and electric motors. DC systems could be easily integrated and powered with Battery Energy Storage Systems (BESS), providing indispensable load-leveling (or supply-demand) and backup power during interruptions or generator outages. DC generators could be easily paralleled, allowing economical operation and improved reliability by using smaller machines during periods of light load [8]. The major drawback with Edison's DC system was that it was not possible to transmit the power more than a couple of kilometers and only customers close to the power plant could access the power supply. As transmission distance increases, voltage drops significantly due to the I^2R power losses and the loads suffered severe voltage variations. The only solution was to increase the transmission line voltage but unfortunately at that time, there was no method to boost or control the DC voltage. To resolve this issue, George Westinghouse (pioneer of the electrical industry) proposed AC distribution and during that time Nikola Tesla had recently invented the induction motor which works on AC [8], [9]. Later, Nikola Tesla developed the transformer which could easily boost the voltage in AC transmission.

This breakthrough made the DC transmission system to be quickly replaced by AC transmission due to the latter's numerous advantages. The first and prominent advantage is that the voltage levels of the AC transmission system could be easily varied by efficiently stepping up the voltage at the transmission level (long-distance power transmission) and stepping down the voltage at the distribution point (for safety reasons) for utilization with reduced losses. Secondly, the AC currents can be easily interrupted due to the natural zero-crossings that occur twice per cycle and the AC circuit breaker can take advantage of this making them more compact and cheaper than the DC breakers [10]. Lastly, AC motors are cheaper and more robust than DC motors as DC machines require commutation brushes. As a result, AC won the "war of currents" and hence the modern electric power systems have been developed using AC rather than DC [11].

Today, the majority of the transmission systems use three-phase HVAC power but with significant developments in power electronics and DC energy sources, interest in DC power transmission has returned [12], [13].

In 1954, the first commercial HVDC link between the mainland of Sweden and the island of Gotland was commissioned. Since then, the total installed power of HVDC transmission networks around the world has increased steadily, with recent spectacular growth in volume. HVDC transmission has proven to be technologically and/or economically superior to HVAC transmission in the following applications-

- *Submarine power transmission longer than about 50 km.* Due to large capacitance in the AC cables, AC transmission is impractical for such distances. As the transmission distance increases, the losses created by the capacitive current becomes unacceptable resulting in the requirement of reactive power compensation (RPC) devices like SVC's and STATCOM's at the middle of the cable incurring significant costs. It might also not be always practical to install an RPC device under the sea. Hence, for long-distance submarine cable transmission, HVDC is more economical and the only feasible technical solution.

- *Bulk power transmission over long-distance overhead lines.* DC transmission is the preferred solution when it comes to transferring large amounts of power over longer distances because the overall cost of the transmission system and the losses are lower than AC transmission. Given the fact that AC transmission won the "war of currents" in the 19th century due to its capability to transmit power over longer distances, HVDC transmission wins the battle back after a century. To transmit the same amount of power, the DC line requires only two conductors per DC circuit (one only for a submarine with earth return) and it allows the supporting towers to be smaller and hence requires lesser right-of-way [14]. Fig. 2.1 shows a comparison of costs for DC and AC transmission lines. The initial capital investment for an HVDC transmission system is higher because of the converter costs but as the transmission distance increases, the benefits of DC counterweigh the capital investment. The cost breakeven distance is in the range of 30–50 km for submarine cables and 600–800 km for overhead lines [12], [15]. Furthermore, intermediate RPC devices like SVC's and STATCOM's have to be installed for long HVAC cables. Also, DC transmission does not have stability limitations unlike AC

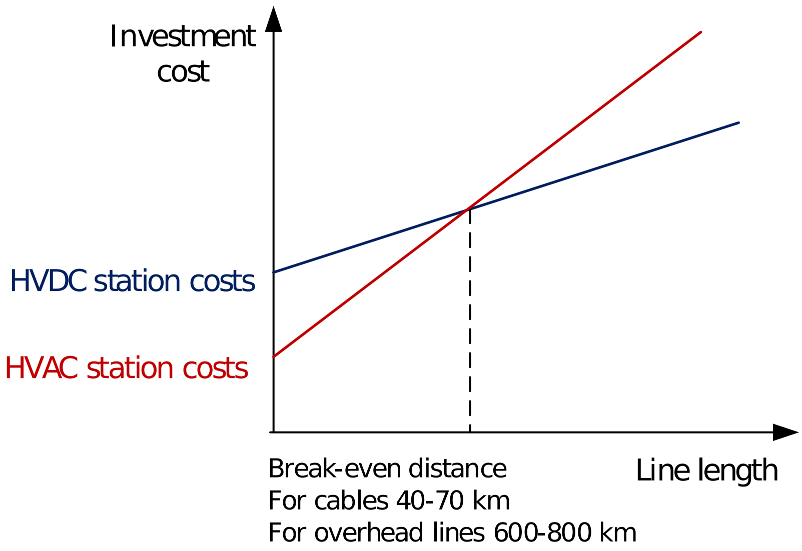

Figure 2.1: HVDC vs HVAC transmission cost comparison.

transmission over longer distances.

- *Interconnection of Asynchronous grids.* AC transmission is impossible between two asynchronous AC systems because of system stability problems or having different frequencies. To overcome this issue, many back-to-back HVDC transmission links have been built as HVDC links are free from stability and synchronization constraints.

- *Short-circuit current.* When new transmission lines are constructed to expand AC networks, the system's short-circuit level will inevitably increase. The AC switchgear in the substation must cope with the short-circuit requirements or an expensive refurbishment will be required. Two AC systems can be connected through an HVDC link without increasing the short-circuit power as the reactive power is not transmitted through the DC link and therefore upgradation of the substation equipment is not required.

- *Losses.* DC transmission does not have inductance unlike AC transmission and hence voltage drop in the line due to inductive reactance does not exist. Skin effect is completely absent in DC transmission line. Corona losses are very low in DC compared to AC line. Dielectric and eddy current losses are also not present in DC transmission lines [12].

- *Power system stability and control.* Another major feature of the HVDC technology is its ability to control a large amount of power flow over an HVDC link hastily and precisely which is beneficial to dampen the low-frequency oscillations in the AC system thereby enhancing the system stability [12]. Due to the absence of inductance in DC transmission, voltage regulation is better than AC transmission. Voltage control is complicated in AC systems due to line charging and voltage drops where intermediate RPC devices are used [15].

- *Firewall protection in Asynchronous ties.* Interconnection of large AC systems increases the complexity of system operation. This has resulted in frequent tripping and major blackouts in North America and Europe [16]. Asynchronous grid interconnection by HVDC links can give a “firewall” protection feature that prevents cascaded AC system outages from spreading from one network to another [17].

- DC transmission line has less *potential stress* on the insulator compared to AC transmission line for the same operating voltage. Hence, DC system requires less insulation than AC system.

- The AC transmission line has more *interference* with neighboring communication lines than the DC transmission line.

2.2 High-Voltage Direct-Current transmission

This section presents the two core HVDC converter technologies that are used in modern transmission systems i.e., LCC-HVDC and VSC-HVDC.

2.2.1 LCC-HVDC

LCCs are conventional, mature and well-established technology used in HVDC applications. The world’s first commercial HVDC link between the mainland of Sweden and the island of Gotland which was commissioned in 1954 employed mercury-arc valves as the converter technology. This trend continued for around two decades. However, the mercury-arc valves suffered from the arc-back fault where the valve conducts in the reverse direction when the voltage across it is negative. This consequently destroyed the converter valve and created high short-circuit currents in the external circuit and also lead to other problems [13]. To overcome these problems, thyristor-based LCC-HVDC technology was introduced in the late 1960s and since then it became the conventional HVDC transmission. LCC or CSC (current-source converters)-HVDC is also known as HVDC Classic due to its capability to transmit bulk power over long distances. The technology now reaches power up to 1.2 GW [18]. The LCC requires a synchronous voltage source to operate.

The basic building block of an LCC is the three-phase, full-wave bridge circuit referred to as a six-pulse converter or Graetz bridge as shown in fig. 2.2. The term six-pulse refers to the fact that there are six commutations each period, resulting in a characteristic harmonic ripple in the DC output voltage that is six times the fundamental frequency. The AC side current harmonics will have frequencies of 6n±1. Each of the six-pulse bridges comprises six controlled switching thyristor valves. To reach the desired DC voltage rating, each valve is made up of a reasonable number of series-connected thyristors. The modern HVDC link is constructed as a 12-pulse converter (as shown in fig. 2.3) using two Graetz bridges connected in series with AC voltage sources phase-shifted by 30° to increase the DC voltage and eliminate some of the characteristic harmonics on the AC and DC sides. In a 12-pulse operation, the AC side current harmonics will have frequencies of 12n±1 and

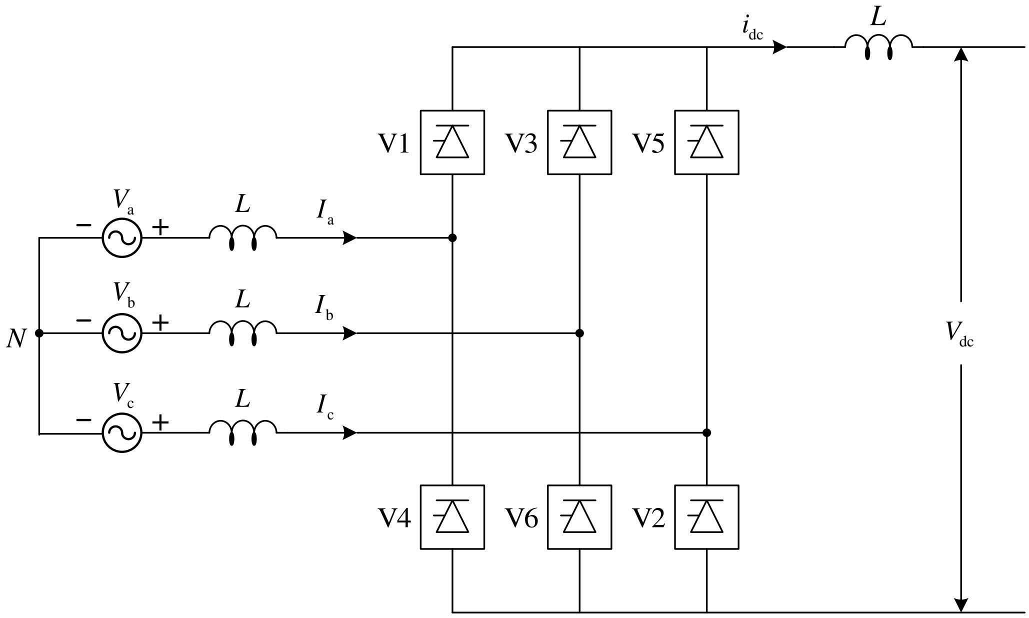

Figure 2.2: Graetz bridge for LCC-HVDC system.

12n for the DC side voltage harmonics. The 30° phase shift is achieved using the star-star-delta connection transformers [19]. The main reason to use such a 12-pulse configuration is to reduce filtering requirements for six-pulse operation. In this case, the fifth and seventh harmonics from the AC side and sixth from the DC side will get canceled out at the primary side of the converter transformer as they are 180° out of phase.

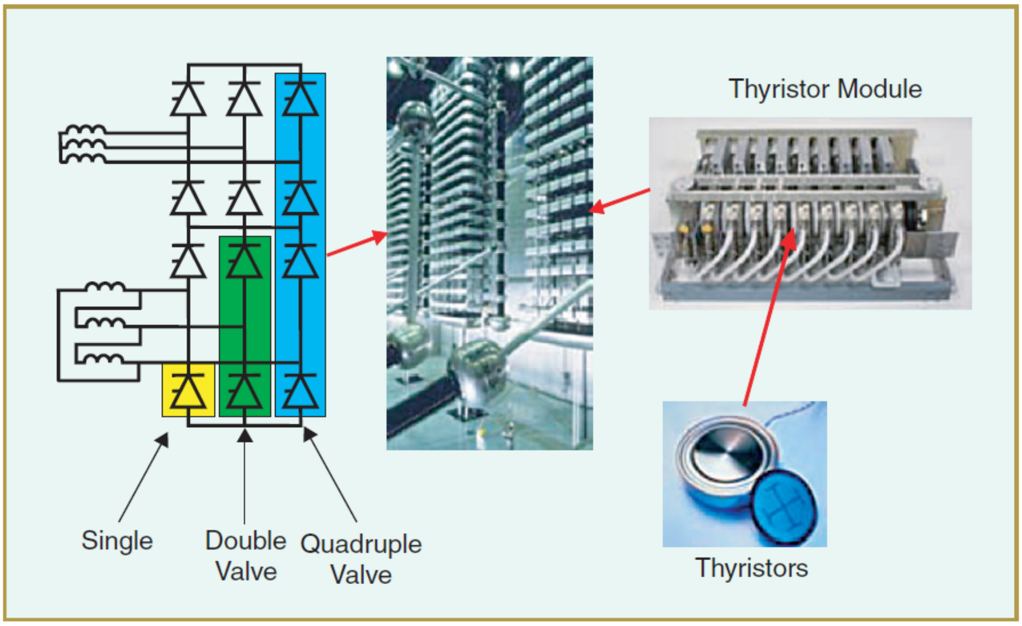

Figure 2.3: 12-pulse LCC [17].

The Graetz bridge can be used for transmitting power in both directions, i.e., the rectifier mode and the inverter mode. This is achieved by regulating the firing angles of the LCC valves. The two operating modes are:

- If the firing angle is less than 90°, direct current flows from the positive terminal of the dc circuit, transferring power from the ac to the dc side.
- If the firing angle is greater than 90°, the direct voltage reverses polarity, and the direct current flows from the dc circuit's negative terminal, transferring power from the dc to the ac side.

Detailed explanation and working of the 12-pulse LCC can be found in [19]–[21].

The LCC-HVDC technology has been very successful with numerous worldwide installations and is still growing in a steady phase. The LCC technology, on the other hand, has several inherent weaknesses as follows:

- *LCC always consumes reactive power* in either mode of operation as they can only operate with the ac current lagging the voltage, and hence, the conversion process requires reactive power. The reactive power consumption of an LCC-HVDC converter station ranges from 50 to 60% of the active power, depending on the firing angles [22]. Large AC filters or capacitors must be connected to compensate for the same and this increases the cost and also the footprint of the converter stations. Furthermore, when connected to a weak AC system, these large filters or capacitors contribute to the HVDC link's temporary overvoltage (TOV) and low-order harmonic resonance issues [23].

- *Commutation failures* are a common problem with the LCC-HVDC system which are often triggered by disturbances in the ac system. The extinction volt-time area of the inverter valve is reduced due to voltage depression or phase-angle shift of the alternating voltage [24], [25]. If the inverter valve's extinction angle is less than 5-6°, the previously conducted valve will regain current, resulting in a commutation failure creating a short-circuit on the dc side, which temporarily halts the power transmission [26]. The converter valves and the ac system are usually unaffected by a single commutation failure but multiple commutation failures may force the HVDC link to trip [27].

- *Weak AC grid interconnection:* The major problem with the LCC-HVDC technology is that the current commutation between the valves relies on the stiffness of the alternating voltage i.e., the strength of the AC grid. If the LCC-HVDC link is connected to an AC system having a low short-circuit ratio (SCR), the system will not operate stably and reliably resulting in problematic interactions between the AC and DC systems. Moreover, low SCR also imposes an upper limitation on the HVDC power transmission [23]. If the LCC is connected to a weak AC grid, static VAR compensators (SVCs), STATCOMs and synchronous condensers will be required to increase the short-circuit level and improve the voltage control [22]. Another problem with weak AC grid interconnections is the low-order harmonic resonances that occur due to the interaction between the high inductances of the AC system with the large capacitors of the HVDC link. This can result in deteriorating the performance of the converter control system.

Hence, LCC is a less attractive technology for weak AC grid interconnections e.g., integration of offshore wind farms.

To address some of these issues, Capacitor-Commutated Converters (CCCs) were introduced in the late 1990s for weak AC system connections, back-to-back applications. It is an extended version of the LCC technology where capacitors are inserted in series between the transformers and thyristor valves as shown in fig. 2.4. The series capacitor automatically provides a part of the reactive power compensation as per the converter's requirement based on the load current and provides a portion of the commutation voltage, thereby enhancing the voltage stability of the

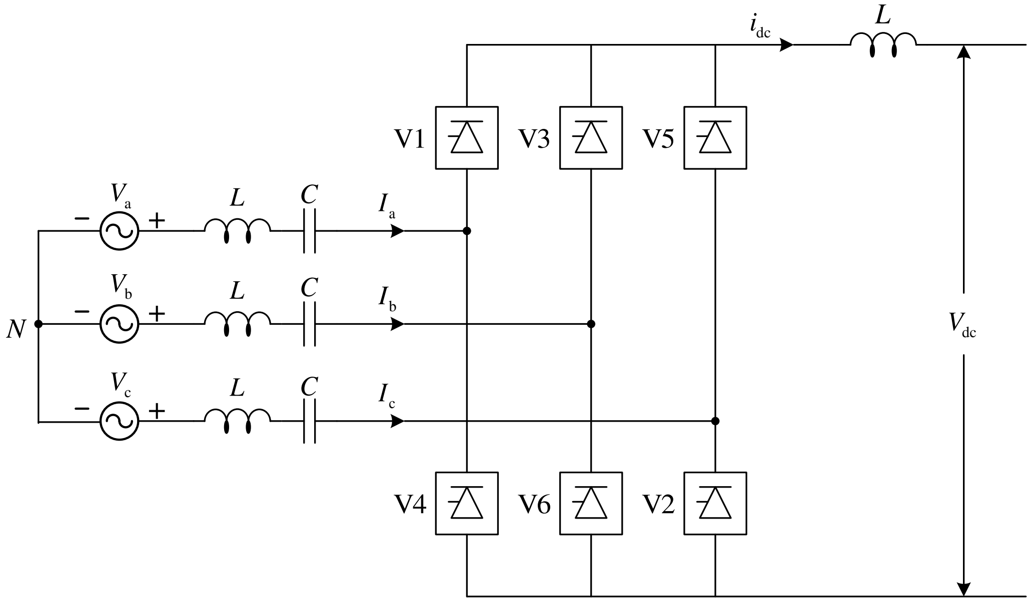

Figure 2.4: Capacitor-Commutated Converter.

system [17]. However, this technology had a major drawback of increased insulation cost of the valves due to series-connected capacitors. Hence, the CCC-HVDC was only applied to a very few projects with back-to-back HVDC links where the voltage level of the valves is much lower.

2.2.2 VSC-HVDC

VSCs are constantly evolving, new converter technology for HVDC transmission. It is commercially known as HVDC Light, introduced in 1997. The first commercial VSC-HVDC link with a rating of 50 MW, DC voltage of ±80 kV (connected to an OWF of length 70 km) was commissioned in 1999 in Gotland island of Sweden, near to the world's first LCC-HVDC link. The technology now attains a power rating of 3,000 MW and ±640 kV enabling power transmission over 2,000 km that is enough electricity to power several million households [18].

VSCs use self-commutating switches with either gate turn-off thyristors (GTOs) or insulated-gate bipolar transistors (IGBTs) which can be turned on or off rapidly. This is in contrast to the LCC where the thyristor valve has only turn-on control and requires the line voltage to be reversed (reverse biased) or wait until the load current falls to zero or through an external commutation circuit to turn off. A VSC can produce its own sinusoidal voltage waveform with high-frequency pulse-width modulation (PWM) technology independent of the ac system. Several topologies have been investigated for VSCs. Although, for HVDC applications, the choices were limited to two-level, three-level and MMCs [19], [28], [29].

The most simplest grid-connected VSC topology is the conventional two-level three-phase bridge as shown in fig. 2.5. The three-phase bridge consists of six valves and each valve consists of a switching device (typically IGBT) with an anti-parallel diode to ensure four-quadrant operation of the converter. It is suited for low-voltage motor drives and grid-connected applications (e.g. integration of RES). This design benefits from its simplicity and the ease with which power is transferred between the phase legs, resulting in smaller capacitor energy storage requirements.

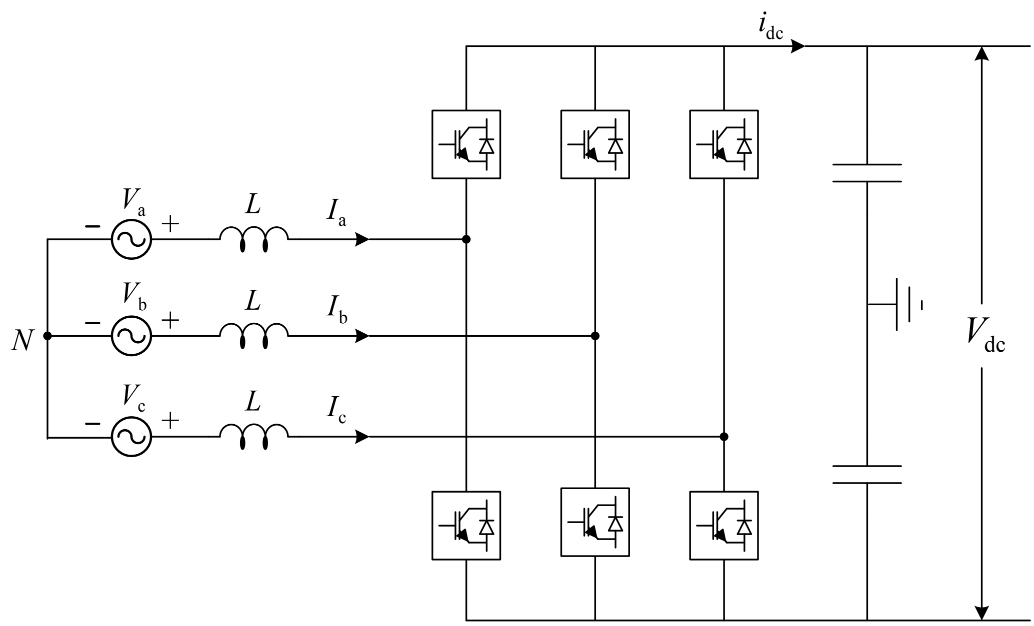

Figure 2.5: Two-level voltage source converter.

The working principle is also very simple. The output AC voltage waveform is produced by varying the width of the pulses and switching very fast between two fixed voltages. The desired fundamental frequency voltage is produced through low pass filtering of the phase reactors and shunt filters. Due to the lack of power semiconductors (switches) with sufficient blocking capability, it is very hard to implement two-level VSCs beyond a few kilovolts. A possible way to realize this is to directly connect the switches in series but it is an expensive technology that has never gained widespread use [28].

Fig. 2.6 shows a three-level VSC or neutral point-clamped (NPC) VSC. This topology is an extension of a two-level VSC where mainly two clamping diodes are added in each phase leg to clamp the switch voltage to half of the dc voltage. As a result, each phase of the VSC can switch to three different voltage levels, i.e., +Vdc,0,-Vdc. By doing this, the output voltage waveform produced by the VSC will be much closer (more sinusoidal) to the reference voltage resulting in lesser harmonic content [29]. Furthermore, the three-level NPC VSC has lower switching losses.

The NPC concept can be further extended to a five-level VSC (or flying capacitor) and even more levels to achieve higher voltage levels which further result in a good sinusoidal output waveform with much lower harmonics and switching losses [29]. However, for high-voltage converter applications, extension to more than three levels is cumbersome as many clamping diodes are required and all of these need to be connected to a common dc link. Additionally, it also complicates the insulation and cooling design of the converter valves. Therefore, the NPC concept with voltage levels higher than three is only applied for medium-voltage applications up to several kilovolts whereas for HVDC applications, voltage levels higher than three have never been considered [28], [29].

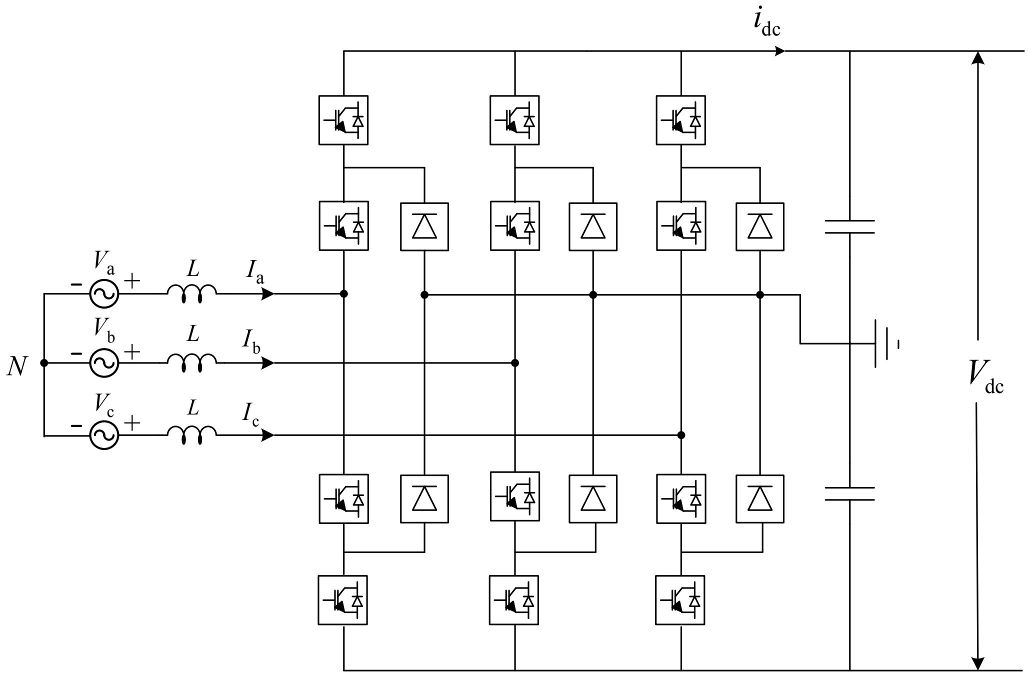

Figure 2.6: Three-level neutral-point-clamped voltage source converter.

To overcome the aforementioned issues, high-power converters that can generate very high voltages came into realization when Professor Marquardt had made a breakthrough in the year 2002 by introducing the concept of MMC with half-bridge submodules [30]. A major feature of the MMC is that no common capacitor is connected at the dc side, unlike the above two topologies.

An MMC comprises of N identical half- bridge submodules that are stacked up in series to form an arm. The upper and lower arm together in one phase represents a phase leg. The configuration of an MMC is shown in fig. 2.7. Small-sized inductors are equipped in the converter arms to suppress the circulating current (negative sequence) and limit fault currents. The half-bridge submodule comprises one two-level phase leg connected in parallel to a DC capacitor which will maintain a direct voltage. The cascaded series-connected submodules split the switched DC-link voltage amongst numerous DC capacitors to avoid the series connection of the IGBTs. The MMC is controlled using a capacitor voltage balancing algorithm.

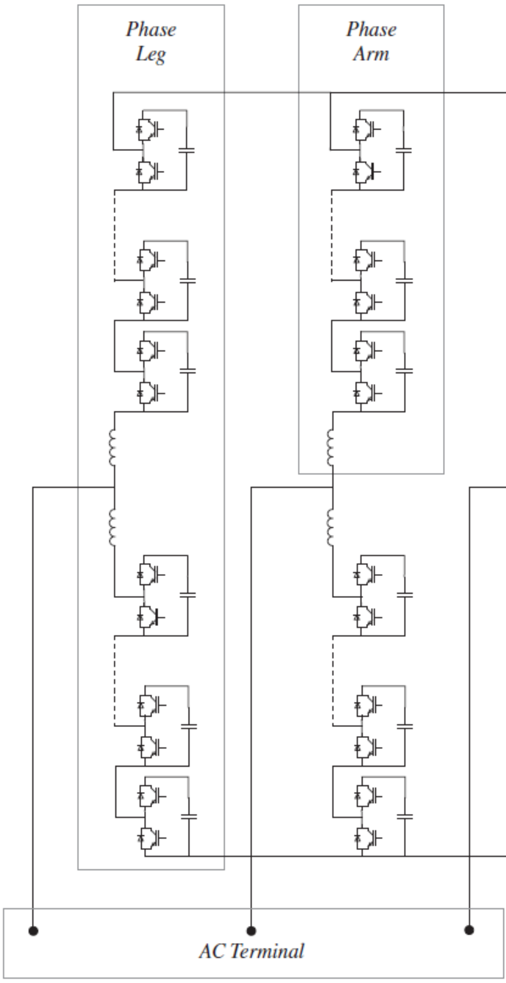

Figure 2.7: Three-phase MMC with half-bridge submodules [28].

The capacitor voltages of each submodules must be balanced to maintain all the DC capacitors on the same voltage level and to distribute the stress (power losses) equally to the power units. The control of an MMC is determined by the number of submodules that have to be inserted or bypassed during each switching cycle. The half-bridge cells generate two output voltage levels due to the two-quadrant operation and the switching states are depicted in table 2.1 and fig. 2.8. The output voltage of each sub-module is given by $V_{\text{sm}} = s.V_c$, where s is the switching function.

Switches on	Cell output voltage
T1	$+V_c$
T2	0 (bypassed)

Table 2.1: Half-bridge switching states.

The capacitor voltages of all submodules (cells) are periodically sampled at a high frequency and sorted in ascending or descending order each time the control demands a cell to be inserted or bypassed. The control system inserts or bypasses a certain

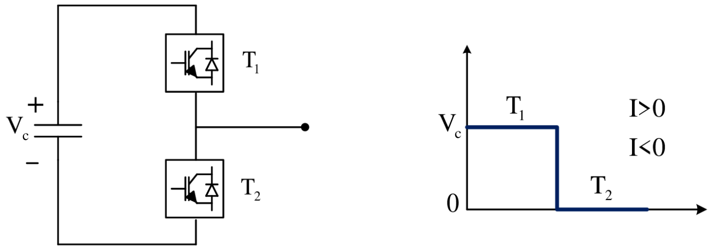

Figure 2.8: Half-bridge commutation cells.

number of cells as per the criteria stipulated in table 2.2.

Cell state	$\mathbf{i}_{ac} > 0$	$\mathbf{i}_{ac} < 0$
Insert cell(s)	Insert and charge cells with the lowest voltages	Insert and charge cells with the highest voltages
Bypass cell(s)	Bypass and prevent charging of cells with the highest voltages	Bypass and prevent charging of cells with the lowest voltages

Table 2.2: Capacitor voltage balancing criteria.

The capacitor voltages of all the cells are balanced continuously by this method ensuring optimized utilization of the stored energy [31]. Fig. 2.9 shows an example of integrating a capacitor balancing algorithm in an MMC control. Further insights on different topologies of MMC are given in [32].

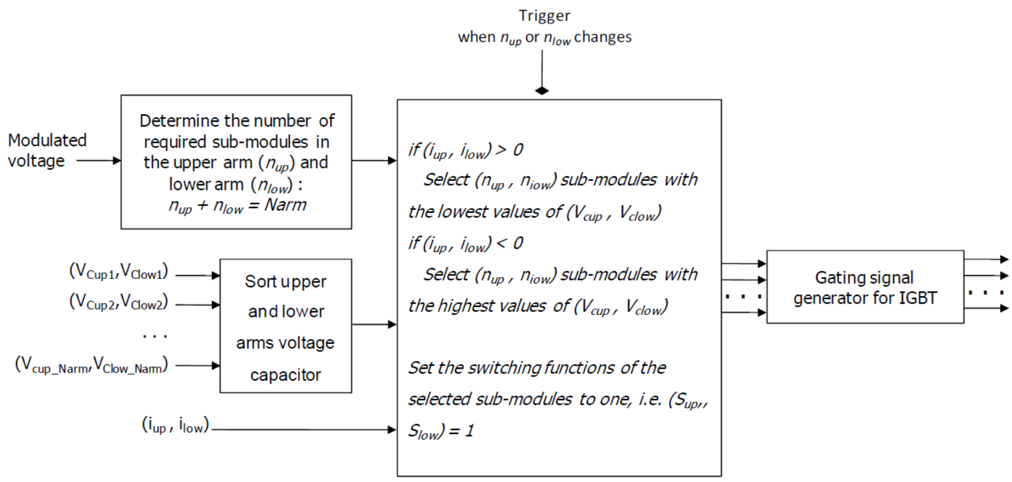

Figure 2.9: Capacitor Balancing Algorithm [18].

The MMC concept stands out especially for high-voltage grid-connected applications due to its modularity, excellent output voltage waveform and superior control characteristics. MMC has become the foremost promising technology due to its robust design, high efficiency and reliability [28], [31]. It can be easily scaled to different high-power and voltage levels by simply stacking up the submodules .

Furthermore, in high-voltage grid-connected applications, the number of submodules in each phase leg would be approximately 100, and each module theoretically only needs to be switched on and off once in a time period which greatly reduces the switching losses of the valves. The switching frequency is also greatly reduced to just a few times the fundamental frequency [28]. The MMC delivers an excellent harmonic performance which may eliminate the requirement of additional filtering equipment. As the submodules are modular and identical, it reduces the time in the design and manufacturing process making it more available [28]. Another advantage of the MMC is that the control system has more flexibility in dealing with dc side faults. During dc faults, the capacitors are not necessarily discharged and as a result, the fault recovery can be faster [33].

On the negative side, the number of components is significantly increased. The design and control of the MMC are complex. Furthermore, at low frequencies, MMCs suffer from significant internal energy fluctuations, which must be absorbed by the submodule capacitors [28]. This implies that the total energy stored in the capacitors needs to be much larger at least than a two-level converter resulting in a bigger capacitor size and hence an increase in cost.

It is also indispensable to consider the converter's limitations in terms of active and reactive power transfer capability for control design and stability analysis. The active power capability of the VSC is determined by the converter-current limitation which is imposed by the current-carrying capability of the converter valves. Since both, active and reactive power contributes to the current flowing through the valves, this limitation appears as a circle in a P-Q diagram as depicted in fig. 2.10. The maximum active power of the converter has to be limited when the VSC is supporting the AC system by supplying or consuming reactive power to ensure that the valve current is within its limit.

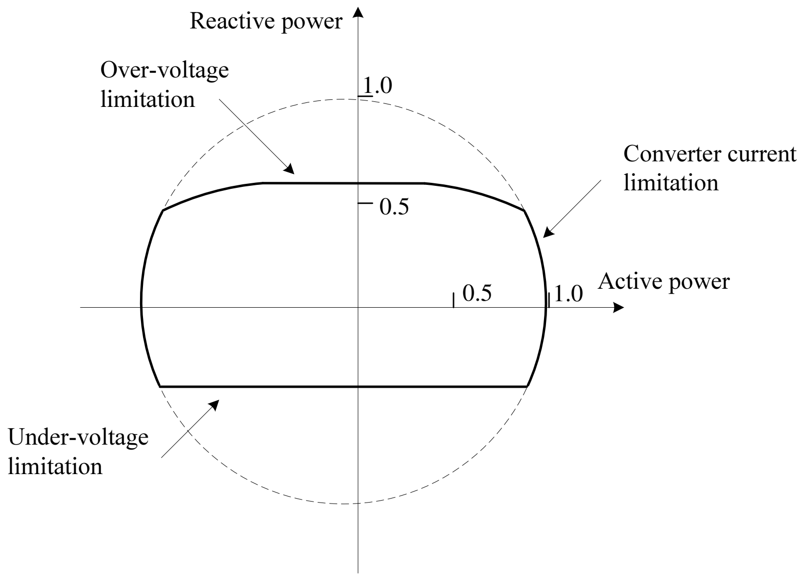

Figure 2.10: P-Q diagram for a typical VSC-HVDC converter [26].

The reactive power capability of the MMC is determined by the under/over voltage magnitude of the VSC (known as modulation index limitation). The VSC's direct-voltage level imposes an overvoltage limitation. The under-voltage limit is imposed by the main-circuit design and the active-power transfer capability, which requires a minimum voltage magnitude to transmit the active power [26]. In this regard, the converter transformer's tap-changer can play a vital role in extending the VSC's reactive-power restriction and this could be an argument to use converter transformers in VSC-HVDC systems. Fig. 2.10 illustrates the active and reactive power capability curve with the aforementioned limitations for a typical VSC-HVDC converter [18].

The fundamental base apparent power is defined as $S_b = P + jQ = \sqrt{3} \,.\, V_c \,.\, I_c^*$ The control of the active power flow between the converter and the AC system is achieved by varying the phase angle (θ) between the fundamental frequency voltage generated by the converter V_c and the AC bus voltage V_n. If the reactor X_l is assumed to be lossless, the power is calculated by

$$P = \frac{V_c \, V_n \, \sin\theta}{X_l} \tag{2.1}$$

Similarly, the reactive power flow between the converter and the AC system is controlled by varying the amplitude of the converter by adjusting the width of the pulses from the VSC.

$$Q = \frac{V_c^2 - V_c \, V_n \, \cos\theta}{X_l} \tag{2.2}$$

The converter's maximum fundamental voltage is determined by the DC voltage. An HVDC Light converter's reactive power generation and consumption capability can be utilized to compensate for the needs of the connected network while staying within the converter's rating. This makes the VSC-HVDC technology flexible for long-distance transmission of electricity without the need for any additional reactive power compensation devices. The reactive power can be controlled independently in both rectifier and inverter stations. Additionally, as mentioned earlier there is no reactive power flow in an HVDC link which significantly reduces the losses. The reactive power capabilities of an MMC can be traded against the active power capability as the converter ratings are based on maximum currents and voltages [34].

VSC-HVDC technology overcomes most of the inherent weaknesses of the LCC-HVDC technology, especially the interconnection of weak ac systems where the LCC technology requires a certain minimum network strength to ensure stable operation. The two notorious weak ac system-related problems such as Temporary Overvoltage (TOV) and low-order harmonic resonances are no longer major issues when VSC-HVDC technology is deployed. VSC-HVDC has made the integration of RES easy. It can provide black-start functions and in an emergency scenario, it can function as the last defense to prevent the grid from blackouts [2]. From a system point of view, the VSC acts like a motor or generator without mass that can instantaneously control active and reactive power independently. Moreover, it does not contribute to the short-circuit power as the AC current can be controlled. As discussed earlier, no additional RPC devices such as huge capacitors, SVC's and

STATCOMs are required when VSC-HVDC technology is employed. With enormous technology advancements in IGBT switching and conduction losses, increased voltage and current rating per device (6.5 kV/2000 A), compact MMC design, efficient PWM switching techniques, and overall control system design and optimization, today, the losses per converter station are brought down to less than 1% [10], [35].

Further advantages compared to the LCC-HVDC technology are the smaller footprint of the converter station site, insignificantly small filters, fast active power reversal, and inherent dynamic reactive power support in each converter station. The VSC avoids commutation failures arising from disturbances in the ac network. The extruded polymeric cable system enables long stretches of land cable installation and reduces the cable cost [36]. This technology also minimizes environmental impact and improves the quality of the power supply. By utilizing VSC-HVDC technology, power can be manipulated as per the grid-code requirements and also maintain power security.

Aside from the advantages listed above, the most salient feature is that a VSC-HVDC system has an unlimited connection capability with ac systems, meaning that with properly designed control systems, a VSC-HVDC system may be connected to any type of ac system (especially connecting asynchronous grids) with N number of links. The HVDC Light technology has taken great strides with outstanding features and has arguably become one of the two main alternatives for HVDC transmission eventually extending the dc transmission technology to ever broader application fields. This technology will be the backbone of a DC Super grid to transmit bulk power through congested areas. These massive overall advantages make the VSC-HVDC technology the most attractive choice for integrating large OWFs.

2.3 Application of Flexible AC Transmission Systems

FACTS are power electronic-based devices that are mainly used to regulate the bus voltage and enhance the active power transfer capability of the power system. Also, FACTS devices are used at the distribution level to enhance power quality. These devices alleviate large dynamic swings between different parts of the system and bottlenecks in the transmission lines thereby improving the reliability of the power system [37]. They are very much flexible in control. The application of FACTS is categorized into transmission level and distribution level:

- At the *transmission level*, FACTS devices are mainly used for power flow enhancement and control, voltage and reactive power control, power oscillation damping, maintaining system stability and stabilizing voltages in weak networks. These deal with the system dynamics.
- At the *distribution level* (1 kV - 38kV), FACTS devices are mainly used for voltage dip mitigation, interruption mitigation, flicker mitigation, active filtering and reduces reactive power absorbed from the main AC grid. These deal with the power quality and custom power devices are typically used.

2.3.1 Power Quality

In order to meet the ambitious 'Carbon-Neutral 2050' goal set by the EU, tremendous efforts are being made to decommission the existing fossil fuel-based power plants and to generate sustainable green energy through RES like wind, solar, hydro, etc. Huge projects in terms of RES integration are being planned and executed all over the world today. When this bulk power is being generated, it is indispensable to ensure that the generated power is efficiently integrated into the existing grid and utilized with the least possible losses. For this, the quality of the power should be maintained well throughout the system right from generation to transmission and distribution. To address the power quality issues, FACTS and custom power devices are deployed.

Power quality includes all possible circumstances in which the waveform of the supply voltage (voltage quality) or the load current (current quality) deviates from the sinusoidal waveform at the rated frequency with amplitude corresponding to the rated value for all three phases of a three-phase system. The power quality phenomena can be classified into two categories:

1. **Voltage quality phenomena.** The quality of the voltage is affected due to the following disturbances that occur from the source side:
   - Lightning surges on an overhead transmission line can cause transient overvoltages in the power system.
   - Switching surges can occur while energizing or disconnecting a transmission line and during capacitor switching resulting in transients or TOV in the system.
   - Another most common cause is the short-circuit faults in the power system which causes voltage dips/sags.

   These phenomena cause overvoltage and undervoltage issues. Overvoltages can permanently damage a sensitive load while undervoltages can cause malfunctioning of the equipment.

2. **Current quality phenomena.** The quality of the current is affected due to the following disturbances that occur from the load side:
   - Starting of huge induction motors in industries can cause transient overcurrents in the power system. The motors draw a significant amount of reactive power from the grid thereby increasing the load current.
   - Non-linear loads such as diode or thyristor rectifiers produce a lot of harmonics in the system.
   - Rapidly varying loads such as arc furnaces can cause periodic current fluctuations leading to power-line flicker.

   These phenomena cause overcurrents and harmonic current distortion issues. Overcurrents heats the system and permanently damage a sensitive load while harmonic current distortion can cause increased losses and overheat. Moreover, a distorted current affects the voltage quality of the system as current and voltage are tightly co-related.

To combat all the aforementioned power quality problems, appropriate FACTS devices are installed in the AC system. A list of FACTS devices with their application

Power Electronics Applications in Power Systems			
Transmission level		**Distribution level**	
Device	**Function**	**Device**	**Function**
SVC elements such as Thyristor Controlled Reactor (TCR), Thyristor Switched Capacitor (TSC).	Shunt connected devices that regulate bus voltage.	SVC	Reactive power compensation.
STATCOM or Static Synchronous Condenser (STATCON)	Shunt connected power electronics-based VSC used for reactive power compensation. Dynamic operation due to fast switching times of the IGBT's.	Distribution Static Compensator (D-STATCOM)	Voltage regulation and reactive power control, flicker mitigation, current active filtering. Mitigation of voltage dips and short interruptions is possible by integrating energy storage.
Thyristor Controlled Series Compensation (TCSC)	Series compensator used to enhance active power flow, boosts transmission capability, dampen power oscillations, improved voltage regulation and reactive power balance.	Static Transfer Switch (STS)	Mitigation of voltage dips and interruptions by fast load transfer.
Static synchronous series compensator (SSSC)	Series variant of STATCOM used to regulate active and reactive power, dampen power oscillations. Drawback- problematic protection issues with the VSC.	Dynamic Voltage Restorer (DVR)	Mitigation of voltage dips, voltage active filtering. Drawback- Cannot mitigate interruptions due to series connection and also complex issues with protection schemes.

Table 2.3: FACTS devices and functions.

is shown in table 2.3. From table 2.3, it is evident that the STATCOM's are capable of carrying out more functions in both the transmission and distribution level.

The STATCOM's are an attractive choice especially for providing dynamic voltage support in interconnecting weak ac grids eg., integrating OWFs and hence the STATCOM will be used in the analysis of the thesis. A detailed explanation of the FACTS devices and their applications can be found in [37], [38].

2.4 Types of Grid-connected Wind Turbine Generators

1. **Type 1: Induction generator (WT-IG)**
   This type is a fixed-speed wind turbine system equipped with a multiple-stage gearbox and a standard squirrel-cage induction generator (SCIG) which is directly connected to the grid through a step-up transformer as shown in fig. 2.11. The induction machine (IM) rotates with a rotor speed (close to the synchronous speed) which is determined by the frequency of the grid and it does not need to be controlled. Since the SCIGs always draw reactive power from the grid, typically, this type of WTGs is equipped with mechanically switched capacitor banks to provide the necessary reactive power compensation. The circuit breaker acts as a protection device that disconnects the generator and the capacitor from the grid in the event of a fault.

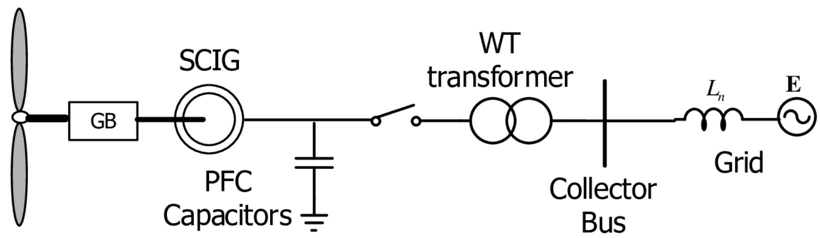

Figure 2.11: Type 1 WTG

   This basic concept is robust, easy and comparatively cheap for mass production. It enables stall-regulated or pitch-controlled WTGs to operate at a constant speed and frequency when connected to a large grid [39]. The main disadvantage is that the speed is not controllable (fixed rotor resistance) and variable only over a very narrow range. Furthermore, the system is subjected to severe mechanical and fatigue stresses due to the fixed speed concept where the wind speed fluctuations are directly transformed into electromechanical torque variations [39].

2. **Type 2: Wound rotor induction generator (WT-WRIG)**
   This type is similar to type 1 WTG but uses a WRIG with variable rotor resistance (VRR) connected to the rotor and is controlled using power electronics as shown in fig. 2.12. The machine's stator is directly connected to the grid. In this way, the torque (rotor speed) of the generator can be controlled by

varying the slip [40]. Typically, the limited variable speed range is less than 10% above the synchronous speed. The major drawback of this concept is that big resistors are required to have a good dynamic speed control range but this eventually also results in significant power loss [39].

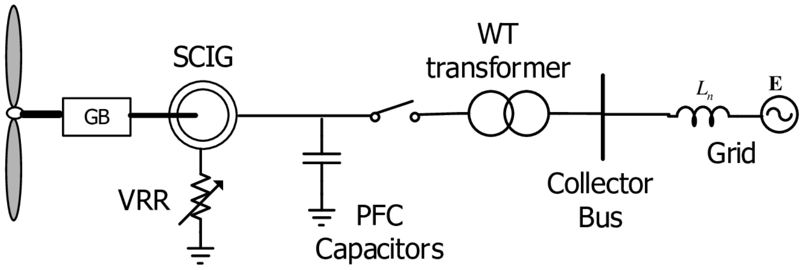

Figure 2.12: Type 2 WTG

3. **Type 3: Doubly-fed induction generator (WT-DFIG)**
   This type utilizes a DFIG machine which is a variable speed wind turbine with a WRIG as shown in fig. 2.13. The rotor is connected to partial-scale back-to-back voltage source power electronic converters (PECs), typically 25-30% of the size of DFIG [39]. The machine's stator is directly connected to the grid. Conventionally, the rotor side converter (RSC) regulates the generator's active and reactive power, while the grid side converter (GSC) regulates the DC-link voltage to maintain DC voltage stability [40].

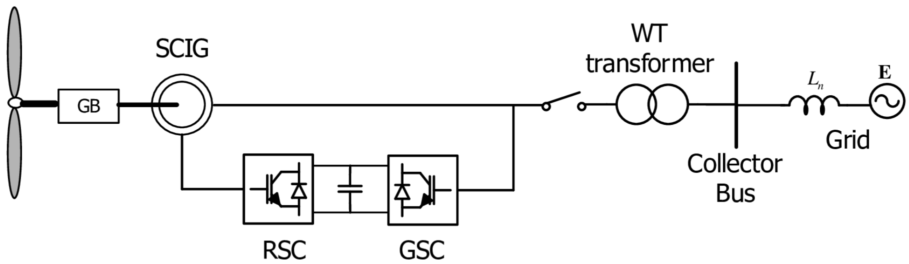

Figure 2.13: Type 3 WTG

The PEC controls the rotor frequency and speed. This concept utilizes and controls the energy in a much efficient way rather than dissipating the energy (loss) through the VRR as in type 2 WTG. In this way, the rotor speed of the DFIG is controlled in a much wider range converter, typically, the variable speed range is ±30% around the synchronous speed [39]. The active and reactive power can be effectively controlled from the WTG to the grid through the PEC and hence the need for a capacitor bank is eliminated. This concept is also attractive from an economic point of view due to the small-sized PEC. Furthermore, type 3 WTGs have FRT capability but during severe grid fault conditions, this becomes an issue as the large stator currents induce large rotor currents, so the PEC has to be protected from getting damaged [39]. Large stator peak currents, on the other hand, may result in significant torque loads on the drive train of wind turbines. As the speed range for a DFIG is far from an ordinary turbine speed of 10–25 rpm, a multi-stage gearbox is still necessary for the drive train. Moreover, slip rings are required to transfer the rotor power along with the PEC which requires regular maintenance and might also result in machine failures and losses.

4. **Type 4: Induction or Synchronous generator with full-scale converter interface (WT-PMSG)**
   This type utilizes an IG or PMSG (Permanent Magnet Synchronous Generator), a variable speed wind turbine with a direct-drive generator (without a multi-stage gearbox) connected to the grid through a full-scale back-to-back PEC with the same power rating as the machine as shown in fig. 2.14. The

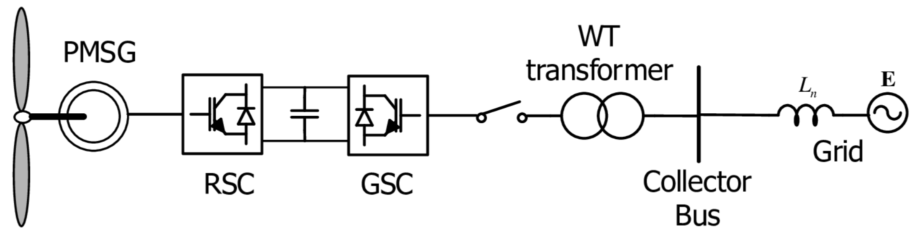

Figure 2.14: Type 4 WTG

control scheme of the RSC and GSC is the same as type 3. Type 4 is a more attractive technology as it overcomes the problems of type 3 WTGs. The full-scale PEC can perform smooth grid connection over the entire speed range as compared to type 3. The type 4 WTG has good isolation from the grid side disturbances and hence, it offers better reactive power compensation and LVFRT capability compared to type 3. Additionally, by omitting the gearbox, heat dissipation from friction, regular maintenance and noticeable noises are eradicated giving a robust performance [39]. The drive train is also simplified. Typically, PMSG with self-exciting magnets in the rotor is used as it has a higher power factor and efficiency [40]. Furthermore, the absence of rotor windings reduces the excitation losses and size of the generator and also very low maintenance. The drawback is that this technology is costly due to the full-scale PEC and also higher power losses from the power electronics since all the generated power has to pass through the converter. This also makes the protection system complex. As the overall advantages of type 4 WTGs outweigh type 3, type 4 is a more attractive and promising option that is typically used in OWFs. Therefore, in this thesis type 4 WTG is used.

2.5 Challenges in interconnecting Offshore Wind Farms

- The main challenge lies in transmitting the bulk power that is generated from the OWF to the onshore AC grid as efficiently as possible with minimum losses. Losses are the biggest "enemy" when it comes to electric power transmission for longer distances. To realize the full potential of the OWF, new electric connections and cost-effective designs with improved reliability and efficiency are required.
- A critical issue of the HVDC-based OWFs is the LVFRT, in which the wind farms are required to be connected to the AC grid during grid faults and disturbances. The OWF system should have LVFRT capability for effective resilient grid operation during severe faults.
- As the existing synchronous generators are being de-commissioned to pave way for 100% RES in the future, the voltage and frequency stability is lost. To overcome this major problem, grid-forming converters must be integrated to provide the necessary voltage and frequency support during island mode operation and blackouts.

2.6 Strength of the Grid

As discussed in section 2.2.1, the strength of the AC grid affects the operation of an LCC-HVDC system. The strength of an AC system is measured by the SCR which is the ratio of the AC system's short-circuit power to the rated power of the HVDC link. If this value is less than 2-3, the AC system is considered weak. As per [23], SCR is defined as

$$SCR = \frac{S_{\mathrm{ac}}}{P_{\mathrm{dc}}} \tag{2.3}$$

where P_{dc} is the rated DC power of the HVDC link and S_{ac} is the short-circuit capacity of the AC system at the filter bus which is expressed as

$$S_{\mathrm{ac}} = \frac{V_f^2}{Z} \approx \frac{V_f^2}{\omega_1 L_n} \tag{2.4}$$

where Z is the equivalent impedance of the ac system, ω_1 is the angular frequency of the ac system and L_n is the inductance of the ac system. Eq. 2.3 can be further simplified by assuming the filter-bus voltage to be identical to the base value of the AC system, i.e., $V_f = V_{\mathrm{ac}}$ and P_{dc} to be equal to the base power of the ac system, i.e., $S_{\mathrm{ac}} = P_{\mathrm{dc}}$. If $\omega_1 L_n$ is expressed in per unit value, then from eq. 2.3 and 2.4,

$$SCR = \frac{1}{\omega_1 L_n} \tag{2.5}$$

The strength of the AC system as per [23] is classified as shown in table 2.4.
In a weak AC system, reactive power can be compensated by placing RPC devices such as SVCs, STATCOMs and synchronous compensators at the point of common

SCR of AC system	Strength of the grid
SCR >3	Strong
2 <SCR <3	Weak
SCR <2	Very weak

Table 2.4: SCR and strength of the grid

coupling (PCC) to improve the SCR [41]. The characteristics of a strong and weak grid are given in table 2.5.

No.	Strong grid	Weak grid
1.	High inertia and low equivalent impedance of the AC network.	Low inertia (e.g. island mode) and high equivalent impedance of the AC network.
2.	High short-circuit current capacity and protection capability against faults.	High short-circuit current capacity and vulnerable to faults.
3.	More stable against perturbations.	Unstable against perturbations.
4.	High damping against destabilizing torques.	Very low damping effect.
5.	Good voltage and frequency regulation capability and hence, lesser voltage and frequency fluctuations.	Unstable voltage and frequency, and thus prone to flickering and outages.

Table 2.5: Strong grid vs Weak grid

2.7 Grid-Following versus Grid-Forming Control

Grid-following (GFL) employs voltage-based synchronization that measures or estimates the voltage angle and frequency of the grid to synchronize the converter with the grid. If a converter's control strategy does not employ a voltage regulator and the frequency is obtained from sensing the phase of the voltage bus, then the frequency is locked to the corresponding bus by a Phase-locked loop (PLL), then it's called grid-following control. It is called GFL control since they follow the phase of grid voltage. A generic control structure of a GFL control is shown in fig. 2.15. GFL controls the current injection and phase angle with respect to a PLL. Existing grid-tied converters operate as grid-following sources that rely on the high stiffness of the grid as it works with vector current control (VCC) for regulating the active and reactive power exchanged with the grid. In this way, the active and reactive power can be controlled independently through decoupling similar to the control of flux and torque of a motor with d and q- axis control. In GFL control the active and reactive power is controlled d and q- axis current respectively. The obtained current reference generates the three-phase voltage reference to the converter. As the control strategy works on VCC, it does not work well with weak grid conditions

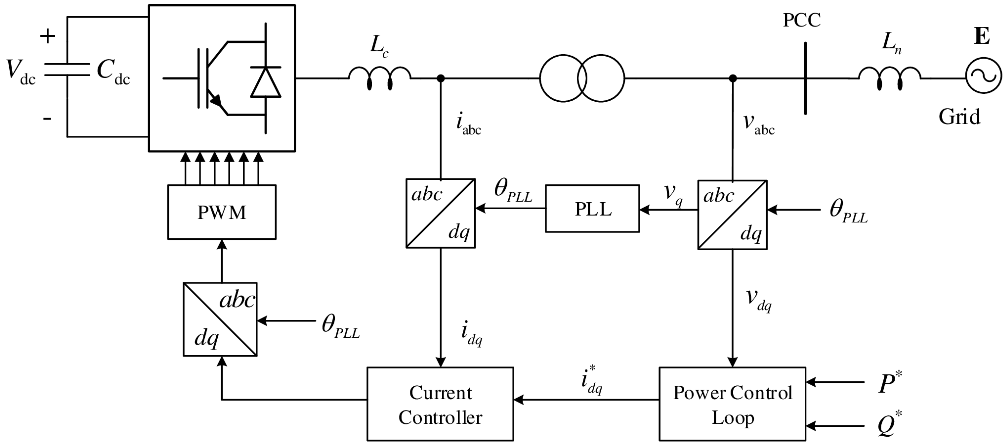

Figure 2.15: Generic structure of a grid-following control

that require self voltage and frequency regulating capability. Standalone operation is not possible.

Grid-forming (GFM) employs power-based synchronization to utilize the active power-frequency droop control similar to the synchronization of SGs to synchronize the converters with the grid. If a converter's control strategy directly incorporates a voltage regulator by giving the desired voltage reference and if its frequency is generated (and not sensed from the voltage bus), then it's called grid-forming control. GFM converter can generate and control the required voltage magnitude and frequency of the grid. A generic control structure of a GFM control is shown in fig. 2.16.

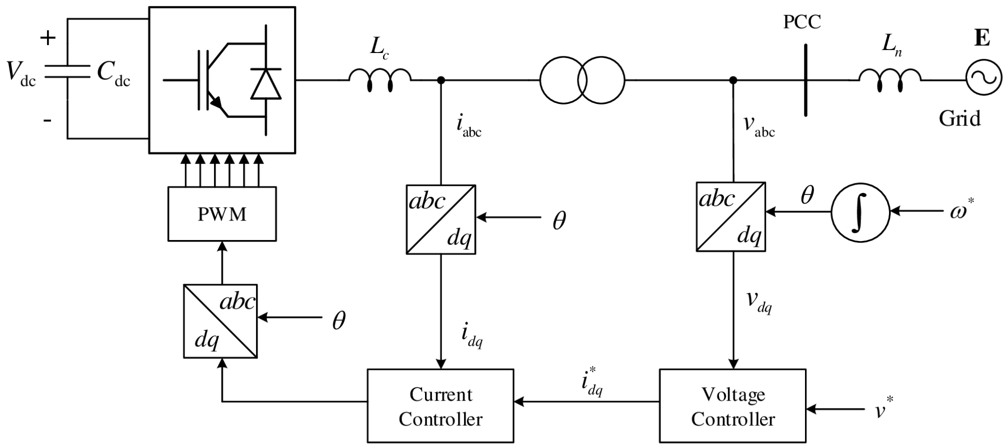

Figure 2.16: Generic structure of a grid-forming control

GFM converter can operate AC grids with or without rotating machines. GFM strategy allows a VSC to mimic synchronous generators for droop-based load-sharing, synthetic inertial-emulation, synchronized and blackstart capability. GFM converter behaves as a voltage source that can be fully utilized in weak grid conditions such as the interconnection of large OWFs and photovoltaic systems, standalone operation (island), and HVDC systems. As the current electricity generation is aiming towards 100% RES in the future to meet the de-carbonization goals, GFM must be a requirement to have grid resiliency and smooth operation after severe faults and blackouts in the system. Further insights on GFL and GFM control strategies can be found in [3], [42]–[44]

2.8 Power-Synchronization Control

PSC is a grid-forming control introduced in [26]. PSC strategy is used in this thesis as it has demonstrated strong performance in weak networks such as the interconnection of OWF. Two major problems of vector current control in weak AC system interconnection are resolved using PSC. First, the presence of low-order harmonic resonances can interfere with the fast-inner current control loop which in turn limits the control performance of the VSC [45], [46]. Second, the resonances and non-linearities due to the interaction between the PLL and AC filter which again induces difficulty in controlling the VSCs [46]–[48]. By using PSC, these problems are avoided.

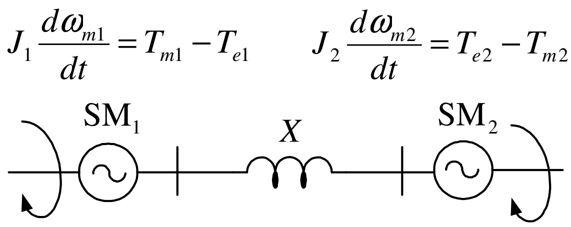

Figure 2.17: Synchronization mechanism between SMs in an ac system

PSC emulates the principle just like the synchronization mechanism between synchronous machines (SMs) connected to an AC grid as shown in fig. 2.17. SM1 and SM2 operate as a generator and motor respectively. X denotes the total reactance of the SMs and the AC line interconnecting the machines. The maximum power that can be transmitted from SM1 to SM2 is given by

$$P = \frac{E_1 E_2 \sin\theta}{X} \tag{2.6}$$

where θ denotes the angle between Electromotive Forces (EMFs) E1 and E2. The well-known Swing equation governing the synchronization of a synchronous machine is given by

$$J\frac{d\omega_m}{dt} = T_m - T_e \tag{2.7}$$

where J is the total moment of inertia of the rotor mass, ω is the rotor speed, T_m is the mechanical torque supplied by the prime mover and T_e is the electrical torque output of the alternator.

As $P = \omega T$, the generated power of an SM is directly proportional to the torque. Hence eq. 2.7 becomes

$$J\omega\frac{d\omega_m}{dt} = P_m - P_e \ , \ \frac{d\omega_m}{dt} = \theta \tag{2.8}$$

where P_m and P_e respectively are the mechanical and electrical power. Disparate the swing equation where double integration is required to obtain the electrical angle from the electric power; which inherently leads to low stability due to poor phase margin, the Power-Synchronization loop (PSL) directly gets the phase angle by only employing a single integration as eq. 2.9

$$J\frac{d\Delta\theta}{dt} = K_p\left(P_m - P_e\right) \tag{2.9}$$

which yields a higher stability margin [26]. Just like a synchronous machine, the terminal of the VSC can provide strong voltage support for a weak AC grid interconnection system. The PSC strategy controls the active and reactive power directly using the phase-angle and voltage magnitude of the AC system without using the PLL.

2.8.1 Power-Synchronization Control of Grid-connected VSCs

This section describes the overall control design of the MMC-HVDC with PSC used in the thesis. The overview of the control loops is shown in fig. 2.18

- *Power-Synchronization Loop (PSL).* The control law is given by

  $$\theta_v = \frac{K_p}{s}(P_{\text{ref}} - P) \tag{2.10}$$

  where θ_v provides the synchronization angle to the MMC, i.e., $\omega t = \omega_{\text{ref}}\, t + \theta_v$. This is the fundamental control loop of the PSC which maintains synchronism between the MMC and the AC system, and is also the active power control loop as shown in fig. 2.18. The output signal ωt is obtained by converting the power control error between the measured PCC (point of common coupling) power and the reference power to a frequency deviation and then integrating it to an angle increment. The converter voltage reference V^c_{ref} is transformed from dq to stationary frame with the angle information provided by ωt signal [49]. The mathematical steps involved in the abc to dq transformations is described in appendix A.1

- *Alternating Voltage control (AVC).* The control law is given by

  $$\Delta V = \frac{k_v}{s}(V_{\text{ref}} - V_f) \tag{2.11}$$

  where ΔV provides the change in the voltage magnitude which is then fed to the voltage control law as the reference. The AVC loop is designed as an integrator with a gain to suppress high-frequency disturbances.

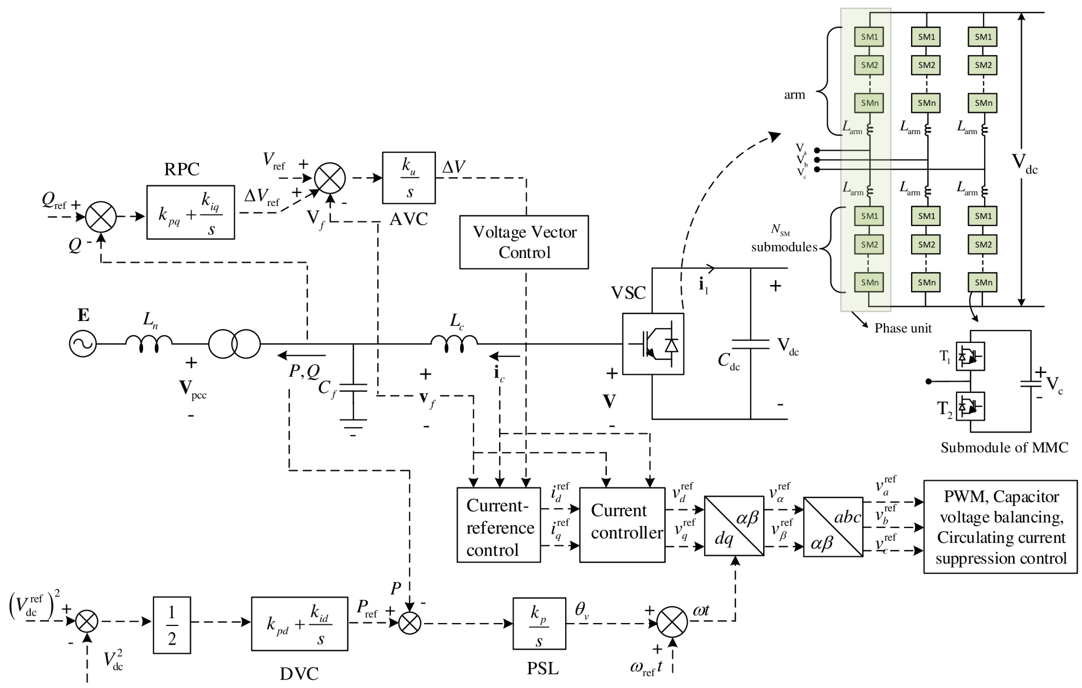

Figure 2.18: Overall control scheme with Power-Synchronization Control

- *Reactive Power control (RPC).* The control law is given by

$$\Delta V = \left(K_{pq} + \frac{K_{iq}}{s}\right)[Q_{\text{ref}} - Q] \tag{2.12}$$

  It is recommended to operate the MMC-HVDC in AVC mode to give the AC system best possible voltage support especially when the system is interconnected to a weak system. Reactive power control could be added to the reference of AVC loop if required and then the added amount should be limited [26].

- *Voltage Vector Control (VVC).* The proposed control law for the voltage vector of the MMC is given by

$$\mathbf{v}^c_{\text{ref}} = (V_0 + \Delta V) - H_{\text{HP}}(s)\,\mathbf{i}^c_c \tag{2.13}$$

  where V_0 is the nominal voltage 1 p.u. and ΔV is derived from the AVC. $H_{\text{HP}}(s)$ is a high-pass filter that is used to dampen out the grid-frequency resonant poles for low resistance grids, expressed by

$$H_{\text{HP}}(s) = \frac{K_v s}{s + \alpha_v} \tag{2.14}$$

  where bandwidth α_v is selected low enough in the range 30 rad/s - 50 rad/s to cover all the possible resonances in the AC system and the gain K_v determines the level of damping effect which is mostly selected between 0.2 p.u. and 0.6 p.u. [26].

- *Direct Voltage Control (DVC).* The control law is given by

$$P_{\text{ref}} = \left(K_{pd} + \frac{K_{id}}{s}\right) \frac{(V_{\text{dc}}^{\text{ref}})^2 - V_{\text{dc}}^2}{2} \tag{2.15}$$

If the MMC is assumed to be lossless with a much faster AC control loop than the direct voltage control loop, the power that goes into the DC-link is the input active power from the PCC, i.e., $i_1 = P/V_{\text{dc}}$. The energy stored in the DC capacitor is $C_{\text{dc}}V_{\text{dc}}^2/2$ Then the DC-link dynamics can be written as [46]

$$\frac{1}{2}C_{\text{dc}}\frac{dV_{\text{dc}}^2}{dt} = P - P_L \tag{2.16}$$

$$C_{\text{dc}}V_{\text{dc}}^0\frac{d\Delta V_{dc}}{dt} = \Delta P - \Delta P_L \tag{2.17}$$

where $P_L = V_{\text{dc}}\,i_2$ The closed-loop dynamics will depend on the operating point V_{dc}^0 if the DVC directly operates on the error between $V_{\text{dc}}^{\text{ref}} - V_{\text{dc}}$. To overcome this issue, the DVC is designed as a PT controller that operates on the error between $[(V_{\text{dc}}^{\text{ref}})^2 - V_{\text{dc}}^2]/2$ [46], [50].

- *Backup Phase-Locked Loop.* The PSL cannot be applied in two scenarios. First, when the MMC is blocked and during this period, the PLL provides the synchronization angle before deblocking the MMC. Second, during AC system faults, the converter has to limit the fault current, so it switches to backup PLL. This is due to the fact that during the current limitation process of the converter valve, it follows the vector current control and moreover PLL works by the coordination of the VCC whereas PSL cannot be applied as it works on voltage control law. The backup PLL and PSL switching scheme is shown in fig. 2.19

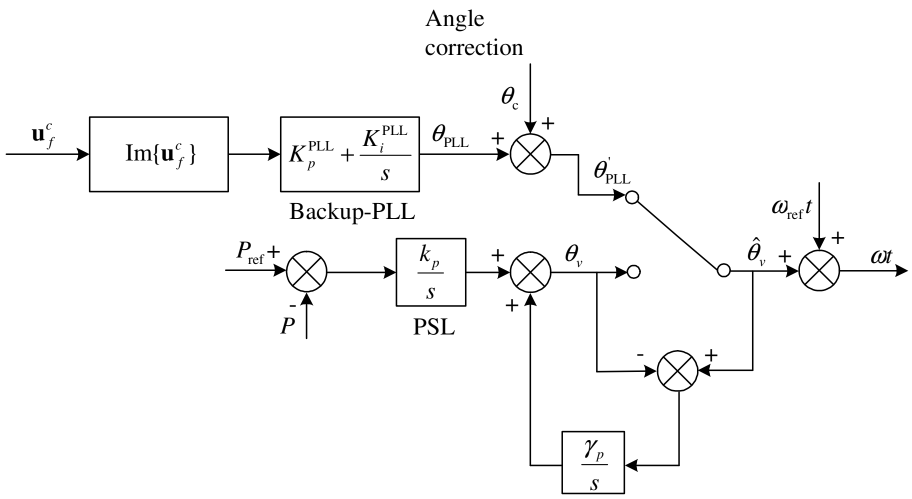

Figure 2.19: Bumpless-transfer angle synchronization scheme [26].

- *Anti-windup scheme for AVC.* With PSC strategy, the AVC controls the d component (voltage-oriented system) of the voltage reference (V_d^{ref}) which is the magnitude of the VSC. However, Vdref might be limited during AC system faults or transients. During such scenarios, occasionally, V_d^{ref} becomes higher than the maximum value of voltage that the VSC can produce resulting in over-modulation. This is more common with weak ac network connections, where a relatively higher VSC voltage magnitude is required to maintain the filter-bus voltage at its nominal value. In such scenarios, it is important to design the anti-windup for the AVC. The anti-windup scheme of the AVC works on the same principle as the bumpless-transfer strategy of the PSL as shown in fig. 2.20 When the AVC is limited, the anti-windup scheme integrates the error between V_d^{ref} and $\hat{V}_d^{\text{ref}}$, and feeds it back to cancel the integrator of the AVC [26]. γ_E is chosen large enough such that the output V_d^{ref} tracks the limited d component reference $\hat{V}_d^{\text{ref}}$ and once the limitation is lifted, the AVC resumes normal operation.

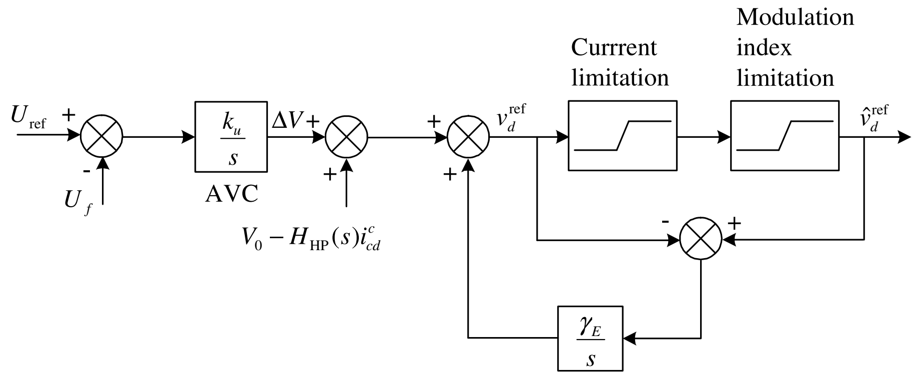

Figure 2.20: Anti-windup scheme for alternating voltage controller [26].

- *Current-Limitation Controller (CLC).* As the PSL cannot limit the over-current during the fault, a current controller as eq. 2.18. is proposed in such a way that during fault scenarios it limits the current to the maximum current rating of the valve (IGBT) and during normal operation simplifies itself to voltage vector control law (inserting eq. 2.18 in eq. 2.19 gives eq. 2.13). Hence, during a fault, the converter control goes to CLC mode and at the same time generates a signal to seamlessly switch to PLL to keep the MMC synchronized with the AC system [26]. Once the fault is cleared, the system resumes normal operation by switching back to PSL.

$$\mathbf{i}_{\text{ref}} = \frac{1}{\alpha_c L_c}\left[(V_0 + \Delta V) - H_{\text{HP}}(s)\,\mathbf{i}_c^c - H_{\text{LP}}(s)\mathbf{V}_f^c - j\omega_1 L_c \mathbf{i}_c^c\right] + \mathbf{i}_c^c \tag{2.18}$$

$$\mathbf{v}_{\text{ref}}^c = \alpha_c L_c\left(\mathbf{i}_{\text{ref}} - \mathbf{i}_c^c\right) + j\omega_1 L_c \mathbf{i}_c^c + H_{\text{LP}}(s)\mathbf{u}_f^c \tag{2.19}$$

2.9 MMC Control and Design

In this section, a brief explanation of the lower-level controls and design aspects of the Modular Multilevel Converter are given.

2.9.1 Lower level controls

The lower level controls generate the firing pulses for the submodules to produce the desired AC voltage waveforms. The three-phase voltage references generated by the upper-level controls are fed as input to the lower-level controls. The lower level controls are responsible for the modulation scheme, capacitor voltage balancing controller (explained in section 2.2.2) and Circulating Current Suppression Control (CCSC).

- *Phase-shifted Pulse-Width Modulation (PS-PWM)* is a carrier-based PWM that defines the switching pattern of the IGBTs in the submodules . Due to the N number of submodules in each arm, N number of triangular carrier waves is required. All triangular carriers have the same frequency and peak to peak magnitude but phase-shifted between two adjacent carrier waveforms given by $\theta = 2\pi/N$. Due to the phase-shift between the carriers, the first band of harmonics gets shifted more towards the higher side of the harmonic spectrum and hence the resultant voltage waveform's harmonic content is extremely low. The modulating reference signal is a sinusoidal wave with adjustable magnitude, frequency and phase angle. The firing pulses are generated by comparing the modulating wave with the carriers as shown in fig. 2.21. By having high MMC levels with an effective switching frequency, the total harmonic distortion (THD) is very low ($< 2\%$) and as a result, different modulation schemes exhibit similar harmonic performance [51]. The requirement of a filter is almost eliminated due to excellent harmonic performance.

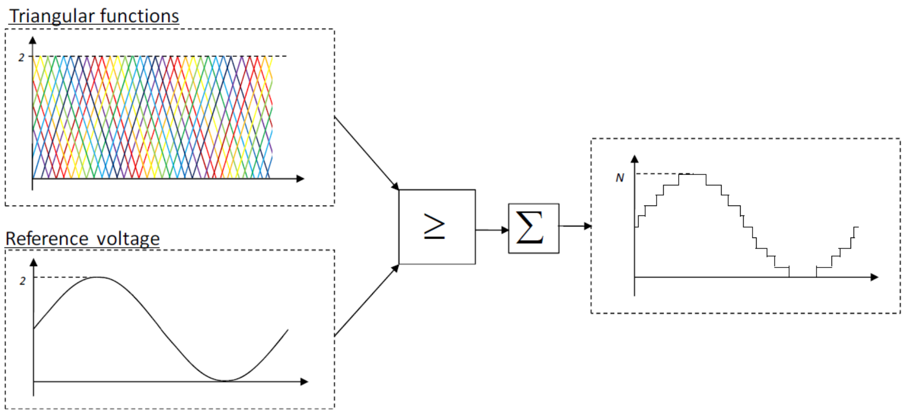

Figure 2.21: PS-PWM technique [51].

- *Circulating Current Suppression Control (CCSC)*. As the three-phase legs of the MMC are stacked with several cells that are connected in parallel to a DC terminal, there exists an inner-circulating current between the phase legs that rotates with a double-fundamental frequency (negative sequence) due to the inequality between the three-phase generated voltages [52]. This circulating current distorts the arm current and hence the quality of the sinusoidal waveform is affected. This problem can be reduced by increasing the size of the arm inductors, but the cost incurred would be high. Hence, the CCSC is implemented based on the double-fundamental frequency to eliminate the inner circulating currents by transforming the three-phase circulating currents to dq frame and then controlled separately by PI (Proportional Integral) controllers as shown in fig. 2.22 [52]. The outer dynamics (voltages and currents) of the MMC at the AC side are not affected due to this control strategy. Detailed explanation of CCSC is given in [52].

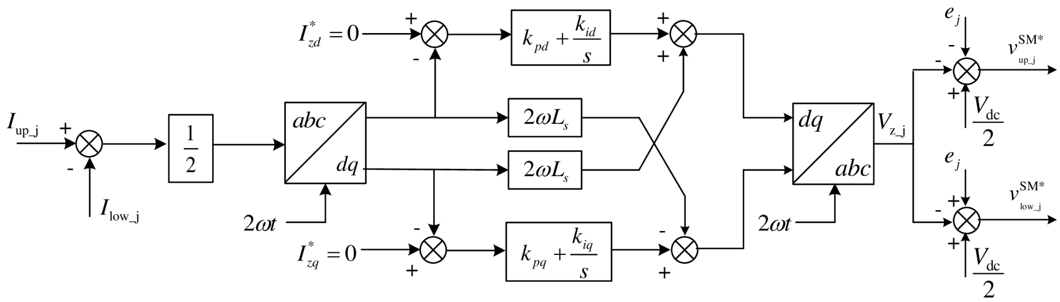

Figure 2.22: Circulating Current Suppression Control in dq frame.

2.9.2 Selection of Number of Submodules and Redundant Submodules

The number of submodules (SMs) is calculated in such a way that the total voltage of one arm sums upto the DC link terminal voltage, i.e., $V_{\mathrm{arm1}} = N_{\mathrm{sm}}.V_c = V_{\mathrm{dc}}$ where N_{sm} is the number of SMs, V_c is the DC capacitor voltage rating of the SM or IGBT voltage rating. Therefore, $N_{\mathrm{sm}} = V_{\mathrm{dc}}/V_c$.

It is also important to consider the redundant submodules while designing the MMC because the highest failure rate of the components in any converter valve occurs from the power electronics part such as the IGBT module and its driving electronic circuit [36]. In case of such sub-module failures, the MMC must continue its normal operation without deteriorating its performance and to achieve this fault-tolerant operation additional SMs called Redundant SMs are integrated into the arms [53]. Due to these redundant submodules, even if a sub-module fails, the faulty submodule will be shorted out and the healthy ones will continue their normal operation without any interruption. The faulty IGBT can be replaced during the time of the next scheduled maintenance. In this thesis, 10% redundant SMs are added [53].

2.9.3 DC Capacitor sizing of Submodules

The size of the DC capacitors must be significant enough to maintain an approximate constant direct voltage while carrying significant currents at low harmonic order, usually fundamental and second [28]. Oversizing the submodule capacitance simply increases the overall cost of the MMC significantly whereas an insufficient capacitor value produces a high voltage ripple. A detailed methodology is presented in [54] for calculating the energy storage requirements in an MMC. The nominal energy stored in one submodule capacitor is given by

$$E_{\text{sm}} = \frac{1}{2} C_{\text{sm}} V_{\text{sm}}^2 \tag{2.20}$$

where C_{sm} is the SM capacitance and V_{sm} is given by

$$V_{\text{sm}} = \frac{V_{\text{dc}}}{N_{\text{sm}}} \tag{2.21}$$

where V_{dc} is the DC link voltage and N_{sm} is the number of SMs per arm. The nominal energy storage per arm then becomes

$$E_{\text{nom}} = \frac{N_{\text{sm}}}{2} C_{\text{sm}} V_{\text{sm}}^2 \tag{2.22}$$

Therefore,

$$C_{\text{sm}} = \frac{2\, N_{\text{sm}}\, E_{\text{nom}}}{V_{\text{dc}}^2} \tag{2.23}$$

The required nominal energy storage in the MMC per transferred VA (Volt-Ampere) is approximately 42 kJ/MVA if the system injects nominal reactive power into the grid with the maximum modulation index [54], [55]. In this approach, the nominal energy storage by arm is calculated by

$$E_{\text{nom}} = \frac{42\,\text{kJ/MVA}\,.\,S_{\text{base}}}{6} \tag{2.24}$$

2.9.4 Selection of Arm Inductance

The role of the arm inductance is to suppress the transients in the circulating current (negative sequence) and limit fault currents. For grid-connected applications, the arm inductors could very well be in the range of approximately 0.10 - 0.15 p.u. [28], [54] In this thesis, a value of 0.28 p.u. is chosen as used in [54].

3

Verification and Validation of Power-Synchronization Control

In this chapter, the designed overall control scheme of Power-Synchronization Control will be verified and validated by applying it in the interconnection of two AC grids.

3.1 System description and modeling

The back-to-back MMC-HVDC system is connected to a very weak AC grid of SCR=1 as depicted in fig. 3.1. The back-to-back MMC's are equipped with GFM-PSC. The converter station connected to the weak grid controls the Active power transfer whereas the converter station connected to the strong grid controls the DC link voltage. The technical details of the system are given in appendix B.1. The simulations will be carried out using PSCAD/EMTDC to demonstrate the performance of PSC.

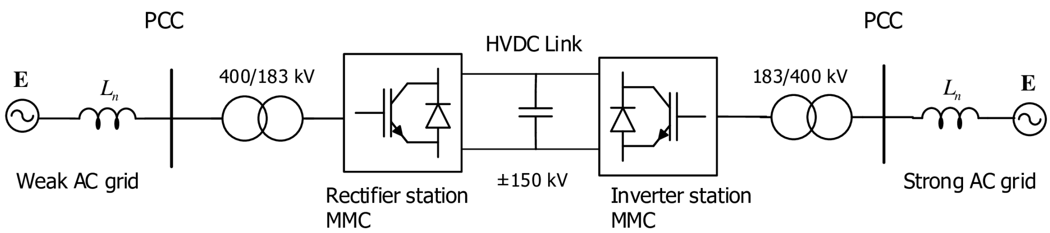

Figure 3.1: Back-to-Back MMC-HVDC interconnected to two AC grids.

3.2 Step tests for Active power control and DC link voltage control

The performance of active power control and DC link voltage control is verified by giving step changes as per [56]. In fig. 3.2, active power is varied in steps of ± 0.2 p.u. to verify whether the controller follows the reference. Initially, the system is energized and the converters are deblocked. The reference steps are manually given from 0.6 s. In fig. 3.3, DC link voltage is varied in steps of ± 0.2 p.u. to verify whether the controller follows the reference.

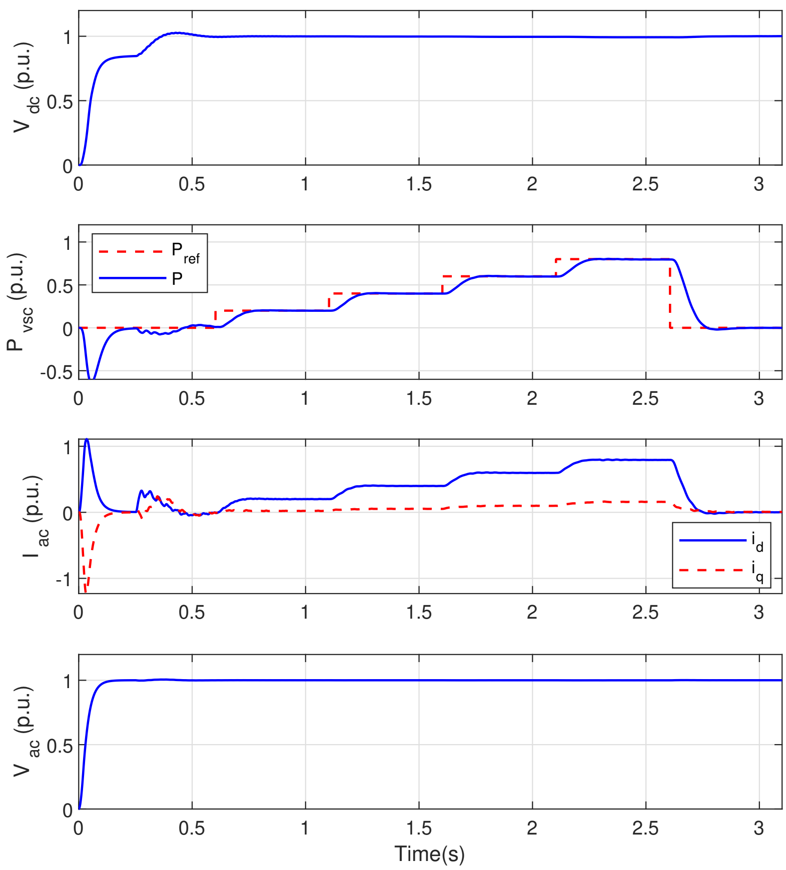

Figure 3.2: Active power control for SCR = 1.

3.3 Low-Voltage Fault Ride-Through Analysis

In this section, the LVFRT capability of the system is analyzed by applying a three-phase fault at the weak ac grid while transferring active power from the weak grid to the strong grid.

Fig. 3.4(a) shows the three-phase voltages at the MMC terminal. Fig. 3.4(b) depicts the deblocking and power ramping-up process of the MMC. From fig. 3.4(c), it is clear that before deblocking the MMC, PLL (θ_{PLL}) is used as its synchronization angle and during this time the PSL angle (θ_{PSL}) is forced to be equal to θ_{PLL}. When the MMC is deblocked at 0.3 s, PSL takes over the synchronization angle and ramps up the active power. As the power is being ramped up, the PLL traces the PSL and becomes equal when the system reaches a steady state. At 1.3 s, a three-phase fault with a duration of 0.2 s is applied on the weak AC grid. The control system on detecting the fault (either by current limitation controller or by sensing

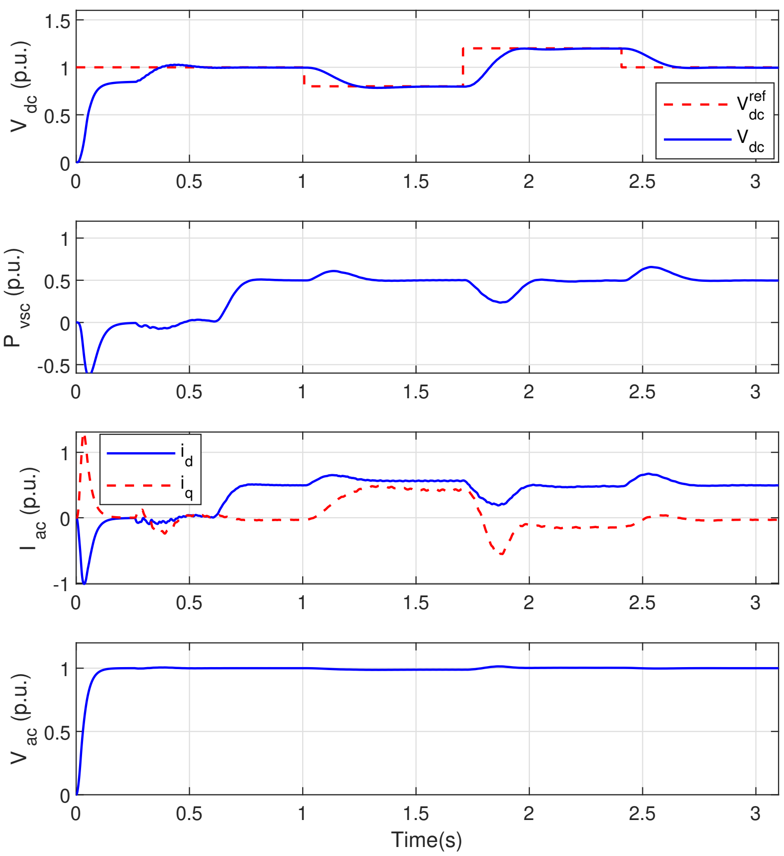

Figure 3.3: Cascaded DC-Link and Active-Power Control.

the voltage magnitude drop of the AC system) switches the synchronization angle of the MMC seamlessly to the backup-PLL. Once the fault is cleared, the PSL takes over the synchronization angle and resumes normal operation. This demonstrates the bumpless-transfer scheme between the PSL and the backup-PLL. The converter valve current increases (over-current) during the fault and after sensing the fault, the current is limited to half of the load current by the current limiter as shown in fig. 3.4(d). Fig. 3.4(e) shows the limitation of the d component of the MMC voltage reference (V_{ref}^{d}) by the current controller during the fault. The anti-windup scheme of the alternating voltage controller is similar to the bumpless-transfer scheme of the PSL, where the voltage output of the AVC is re-directed to follow the limited voltage reference [26]. Fig. 3.4(f) depicts the total capacitor voltages of the upper and lower arms (zoomed).

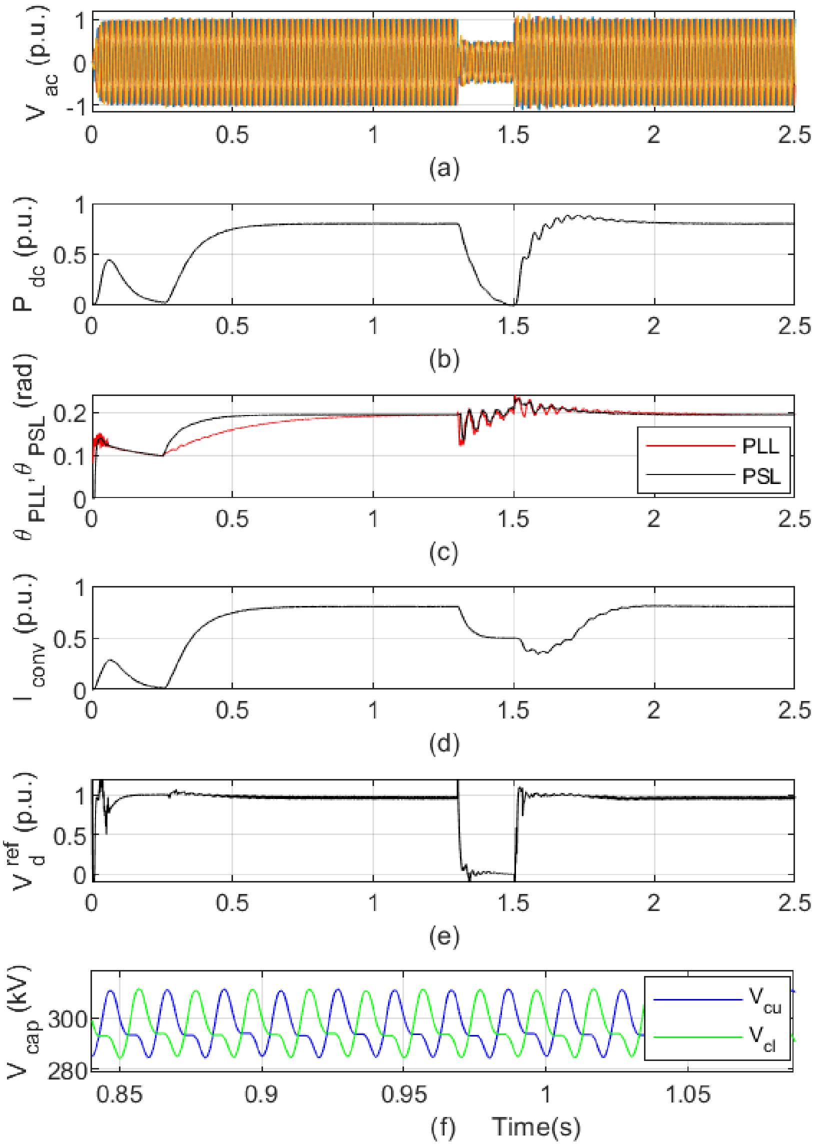

Figure 3.4: (a) Three-phase MMC terminal voltages. (b) Active power of the MMC-HVDC link. (c) PSL and PLL synchronization angle. (d) MMC valve current. (e) d component of the MMC voltage reference. (f) Total capacitor voltages of upper and lower arms (zoomed).

4

Test System 1: Back-to-Back MMC-HVDC

In this chapter, state-of-the-art back-to-back MMC-HVDC system with the interconnection of the Offshore Wind Farm will be modeled and studied. The overall system will be analyzed during LVFRT conditions, island mode and passive mode operations.

4.1 System description and modeling

The back-to-back MMC-HVDC system is connected to an OWF as depicted in fig. 4.1. The wind system is obtained from the PSCAD model which uses the traditional Grid-following-Vector Current Control (GFL-VCC) to control the back-to-back converters of the wind turbine. The GSC regulates the DC link voltage and AC voltage whereas the RSC controls the active power and AC voltage at the terminal of the PMSG machine. Later in the thesis, the control system will be replaced with GFM-PSC to study its benefits.

The back-to-back MMC's are equipped with GFM-PSC. Usually, the onshore MMC controls the DC link voltage and the offshore MMC controls the active power transfer. But, for a weak AC system interconnection, it is recommended to have DVC control on both of the converter stations for faster recovery of the DC link voltage [26]. For instance, if there is a fault on the offshore grid, the onshore MMC can control the DC link voltage and vice-versa so that the DVC can be maintained around its nominal value. The bandwidth of the inner PSC should be atleast four times greater than the DVC loop [26]. The technical details of the system are given in appendix B.1.

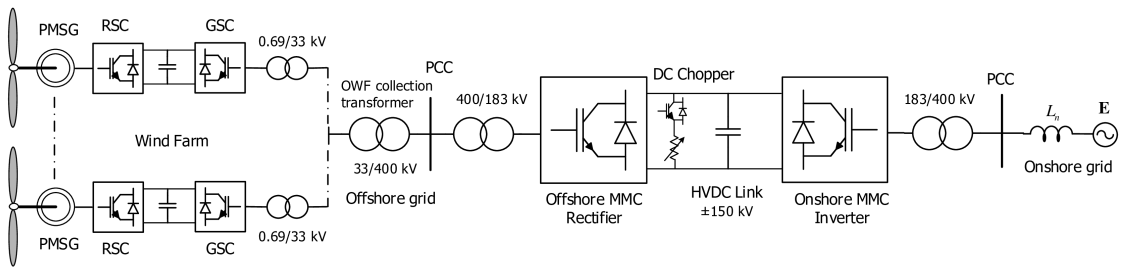

Figure 4.1: Back-to-Back MMC-HVDC interconnected to an offshore wind farm.

4.2 Interconnection of Offshore Wind Farm into AC grids

In this section, the interconnection of OWF into the offshore and onshore grids by the back-to-back MMC-HVDC link is analyzed as shown in fig. 4.1. The performance of the MMC-HVDC system is analyzed with a LVFRT condition at both the converter stations with two scenarios. First, the LVFRT performance is tested by transferring the active power from OWF to the Onshore AC grid. Second, the LVFRT performance is tested by transferring the active power from the Onshore to Offshore AC grid to demonstrate the bi-directional power transfer capability of the IGBT's. The MMC's operate with the GFM-PSC strategy which forms and controls the voltage and frequency of the respective offshore and onshore grids. The simulations will be carried out using PSCAD/EMTDC.

4.2.1 LVFRT Analysis (active power transfer from Offshore to Onshore)

Fig. 4.2 shows the graphs from the onshore station (inverter station). The OWF is deblocked and ramped up to 160 MW at the beginning. The MMC's are then deblocked and the active power is transferred from OWF to the onshore AC grid. At 1.6 s, a three-phase AC fault for 0.2 s is applied at the offshore grid (rectifier station). The HVDC link voltage dips to 0.3 p.u. due to the sudden loss of power from the OWF. The converter valve current of both the stations increase (overcurrent) during the fault and after sensing the fault, the current is limited to half of the load current by the current limiter.

At 3.6 s, a three-phase AC fault for 0.2 s is applied at the onshore grid (inverter station). The offshore grid is not affected by the fault and hence the converter valve current is within the limit but there is an over-current at the onshore side which is limited by the current limiter. During an onshore fault, the HVDC link gets overcharged as the OWF is not affected which continuously pumps power into the HVDC link and it is not possible for the power to be evacuated at the onshore side as the PCC voltage during the fault is zero. To overcome the HVDC overvoltage problem, a chopper is integrated. Chopper resistors that are controlled by IGBT switches are placed on the offshore HVDC converter station. The chopper is designed with a hysteresis control in such a way that the HVDC link voltage does not exceed 1.1 p.u. The chopper gets activated as soon as the HVDC link voltage reaches 1.05 p.u. and will dissipate the excess power using the resistors thereby avoiding an over-voltage situation as shown in fig. 4.2.

4.2.2 LVFRT Analysis (active power transfer from Onshore to Offshore)

From fig. 4.3 shows the graphs from the onshore station (inverter station). In this scenario, the system operation is the same as before except that the active power is transferred from the onshore to offshore AC grid. At 1.6 s, a three-phase

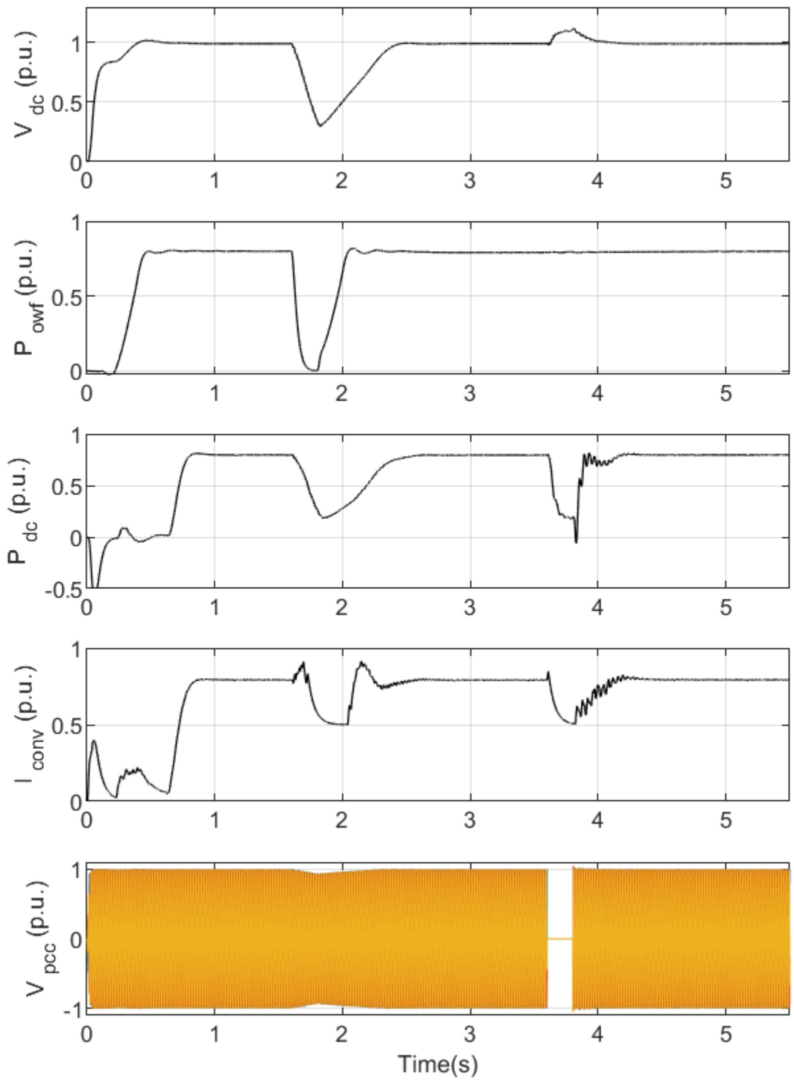

Figure 4.2: LVFRT capability of the MMC-HVDC link during three-phase AC system faults at offshore and onshore grids while transferring active power from OWF to the onshore grid.

AC fault for 0.2 s is applied at the offshore grid (rectifier station). The HVDC link voltage actually increases to around 1.2 p.u as the current from the onshore grid continuously charges the HVDC link during the fault and the power cannot be evacuated similar to the previous case. The chopper gets activated when the HVDC link voltage reaches 1.05 p.u. and prevents it from further over-charging by dissipating the excess power. There is an over-current issue at the offshore side which is limited by the current limiter. The onshore grid is not affected, and the converter valve current is within the limit.

At 3.6 s, a three-phase AC fault for 0.2 s is applied at the onshore grid (inverter station). The HVDC link voltage dips to 0.45 p.u. due to the sudden loss of power from the OWF. The converter valve current of both the stations increase (over-current) during the fault and after sensing the fault, the current is limited to half of the load current by the current limiter. After the fault is cleared, the system resumes its normal operation.

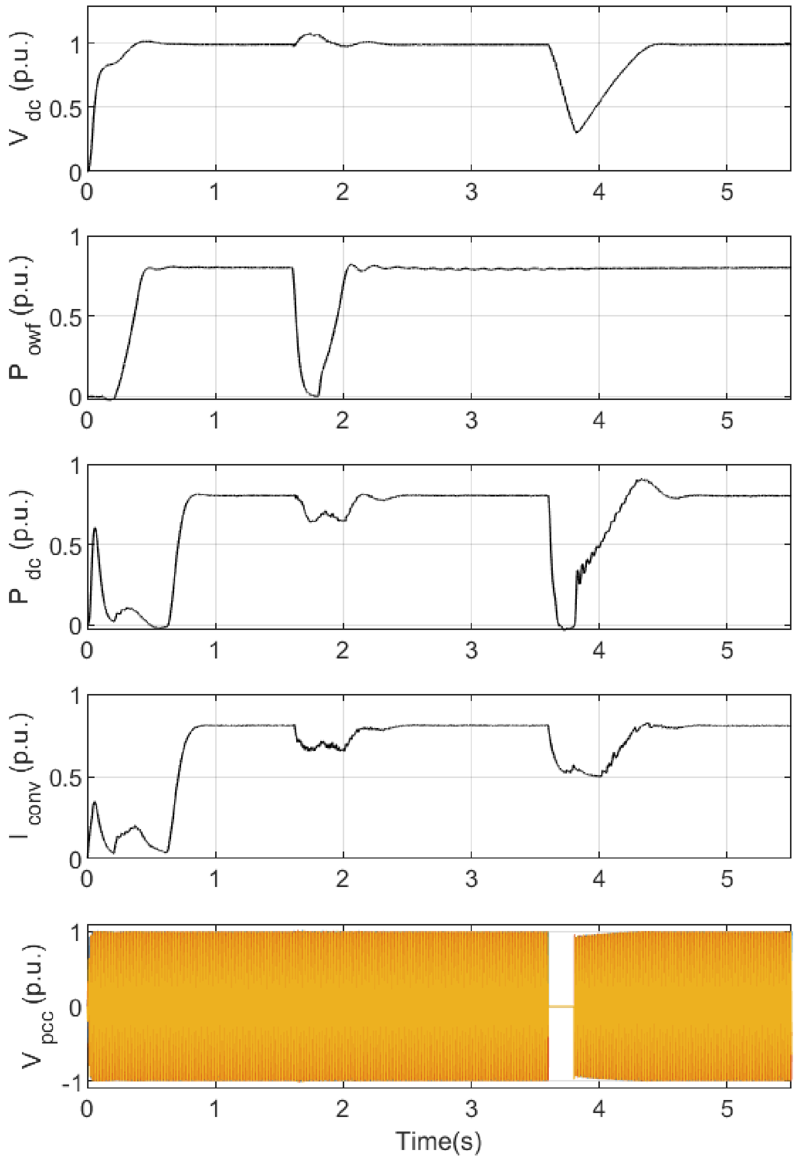

Figure 4.3: LVFRT capability of the MMC-HVDC link during three-phase AC system faults at offshore and onshore grids while transferring active power from the onshore grid to the offshore grid.

These two test scenarios clearly depict the bi-directional power flow capability of the back-to-back MMC's due to the IGBT switches.

4.3 Island mode operation studies

In this section, the island mode operation of the OWF with the MMC-HVDC link is investigated. The islanded system represents a weak grid. The system shown in fig. 4.4 is simulated using PSCAD/EMTDC which represents a typical island system. The island mode operation is demonstrated by tripping the offshore AC grid.

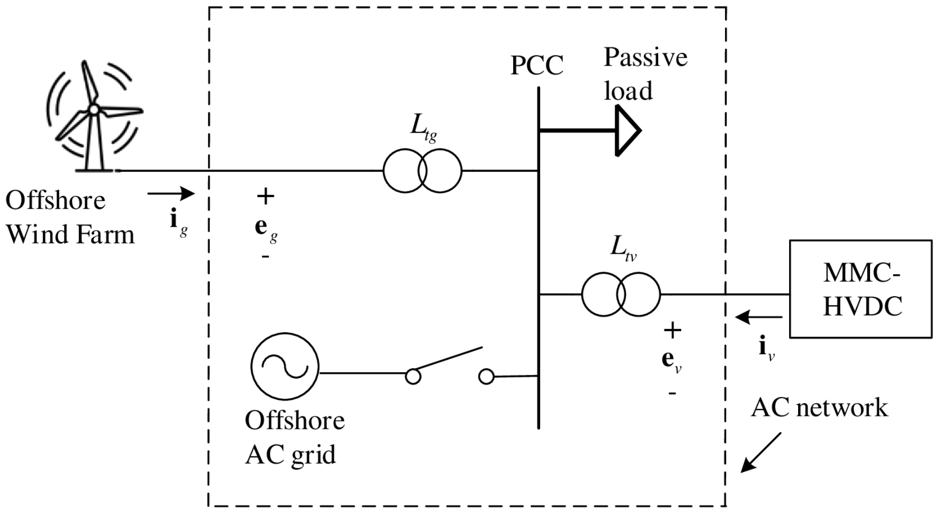

Figure 4.4: A typical island system.

4.3.1 Frequency droop control

During island mode operation, the MMC-HVDC will not have constant power control but it's possible to control the frequency of the system. A frequency controller is proposed with a low-pass filter with a gain as per [26]. A schematic of the same is shown in fig. 4.5

$$\Delta P_{\text{ref}} = \left(\frac{K_f}{1 + T_f s}\right)[\omega_{\text{ref}} - \omega] \tag{4.1}$$

where ω_{ref} and ω are the reference and measured value of the angular frequency respectively. K_f and T_f are the gain and time constant of the frequency controller respectively. ω is measured by taking the derivative of the angle output of the active power controller (PSL) and the output of the frequency controller is added to the power reference of the active power control. The frequency droop of the MMC-HVDC link can be expressed as

$$\Delta\omega = \underbrace{\frac{1}{\frac{1}{K_p} + K_f}}_{R_{\text{vsc}}}(P_{\text{ref}} - P) \tag{4.2}$$

The frequency control gives a frequency droop characteristic and with this feature, the power shared by the MMC-HVDC and the OWF can be determined. If there are any other power generating units in the island system, the load sharing is determined by the frequency droop of each power generating unit which is given by

$$R_{\mathrm{G}} = \frac{\omega_{\mathrm{ref}} - \omega}{\Delta P^{*}_{\mathrm{droop}}} \tag{4.3}$$

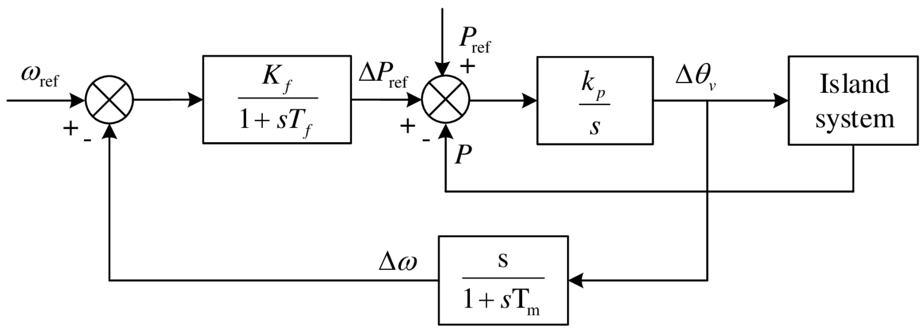

Figure 4.5: Frequency droop controller.

The performance of the MMC-HVDC system is analyzed with a LVFRT condition at the offshore grid in three different scenarios as follows:

4.3.2 Island system exporting active power from OWF to the onshore grid.

This test is to demonstrate the capability of MMC-HVDC during island mode operation while exporting the generated power from the OWF (160 MW) to the onshore AC grid. The MMC-HVDC will provide voltage and frequency support to the offshore grid during island mode operation with GFM-PSC.

From fig. 4.6, the OWF is deblocked and ramped up to 160 MW at the start of the simulation. The MMC's are deblocked at 0.3 s and the generated OWF power is transferred to the onshore grid. The offshore AC system is tripped at 1 s which means that the system is now operating in island mode and the voltage and frequency support is provided by the MMC-HVDC system. At 1.5 s, a three-phase AC fault with a duration of 0.2 s is applied at the offshore grid. The system rides through the fault smoothly. There is an over-current in the converter valve during the fault which is limited by the current limiter. After riding through the fault, the system resumes normal operation. The frequency of the offshore grid is maintained at 50 Hz throughout the entire operation except for slight fluctuation after the fault from 1.7 s to 1.9 s in the range of 49.95 Hz to 50.9 Hz.

4.3.3 Island system feeding the offshore load

This test is to demonstrate the MMC-HVDC's bi-directional power transmission capability during island mode operation. In this test case, the load at the offshore is considered as 160 MW.

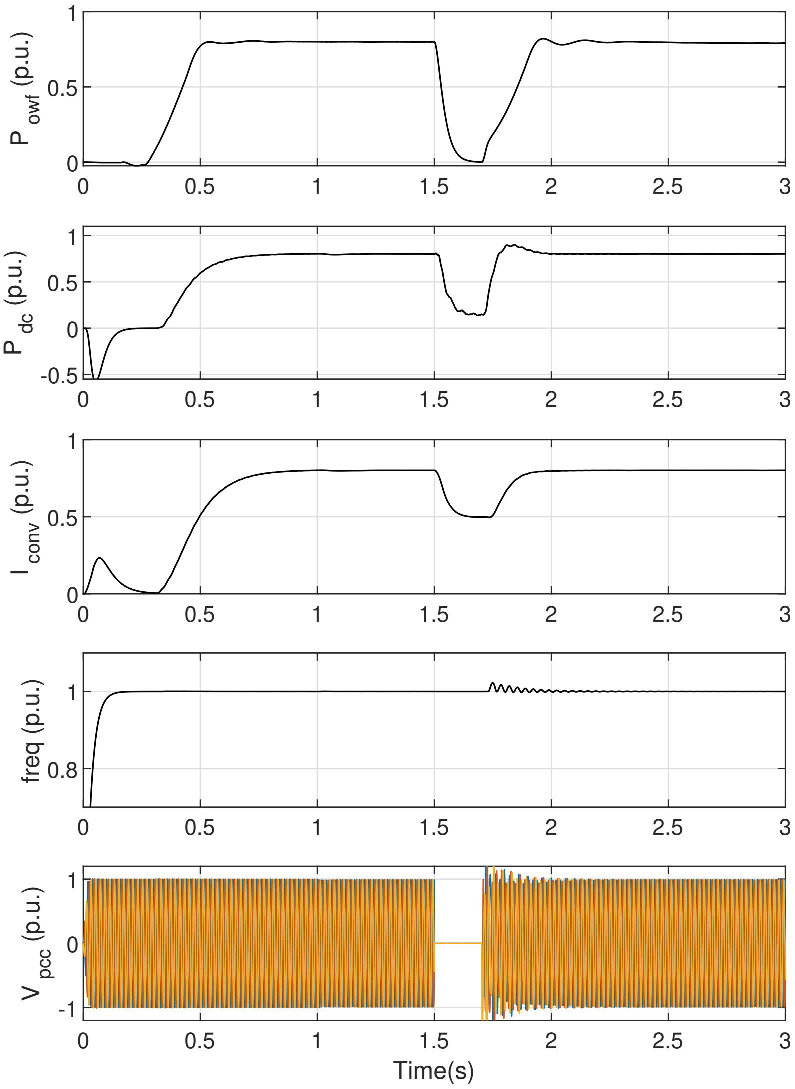

Figure 4.6: LVFRT capability of the MMC-HVDC link during island mode operation.

From fig. 4.7, during normal operation, the OWF will supply 80 MW to the load, 50 MW by MMC-HVDC link with constant power control and the remaining 30 MW is balanced by the offshore grid. After entering into island mode operation at 1 s, the power supply that is lost from the local grid (30 MW) will be powered by the MMC-HVDC with frequency droop control which gets activated by detecting the frequency using a transient frequency measurement device. The frequency of the offshore grid slightly deviates to 49.9 Hz during island mode due to the frequency droop characteristics.

At 1.5 s, a three-phase AC fault with 0.2 s is applied at the offshore grid. There is an over-current in the converter valve during the fault which is limited by the current limiter. Immediately after the fault, the load draws a major portion of the power from the MMC-HVDC link for about 0.2 s until the OWF regains its rated power and this is due to the sudden disconnection and connection of the load during the fault condition. During this transient period, the converter valve current is within its limit. After riding through the fault, the system again resumes normal operation.

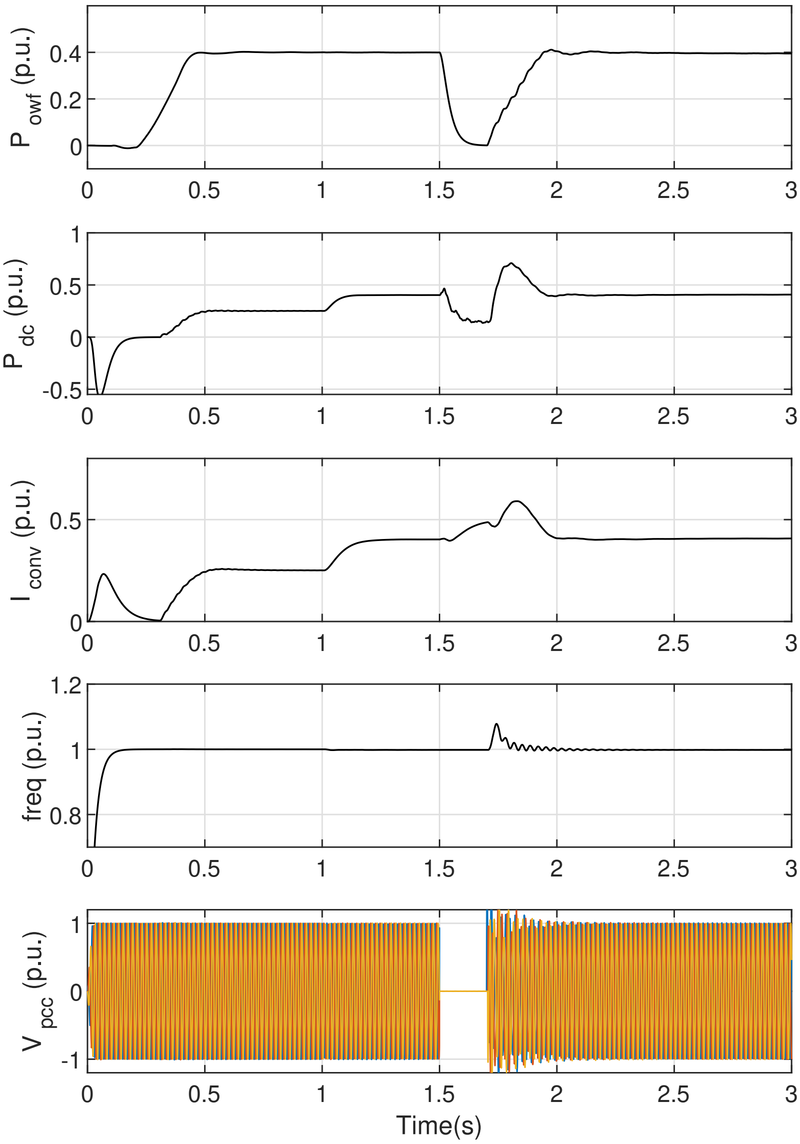

Figure 4.7: LVFRT capability of the MMC-HVDC link during island mode operation, feeding the offshore load.

4.3.4 Passive mode operation

This test is similar to the previous one where the OWF is also tripped along with the offshore AC grid at 1 s, and now it is a passive network with a load.

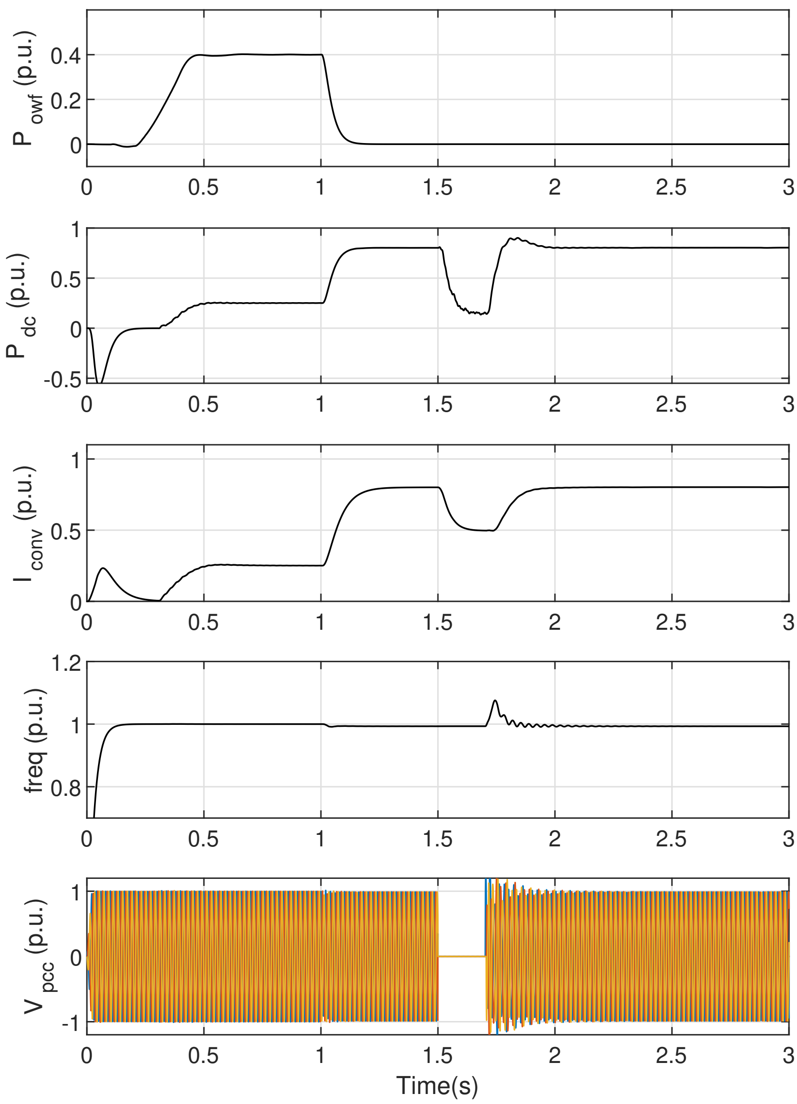

Figure 4.8: LVFRT capability of the MMC-HVDC link during passive mode operation.

From fig. 4.8, the system operation is the same as the previous case except that when both the offshore AC grid and the OWF are tripped at 1 s, the MMC-HVDC link powers the entire load. The frequency of the offshore grid further deviates to 49.7 Hz during passive mode due to the frequency droop characteristics. The power order can be adjusted with the load to keep the frequency constant at 50 Hz. At 1.5 s, a three-phase AC fault with 0.2 s is applied at the offshore grid. There is an over-current in the converter valve during the fault which is limited by the current limiter. The system again resumes normal operation after riding through the fault.

4.4 Summary

The simulation results illustrate the dynamic and versatile performance of the back-to-back MMC-HVDC system during different operating conditions in providing the necessary voltage and frequency support to the grid. This topology provides robust performance during LVFRT scenarios at the offshore and onshore grids, and island mode operations. The bi-directional power flow capability of the IGBT's enables the converter to reverse and transfer the power smoothly in either direction. It is worth noting that when the MMCs are equipped with GFM-PSC, the voltage and frequency are generated by the converters which resemble the behavior of a synchronous machine. With such a control strategy the converter will be able to overcome disturbances originating from the grid. The main highlight of this system is that it provides robust performance while integrating weak grids such as OWFs and that is why it is the preferred solution up to date.

5

Test System 2: DRU-HVDC

In this chapter, the DRU-HVDC system with the interconnection of the Offshore Wind Farm will be modeled and studied. The overall system will be analyzed during LVFRT conditions and island mode operation.

5.1 System description and modeling

The DRU-HVDC system is connected to an OWF as depicted in fig. 5.1. The diode rectifier is the most simple and robust AC-DC converter in high-power applications. A small STATCOM is placed on the offshore grid to provide the system with the required voltage support during island mode operation. Initially, the STATCOM is assumed to be 100 MVA, which is half the rating of the onshore MMC. Later in this thesis, the size of the STATCOM will be reduced as per the requirement during island mode operation. The diode rectifier being a non-linear load distorts the line current thereby introducing harmonics in the range of 12n±1 and hence, filters for the same have been placed to compensate for it.

As the diodes are uncontrollable, the offshore side does not have any controls. The STATCOM does not have an energy storage unit rather has a DC capacitor which is maintained at its nominal value throughout by direct-voltage control. By controlling the direct voltage, the reactive power exchange between the STATCOM and the PCC can be effectively controlled. The onshore MMC controls both the DC link voltage and active power transfer. The MMC and the STATCOM are equipped with GFM-PSC. The technical details of the system are given in appendix B.2.

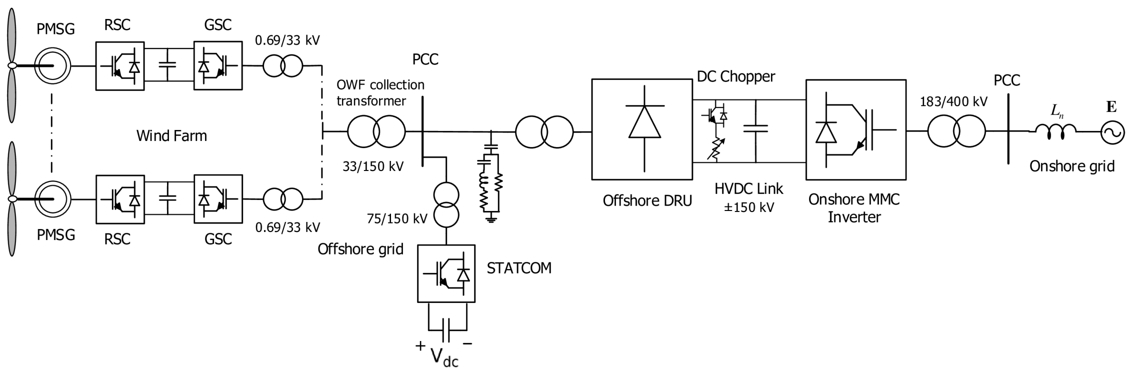

Figure 5.1: DRU-HVDC interconnected to an offshore wind farm.

5.2 Interconnection of Offshore Wind Farm into AC grids

In this section, the interconnection of OWF into the offshore and onshore grids by a DRU-HVDC link is investigated as shown in fig. 5.1. The performance of the DRU-HVDC system is analyzed with a LVFRT condition at both the converter stations. In this test case, STATCOM is not required due to the interconnection of two AC grids. The simulations will be carried out using PSCAD/EMTDC.

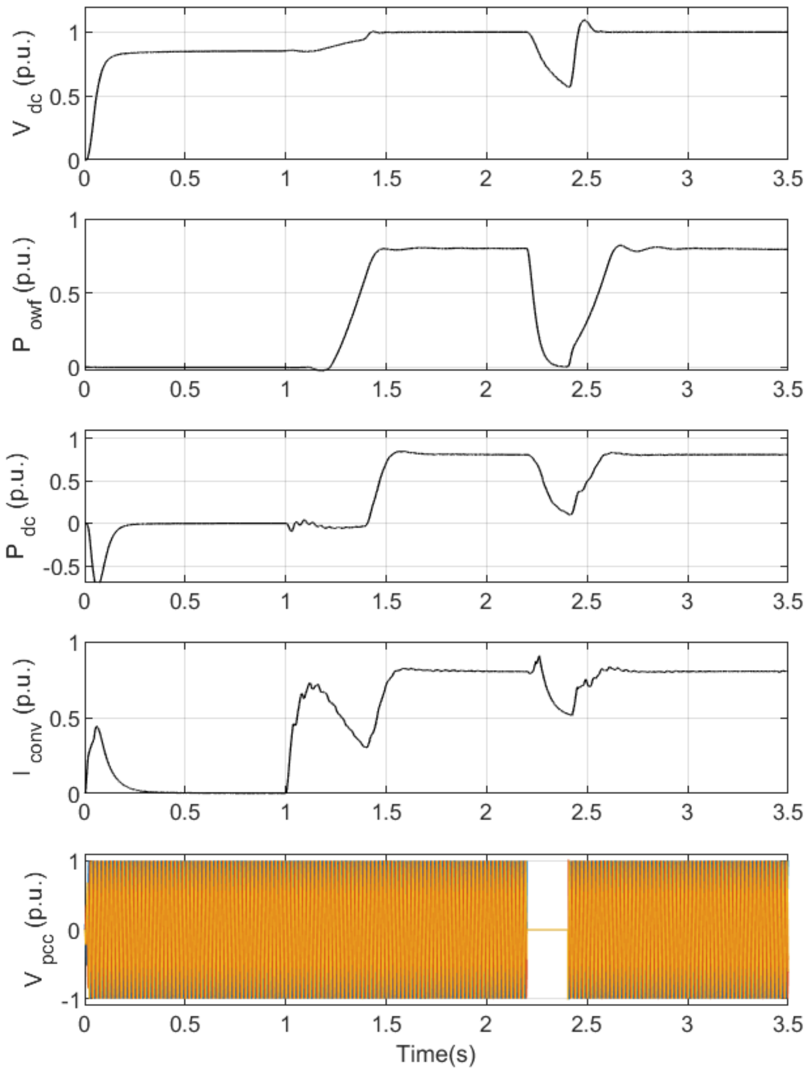

Figure 5.2: LVFRT capability of the DRU-HVDC link during three-phase AC system fault at the offshore grid.

5.2.1 LVFRT Analysis at Offshore grid

In order to transmit the generated power from the OWF to the HVDC link, the input voltage of the DRU should be higher than the HVDC link voltage for the diodes to start conducting. Fig. 5.2 shows graphs from the onshore MMC station (V_{pcc} depicts offshore PCC voltage). From 0-1.5 s, the OWF is ramped up to its rated power (160 MW) and the MMC is deblocked thereby transmitting the generated power to the onshore grid through the HVDC link. At 2.2 s, a three-phase AC fault with 0.2 s is applied at the offshore grid and during this time, the HVDC link voltage dips to 0.6 p.u. due to the sudden loss of power. The fault current at the converter valve is reduced by the current limiter. Once the fault is cleared, the system resumes its normal operation.

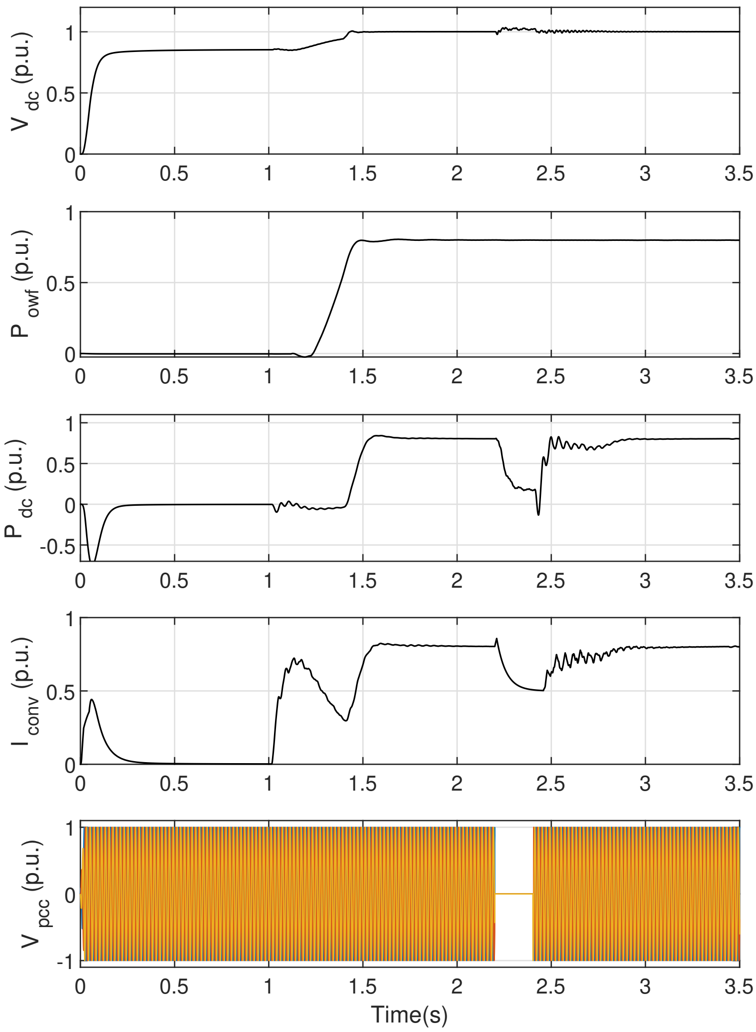

Figure 5.3: LVFRT capability of the DRU-HVDC link during three-phase AC system fault at the onshore grid.

5.2.2 LVFRT Analysis at Onshore grid

Fig. 5.3 shows graphs from the onshore MMC station. The system operates as explained in the previous case but here the fault ride-through performance is analyzed at the onshore side. During the fault, the HVDC link voltage slightly increases to 1.07 p.u. as the current from the OWF is not affected during the fault which keeps pumping power into the HVDC link. The chopper gets activated when the HVDC link voltage reaches 1.05 p.u. and prevents it from further over-charging by dissipating the excess power through the chopper resistors. The power is evacuated after the fault is cleared and the system regains its normal operation again. The current limiter limits the converter valve current during the fault.

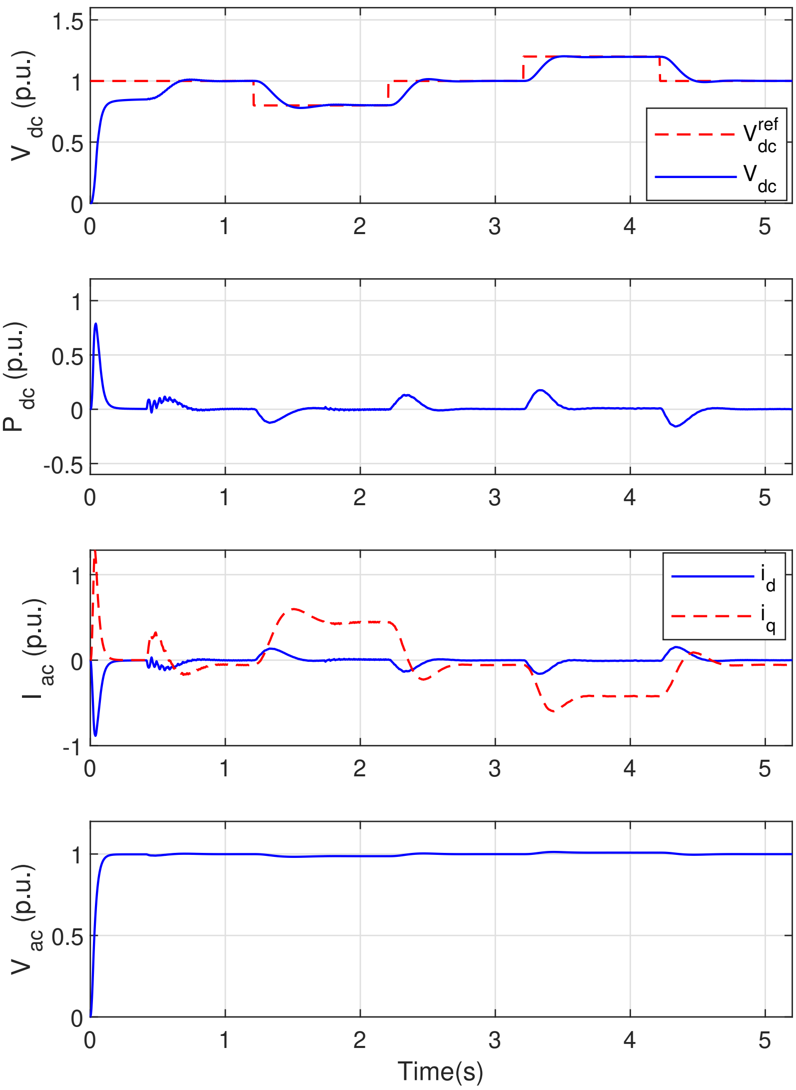

Figure 5.4: DC link control of STATCOM.

5.3 Step test for DC link voltage control of STATCOM

The performance of the DC link voltage control is verified by giving step changes. In fig. 5.4, DC link voltage is varied in steps of ±0.2 p.u. to verify whether the controller follows the reference. Initially, the system is energized and the STATCOM is deblocked. The reference steps are manually given from 0.4 s. As there is no energy storage (e.g. battery) integrated with the STATCOM, the STATCOM cannot supply active power to the grid. It can only inject reactive power to provide the necessary voltage support to the grid. When the grid's PCC voltage is less than the terminal voltage of the STATCOM, the STATCOM injects reactive power.

5.4 Island mode operation studies

In this section, the island mode operation of the OWF with the DRU-HVDC link is analyzed. The system shown in fig. 5.5 is simulated using PSCAD/EMTDC which represents a typical island system. The island mode operation is demonstrated by tripping the offshore AC grid. Unlike the back-to-back MMC-HVDC system where the MMC can provide the voltage support during island mode operation with the GFM-PSC feature, here it is necessary to equip the system with a STATCOM to provide the required voltage support at the offshore grid. The performance of the DRU-HVDC system is analyzed with a LVFRT condition at the offshore grid in two scenarios as follows:

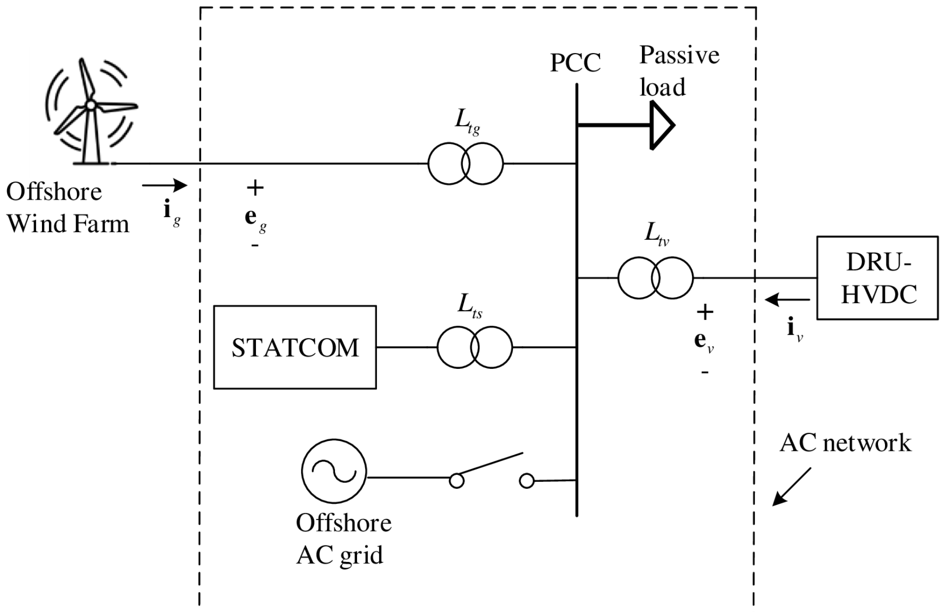

Figure 5.5: A typical island system.

5.4.1 Island system exporting active power from OWF to the onshore grid

Fig. 5.6 shows graphs from the onshore MMC station (V_{pcc} depicts offshore PCC voltage). During normal operation, the generated power from the OWF is transferred to the onshore grid via the DRU-HVDC link. The offshore AC grid is tripped at 1.9 s and hence the system enters island mode operation. The STATCOM provides the necessary voltage support by injecting reactive power (13.8 MVAr) to the grid (negative sign indicates that the STATCOM is supplying reactive power to the grid) and the power transmission is still smoothly generated and transmitted without any interruption as shown in fig. 5.7. This depicts the dynamic nature of the STATCOM in stabilizing the grid.

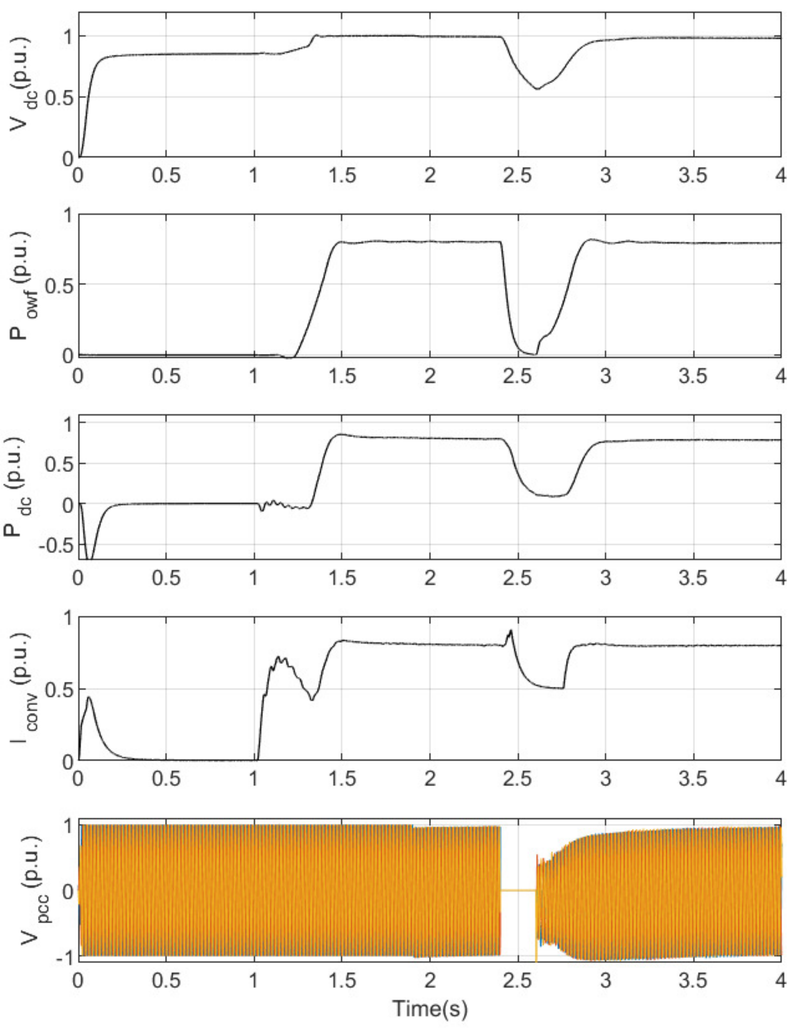

Figure 5.6: LVFRT (offshore) capability of the DRU-HVDC link during island mode operation.

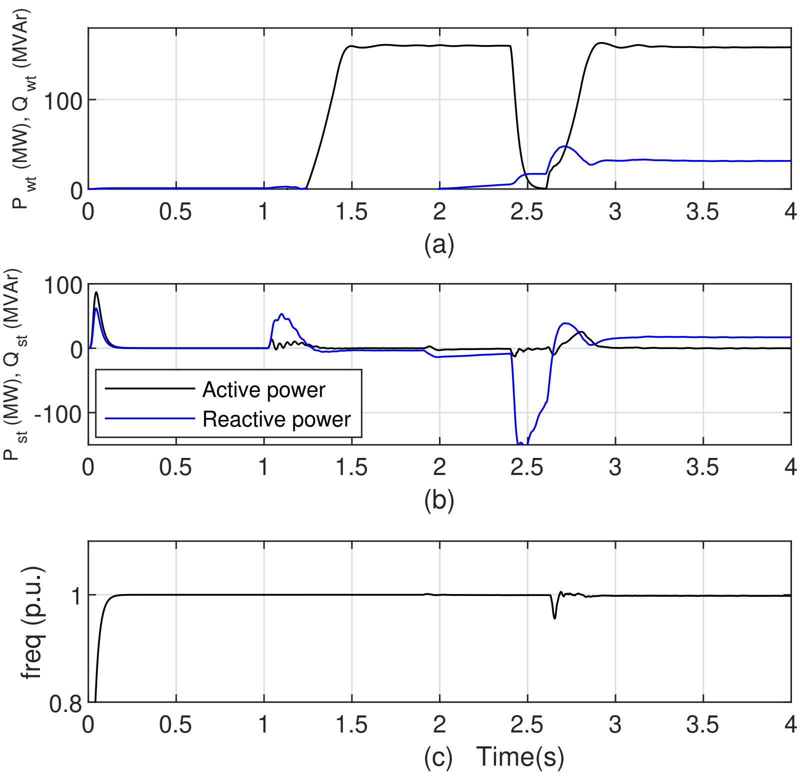

Figure 5.7: (a) Active and reactive power from OWF. (b) Active and reactive power from STATCOM. (c) Frequency of the offshore grid.

At 2.4 s, a three-phase AC fault with 0.2 s duration is applied at the offshore grid. The OWF is tripped during this scenario and the HVDC link voltage drops to 0.56 p.u. due to the sudden loss of power. After detecting the voltage dip, the OWF supplies 31.6 MVAr to support the grid voltage. The excess reactive power (17 MVAr) is absorbed by the STATCOM. The current limiter limits the fault current of the MMC and STATCOM during the fault. The frequency of the offshore grid is maintained at 49.98 Hz during island mode operation except for a slight dip to 48 Hz immediately after the fault for 52 ms.

LVFRT Analysis at Onshore grid

The system operation is the same as the previous case. Fig. 5.8 shows graphs from the onshore MMC station. During an onshore fault, the DRU is still conducting as the offshore side is not affected. Due to this, huge OWF power is fed to the HVDC link (current flows in the lowest impedance path) which charges it continuously (power cannot be evacuated to onshore during an onshore fault as the voltage at the PCC is zero) and will not retain to its normal operation. The solution is to stop the conduction of DRU during fault by reducing the power generation of OWF to 0 [57]. During FRT, instead of having an over-voltage issue, the OWF starts to decelerate at 2.4 s and during this time the HVDC link voltage drops to 0.83 p.u. After the fault is cleared (at 2.6 s), the OWF ramps up to the rated power (160 MW) and

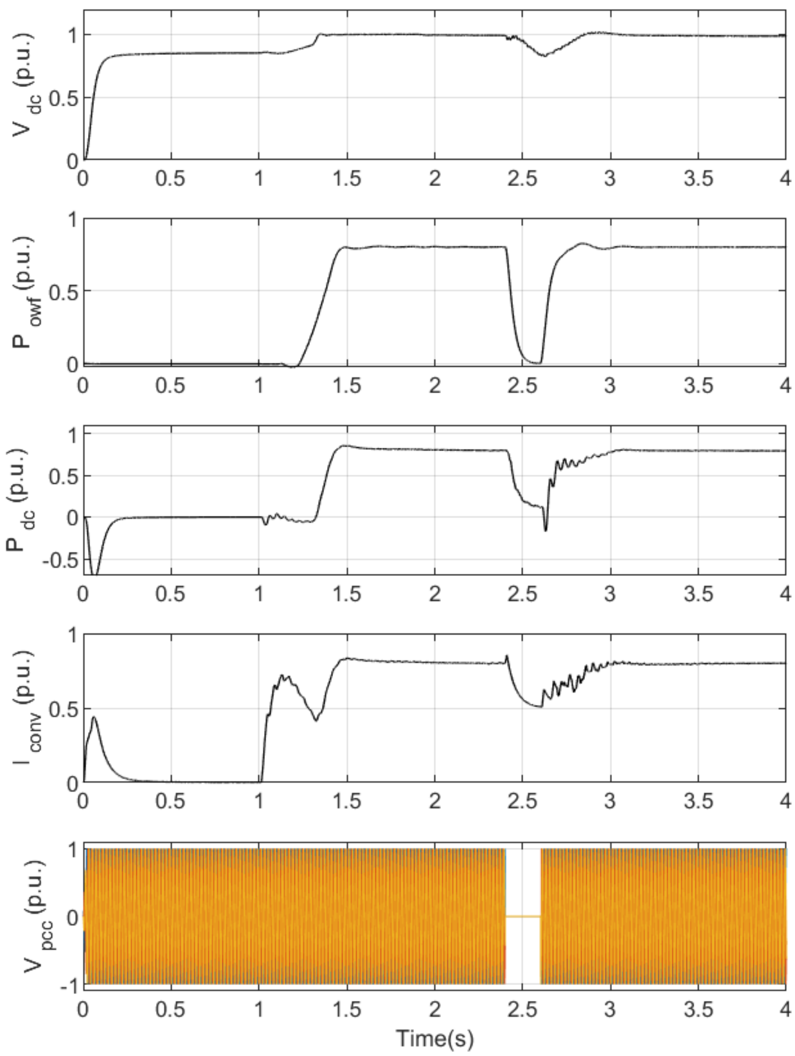

Figure 5.8: LVFRT (onshore) capability of the DRU-HVDC link during island mode operation.

the power is delivered to the onshore smoothly. The STATCOM provides voltage support throughout the operation as shown in fig. 5.9. It is better to have an under-voltage/current rather than over-voltage/current as it would induce more damage to the power system. The fault current of the MMC is reduced by the current limiter. As the fault is on the onshore side, there is no over-current issue in the STATCOM. The frequency of the offshore grid is maintained at 49.98 Hz during island mode operation except for a slight dip to 49.55 Hz during the fault for 9 ms.

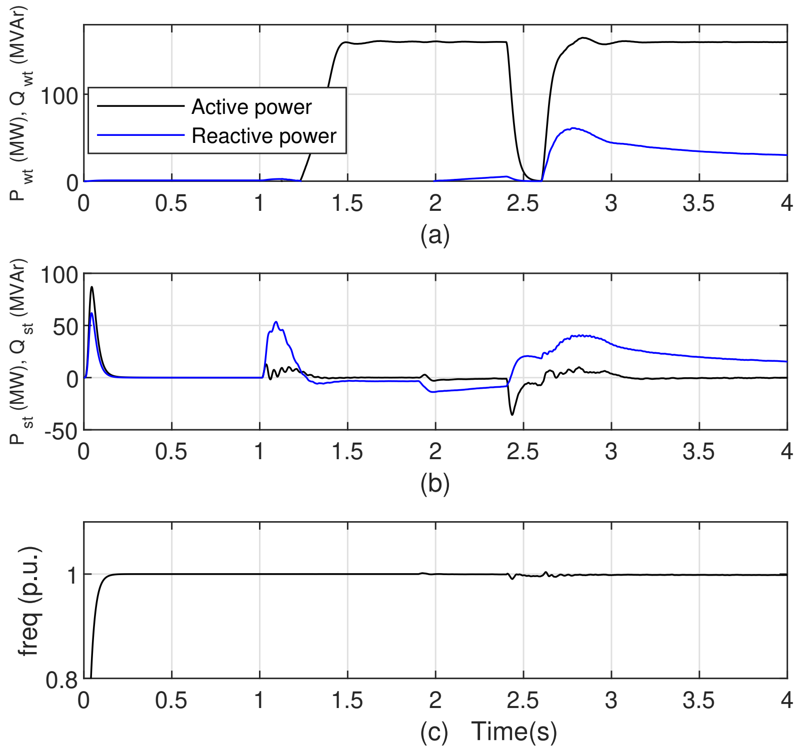

Figure 5.9: (a) Active and reactive power from OWF. (b) Active and reactive power from STATCOM. (c) Frequency of the offshore grid.

5.4.2 Island mode operation feeding the offshore load

In this analysis, the island system with a load of power factor (pf) 0.95 is connected to the offshore grid. The result from this test will also be used to determine the rating of the STATCOM in the next section. In this case, the locally connected load at the offshore side must not exceed the output power of the OWF system due to the uni-directional power flow of the diodes. Unlike the back-to-back MMC-HVDC system where the power flow is bi-directional, here as the DRU system comprises diodes, it is not possible to utilize the HVDC link to transfer additional power to feed the loads connected on the offshore. This is the biggest setback of this topology. A high voltage circuit breaker is used to disconnect the DRU when the power is not transferred to the Onshore.

From fig. 5.10, the OWF is ramped up to its rated power (160 MW) and the power is transferred to the offshore load. At 0.7 s, the system enters into island mode and the STATCOM provides the voltage support by injecting 70 MVAr to the PCC. Compared to the previous case, the reactive power demand is more here due to the additional reactive power requirement by the load. The frequency of the offshore grid is maintained at 50 Hz during island mode operation except for a slight dip to 48.3 Hz after the fault for 56 ms.

Passive mode operation is not possible with this topology due to the uni-directional power flow of the diodes.

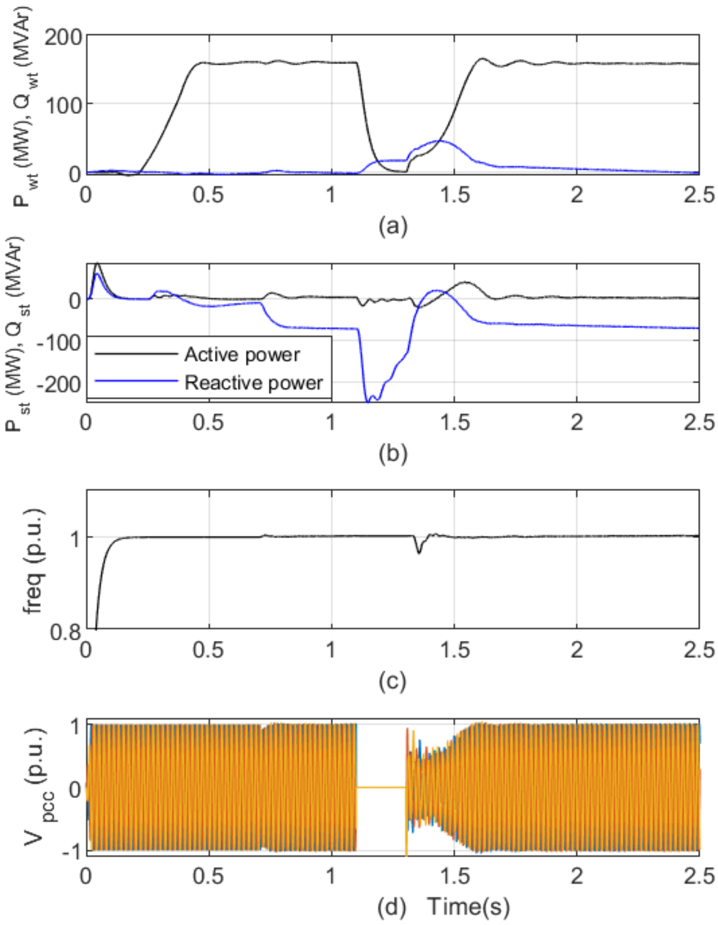

Figure 5.10: (a) Active and reactive power from OWF. (b) Active and reactive power from STATCOM. (c) Frequency of the offshore grid. (d) PCC voltage of the offshore grid.

5.5 STATCOM sizing

The size of the STATCOM also plays a crucial role in determining the overall cost of the system. The size of the STATCOM depends upon the amount of reactive power required during island mode and locally connected load to maintain the offshore PCC voltage at the nominal value. As the requirement of the reactive power increases, the size of the STATCOM also increases. It's also recommended to design the STATCOM with an additional 10% of the required STATCOM rating so that the device operates smoothly without stress throughout the operation. Considering these aspects and from tests 5.4, table 5.1 depicts the required size of the STATCOM.

Typically in large OWF projects, the generated offshore wind power is exported completely to the onshore AC grid and then utilized/distributed from there to feed various loads. In that case, when compared to test system 1 (back-to-back MMC-HVDC), the required STATCOM rating is approximately 19 MVAr. Compar-

No.	Island mode operation condition	Required STATCOM size
1.	160 MW active power transfer to Onshore grid	17/0.9 = 18.89 MVAr
2.	With offshore load S=160 MVA, pf=0.95	70/0.9 = 77.77 MVAr
3.	With offshore load S=160 MVA, pf=0.90	93.5/0.9 = 103.88 MVAr

Table 5.1: STATCOM sizing

ing the size of the STATCOM with the MMC of test system 1, MMC : STATCOM = 200/18.89 = 10.58 times lesser size.

5.6 Summary

The simulation results from the previous sections reveal the dynamic behavior of the STATCOM when utilized with GFM-PSC. The STATCOM instantly injects reactive power to the offshore grid when the PCC voltage is less than the terminal voltage of the STATCOM thereby providing the best possible voltage support. With the support of the STATCOM, the overall performance of the DRU-HVDC system can match the performance of the back-to-back MMC-HVDC system. This topology makes it attractive by reducing the cost of the system and also by eliminating complex controls at the offshore station. The only drawback of this system is that power reversal is not possible due to the uni-directional property of the diodes. On the other side it is also worth noting that in large-scale offshore wind projects, the main goal would be to export the entire generated power from the OWF to the onshore AC grid and then distribute it to various loads. Hence, in such scenarios, it is not mandatory to have a bi-directional power flow feature. As the DRU draws line current harmonics in the frequency range 12n±1, filters are required to compensate for the same. The STATCOM could be eliminated if the wind turbine is equipped with a GFM feature that can form and control the voltage and frequency of the offshore grid. This will be later investigated in this thesis.

6

Test System 3: STATCOM-HVAC

In this chapter, the STATCOM-HVAC system with the interconnection of the Offshore Wind Farm will be modeled and studied. The overall system will be analyzed during LVFRT conditions and island mode operation.

6.1 System description and modeling

The STATCOM-HVAC system is connected to an OWF as depicted in fig. 6.1. This topology is a complete AC solution in contrast to the previous test systems. The wind turbines are equipped with GFM-PSC strategy so that they can form and control the offshore voltage and frequency. The RSC uses the traditional GFL-VCC with decoupled currents where i_d controls the DC link voltage and i_q controls the AC voltage at the machine side. The GSC works with GFM-PSC.

Problems with long-distance HVAC cable: High capacitance, charging current increases and Ferranti effect due to high reactive power flow in AC cables. Due to these reasons, it is indispensable to have a RPC device at the mid-point of the HVAC transmission system. STATCOMs are selected as the RPC device due to their very fast and dynamic behavior which are capable to overcome a variety of problems as discussed in section 2.3. The technical details of the system are given in appendix B.3.

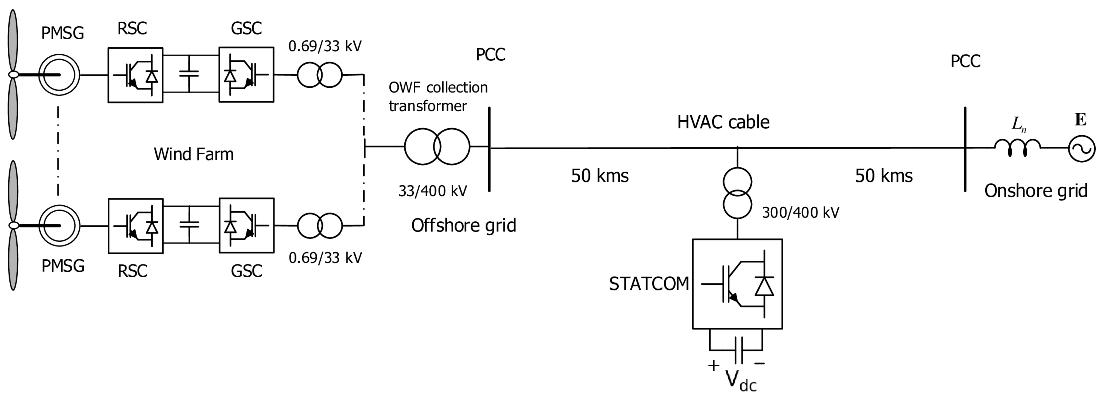

Figure 6.1: STATCOM-HVAC link interconnected to an offshore wind farm.

6.2 Island mode operation and LVFRT studies without STATCOM

In this section, the interconnection of OWF into the onshore AC grid by an HVAC link is investigated as shown in fig. 6.2. Initially, this system is simulated to see how much distance can the power be transferred without the STATCOM? The performance of the system is analyzed with a LVFRT condition at the offshore grid. The simulations will be carried out using PSCAD/EMTDC.

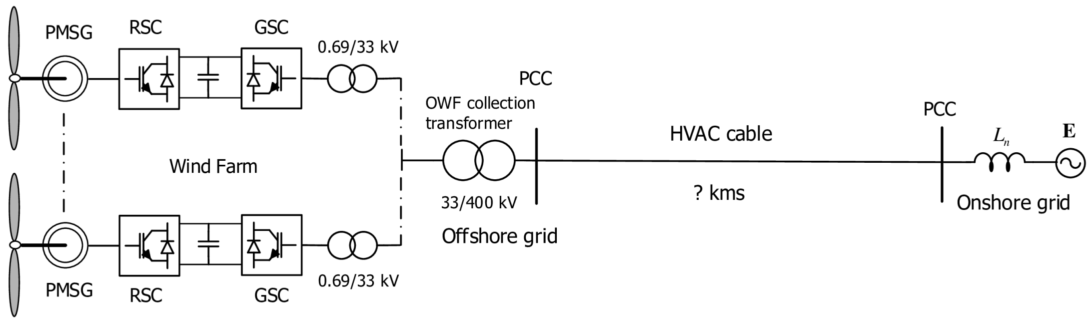

Figure 6.2: HVAC link interconnected to an offshore wind farm.

From fig. 6.3, the OWF starts in island mode and the power is ramped to its rated value (160 MW) and the power is exported to the onshore grid. At 2 s, a three-phase AC fault with a duration of 0.2 s is applied at the offshore grid. The system demonstrates LVFRT capability and smooth grid operation after the fault is cleared. The frequency of the offshore grid is maintained at 50 Hz throughout the operation except for a dip to 45.25 Hz after the fault for 0.13 s. A chopper is used in the WTG to protect the DC link from over-voltage (1.1 p.u. max) as shown in fig. 6.4. The three-phase AC voltages produced by the GSC of the WTG is also shown in fig. 6.4.

6.3 STATCOM sizing

The transmission distance (or cable length) determines the amount of RPC required by the STATCOM. As transmission distance increases, the Ferranti effect increases and hence losses increase. The over-voltage at the receiving end (load side) can damage the equipment such as transformers and wind turbine converters. A number of simulations were carried out with different cable lengths to estimate the rating of the STATCOM as shown in table 6.1.

Typically, in large-scale OWF projects, the distance from onshore would be around 100 km so this distance is chosen and the corresponding RPC for the same is 1055 MVAr. A STATCOM with a rating of 1200 MVAr (with 10% extra) will be used for analyzing the system in the next section.

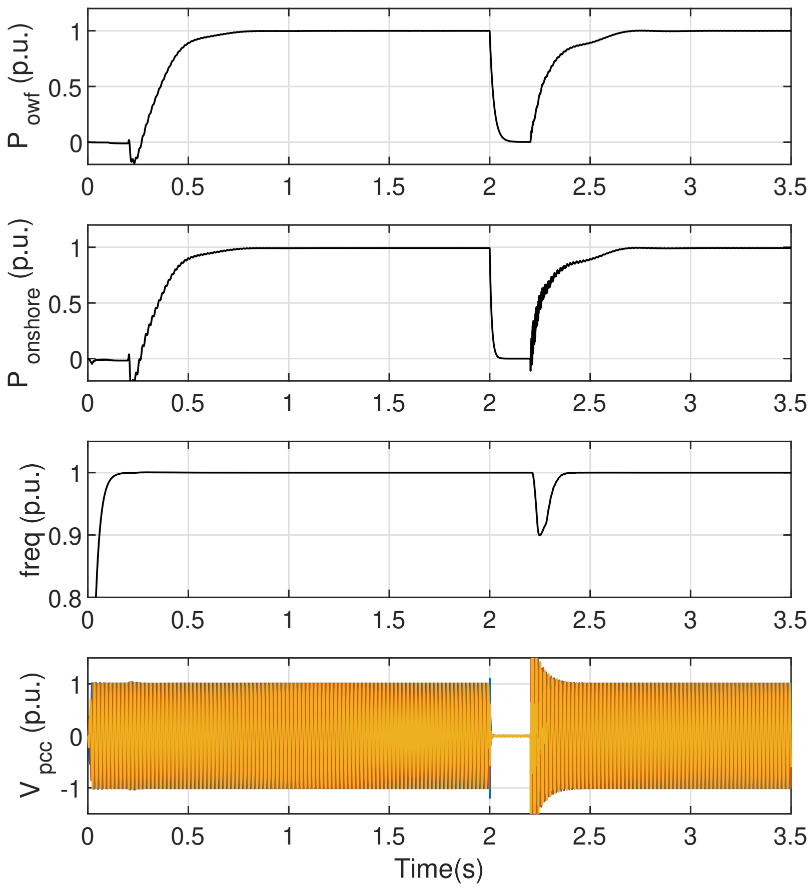

Figure 6.3: LVFRT capability of the HVAC link during island mode operation.

No.	Cable length (km)	Reactive Power generation (MVAr)	Sending end voltage (kV)	Receiving end voltage (kV)	Power loss (MW)
1.	10	78	400	404	1.5
2.	20	160	400	408	2
3.	50	429	400	424	5
4.	**100**	**1055**	**400**	**462**	**10**
5.	150	1900	400	515	20

Table 6.1: STATCOM sizing

6.4 Island mode operation and LVFRT studies with a STATCOM

In continuation from the previous section, a STATCOM is added at the mid-point of the HVAC transmission line for RPC as shown in fig. 6.1. The STATCOM is equipped with GFM-PSC and does not have an energy storage unit rather has a

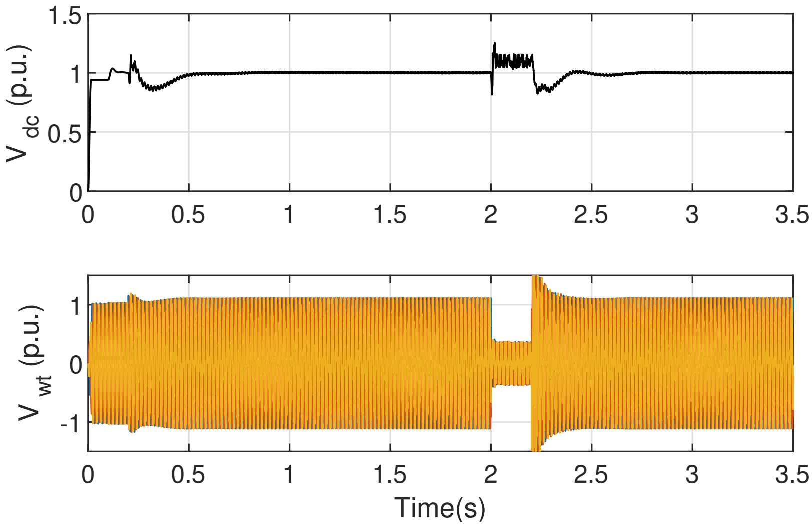

Figure 6.4: Upper plot: DC-link voltage of the WTG. Lower plot: Three-phase AC voltages of the WTG.

DC capacitor which is maintained at its nominal value throughout by direct-voltage control. By controlling the direct voltage, the reactive power exchange between the STATCOM and the PCC can be effectively controlled. The performance of the STATCOM-HVAC system is analyzed with an LVFRT condition at the offshore grid.

From fig. 6.5, the system operates in the same way as discussed in the previous case. When the grid's PCC voltage is higher than the terminal voltage of the STATCOM, the STATCOM absorbs the excess reactive power (produced by the HVAC cables) from the grid to maintain the PCC at 400 kV. The system demonstrates FRT capability and smooth grid operation after the fault is cleared due to the dynamic performance of the STATCOM and grid-forming feature of the wind turbines. The STATCOM absorbs 870 MVAr from the PCC as shown in fig. 6.6. The OWF generates 9 MVAr throughout the operation. During the fault, the reactive power increases. The frequency of the offshore grid is maintained at 50 Hz throughout the entire operation except for a short spike to 50.7 Hz after the fault for 0.15 s.

If this big STATCOM (1200 MVAr) has to be placed in the middle of the sea, a substation should be built which incurs a higher cost to the system. So, rather than placing one big STATCOM at the center of the sea, two STATCOMs with ratings split have been proposed to be placed on offshore and onshore platforms. In this way, the reactive power compensation will also be more effective.

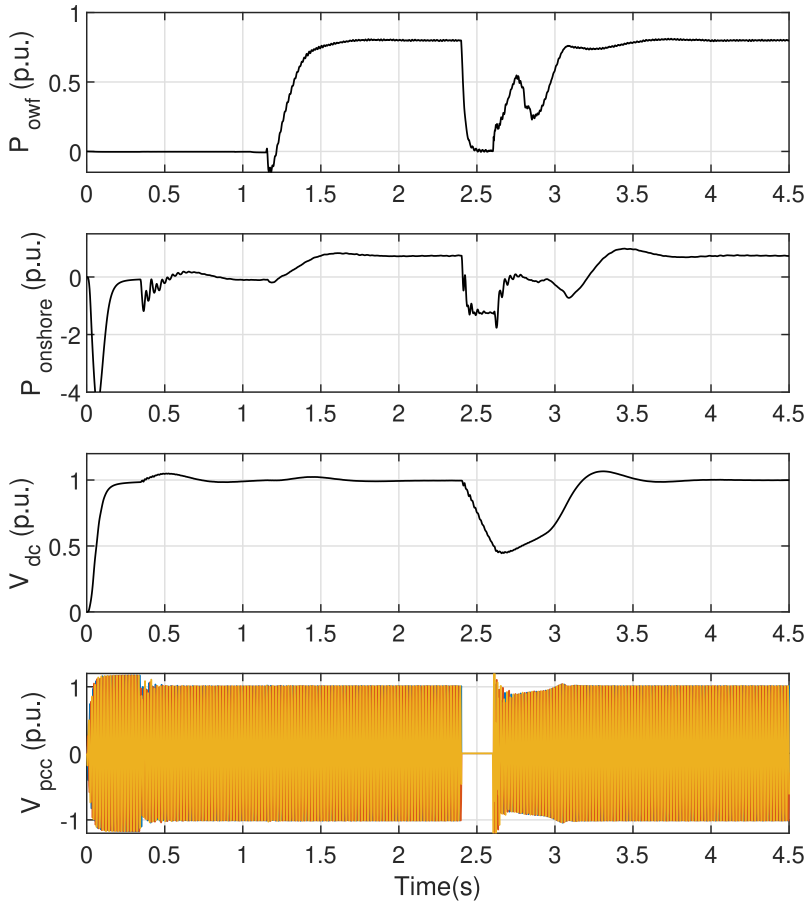

Figure 6.5: LVFRT capability of the STATCOM-HVAC link during island mode operation.

6.5 Island mode operation and LVFRT studies with two STATCOMs

Further to the discussion from the previous case, two STATCOMs each rated 600 MVAr are placed on the offshore and onshore platforms as shown in fig. 6.7. The technical details of the system are given in appendix B.4.

From fig. 6.8 and 6.9, the STATCOM's together absorb 912 MVAr from the PCC (STATCOM1= 490 MVAr, STATCOM2= 422 MVAr) to maintain the offshore and onshore PCC voltage as 400 kV. In the previous case, with one STATCOM placed at the mid-point of the system, the STATCOM absorbs 870 MVAr from the PCC to maintain 400 kV but there was slightly higher voltage at the offshore and onshore PCC (402 kV) and this is again due to the reactive charging current of the HVAC cables. But when two STATCOMs are placed, the inverse effect could be observed where the offshore and onshore PCC voltage is maintained to 400 kV and the mid-point PCC voltage was 402 kV. The STATCOMs are better utilized

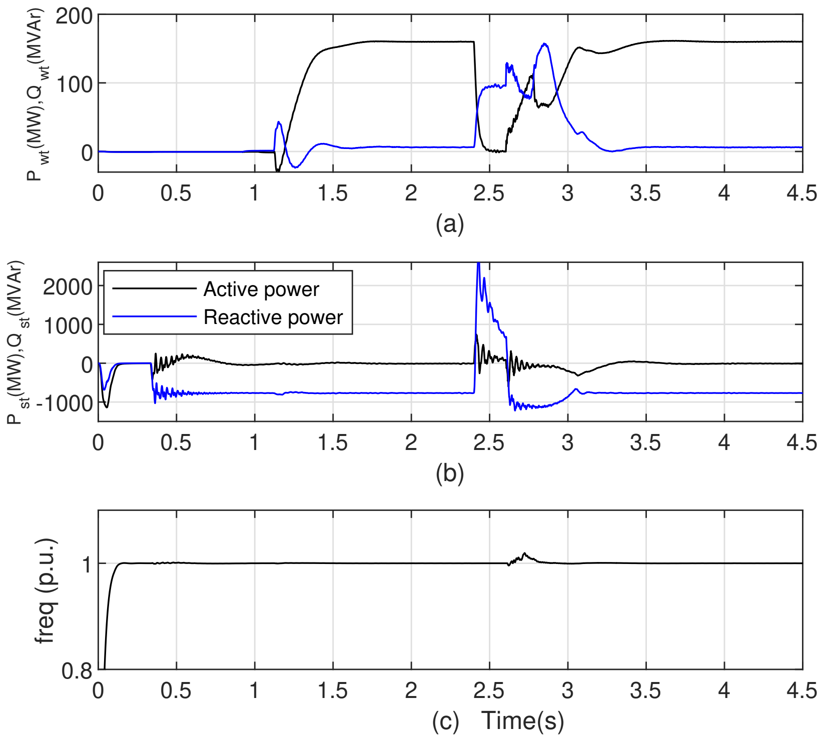

Figure 6.6: (a) Active and reactive power from OWF. (b) Active and reactive power from STATCOM. (c) Frequency of the offshore grid.

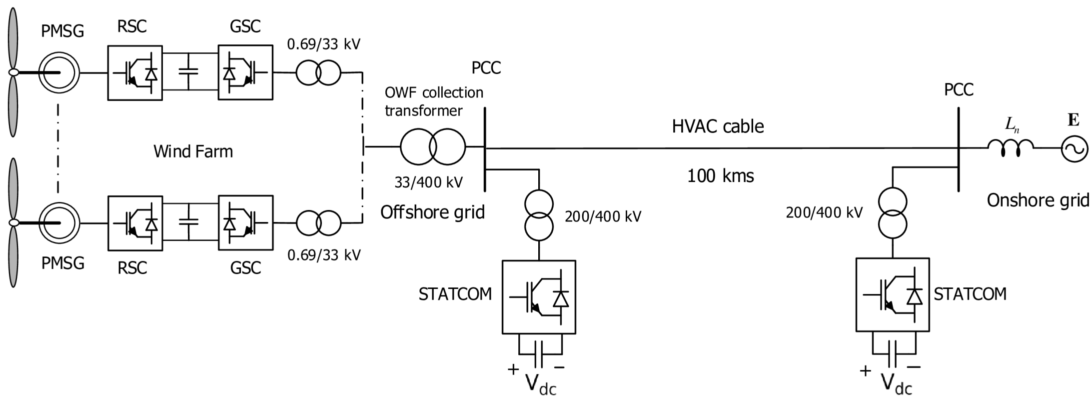

Figure 6.7: Two-STATCOM-HVAC link interconnected to an offshore wind farm.

with this topology. OWF generates 16 MVAr throughout the operation. During the fault, the reactive power increases. The frequency of the offshore grid is maintained at 50 Hz throughout the entire operation except for a short spike to 51.6 Hz after the fault for 0.12 s.This topology is good in terms of performance but the issue with the HVAC cables is still a big problem that makes it not feasible for long-distance power transmission. Of course, the STATCOM size is huge and hence the cost.

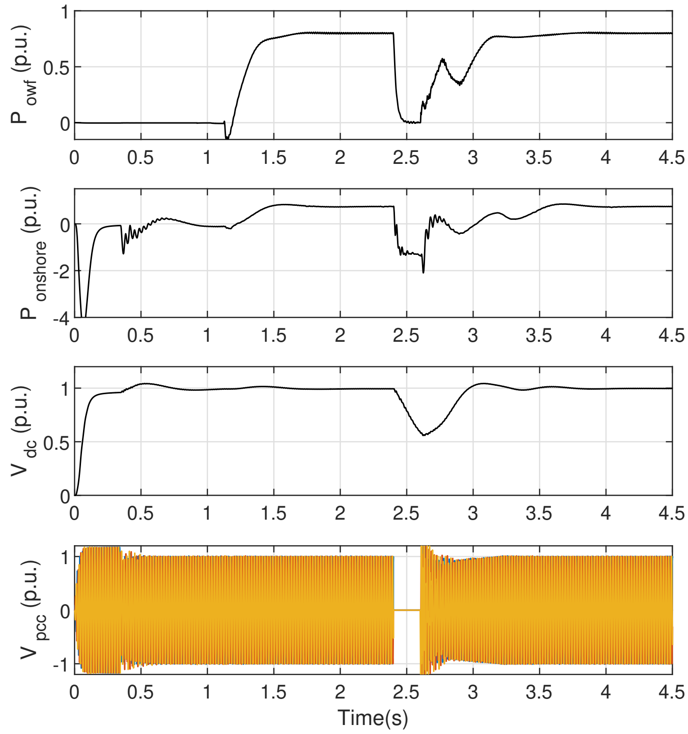

Figure 6.8: LVFRT capability of the Two-STATCOM-HVAC link during island mode operation.

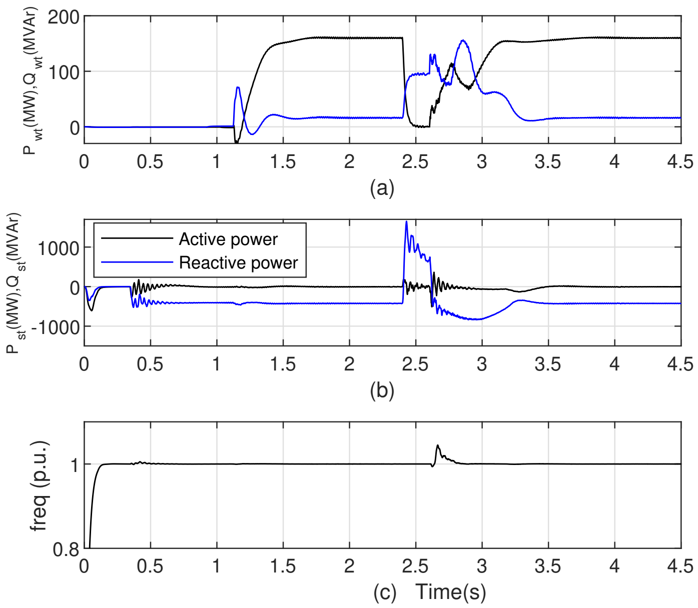

Figure 6.9: (a) Active and reactive power from OWF. (b) Active and reactive power from STATCOM. (c) Frequency of the offshore grid.

6.6 Summary

The STATCOM-HVAC system is not a good choice for interconnecting OWFs mainly because of the reactive charging current of the HVAC cables due to high capacitance. From the simulation results of the previous section, it is evident that GFM control cannot solve this problem. Apart from this major drawback, the system shows good performance when the STATCOMs and the WTs are utilized with GFM-PSC. The sizes of the STATCOM should be big enough to absorb the bulk reactive power from the grid. This increases the overall cost of the system tremendously, in fact, the cost would be more than the back-to-back MMC-HVDC system.

7

Results with OWF GFM-PSC of Test system 1 and 2

In this chapter, test system 1 and 2 is analyzed by replacing the GFL-VCC of the wind turbines with GFM-PSC as modeled in test system 3. The overall system will be analyzed during LVFRT conditions and island mode operation.

7.1 Test system 1 with OWF GFM-PSC

The control strategy of the wind turbines (WTs) with GFL-VCC is replaced with GFM-PSC and interconnected to the back-to-back MMC-HVDC system as shown in fig. 7.1. The performance of the system is investigated with an LVFRT condition during island mode operation at the offshore grid. This test is to demonstrate the capability of the offshore WTs to provide the required voltage and frequency support to the offshore grid during island mode operation with GFM-PSC while exporting the generated power from the OWF (160 MW) to the onshore AC grid. The simulations will be carried out using PSCAD/EMTDC.

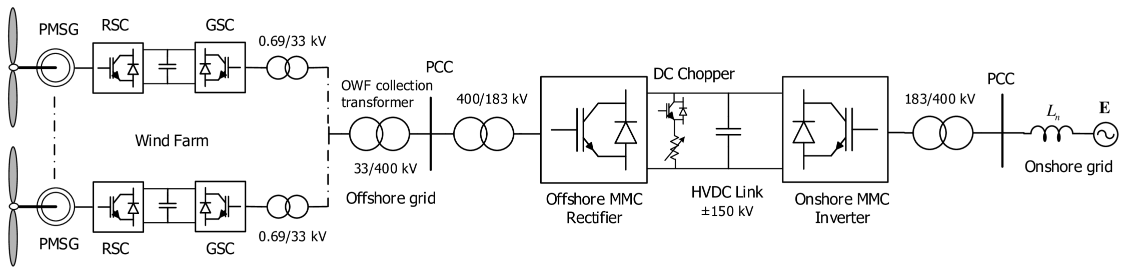

Figure 7.1: Back-to-Back MMC-HVDC interconnected to an offshore wind farm.

From fig. 7.2, the OWF starts in island mode and exports 160 MW to the onshore grid. The OWF supplies 14.4 MVAr throughout the operation for supporting the offshore grid voltage. At 1.5 s, a three-phase AC fault with a duration of 0.2 s is applied at the offshore grid. The system rides through the fault smoothly and resumes normal operation. The over-current in the converter valve during the fault is limited by the current limiter. The frequency of the offshore grid is maintained at 50 Hz throughout the entire operation except for slight fluctuation during the fault recovery. The DC-link voltage and three-phase AC voltages of the WTG are shown in fig. 7.3.

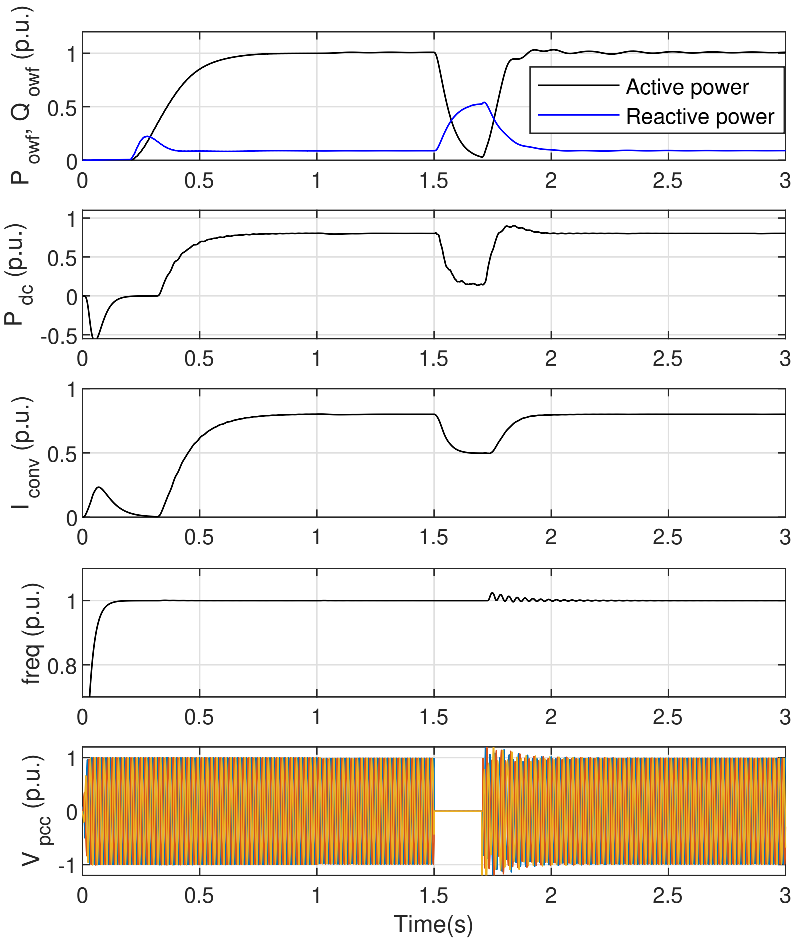

Figure 7.2: LVFRT capability of the MMC-HVDC link during island mode operation.

With the traditional VCC of the WTs in type 4 back-to-back converters, the front-end converter (GSC) relies on the offshore voltage and frequency and hence the offshore wind system's (OWS's) power output will be affected if the voltage and frequency are not maintained leading to overall system instability. During island mode operation, the MMC-HVDC system will provide the necessary voltage and frequency support so that the OWS remains connected with the offshore AC grid throughout.

If grid-forming control is equipped in the WT converters, then the WTs do not have to rely on an external voltage source to keep them connected with the AC grid during severe faults or outages as the WT's can produce their own sinusoidal voltage for a given reference. Likewise, the frequency of the offshore grid can also be controlled using the frequency droop controller discussed in section 4.3.1. With such a control strategy implemented in the WTs, the system can have an added advantage while black-starting the system.

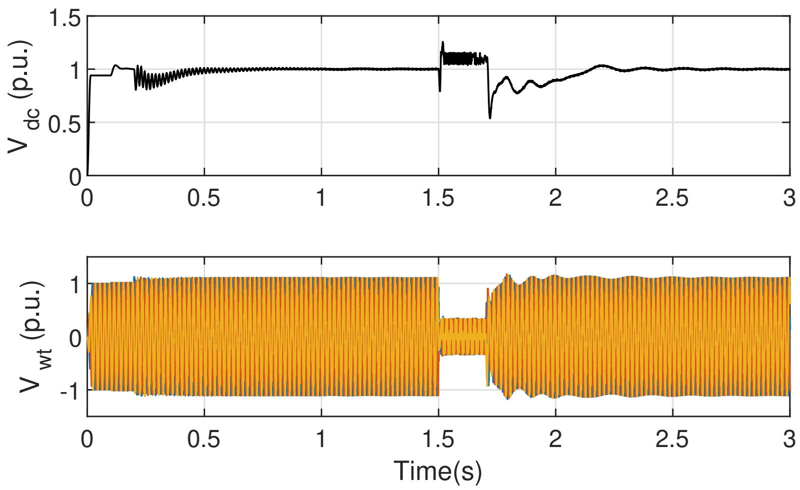

Figure 7.3: Upper plot: DC-link voltage of the WTG. Lower plot: Three-phase AC voltages of the WTG.

7.2 Test system 2 with OWF GFM-PSC

In continuation with the previous section, in this section, the offshore WTs equipped with GFM-PSC are interconnected to the DRU-HVDC system as shown in fig. 7.4. A similar test like the previous section will be carried out to analyze the system.

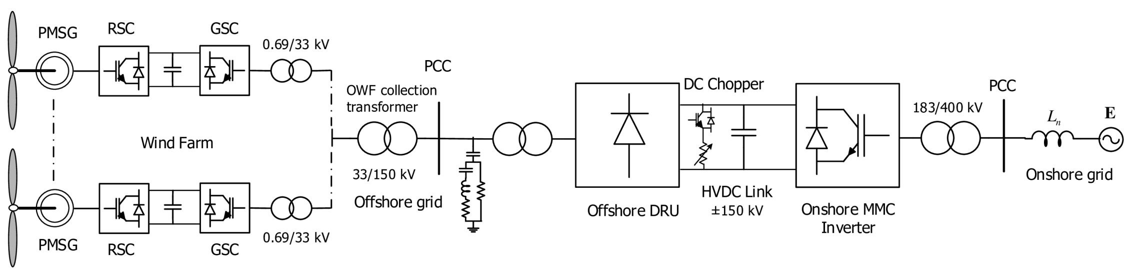

Figure 7.4: DRU-HVDC interconnected to an offshore wind farm.

From fig. 7.5, the operation of the system is the same as discussed in 5.4, except that during island mode, the wind turbines will provide the necessary voltage and frequency support to the offshore grid without the need of a STATCOM. The OWF supplies 24.5 MVAr throughout the operation for supporting the offshore grid voltage. The system rides through the fault and resumes normal operation smoothly. The over-current in the converter valve during the fault is limited by the current limiter. The frequency of the offshore grid is maintained at 50 Hz throughout the entire operation except for a slight dip to 48.5 Hz during the fault recovery. The DC-link voltage and three-phase AC voltages of the WTG are shown in fig. 7.6.

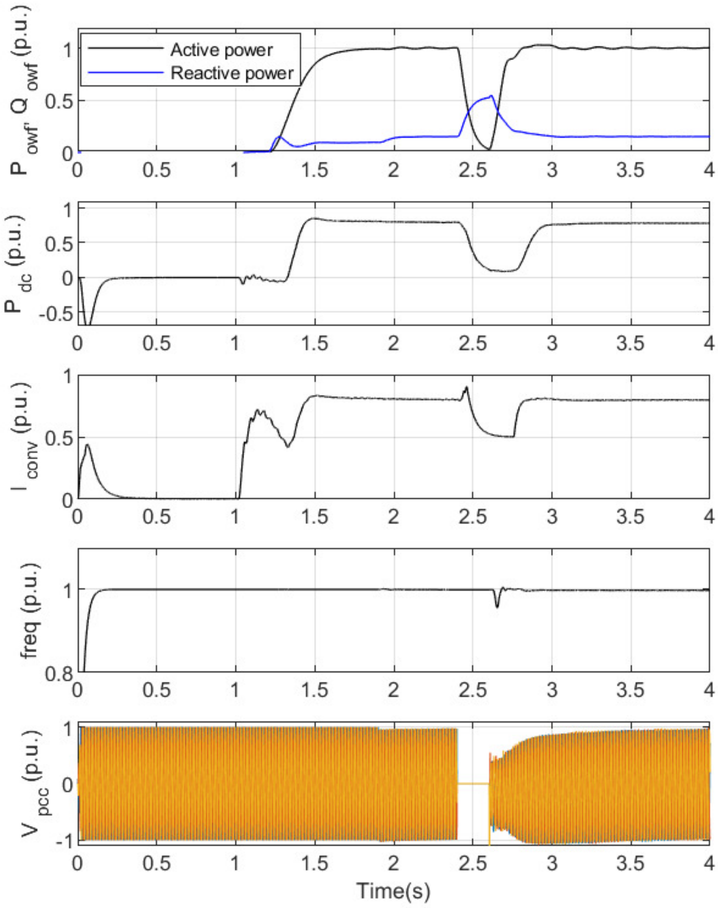

Figure 7.5: LVFRT capability of the DRU-HVDC link during island mode operation.

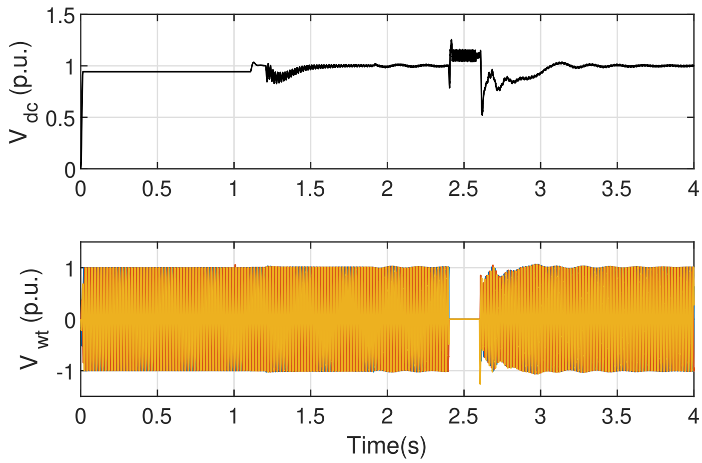

Figure 7.6: Upper plot: DC-link voltage of the WTG. Lower plot: Three-phase AC voltages of the WTG.

This study demonstrates how grid-forming control can play an indispensable role by eliminating the STATCOM. The overall cost of the system is further reduced by eliminating the STATCOM and footprint of the offshore platform.

8

Conclusions and Future Work

This chapter presents the conclusions of the thesis and provides suggestions for future work.

8.1 Conclusions

Three possible OWF design topologies to effectively interconnect the main AC grid have been investigated in this thesis. The comparison of the three test systems are as follows-

Test system 1, i.e., back-to-back MMC-HVDC system exhibited robust performance with the integration of the OWF during island and passive mode operations. The overall system coordination during LVFRT scenarios was also excellent. By equipping the back-to-back MMCs with GFM-PSC, the converter could independently control the active and reactive power of the system. Moreover, the offshore MMC could form and control the voltage and frequency of the offshore grid smoothly during island and passive mode operations with LVFRT situations. The MMC's voltage waveform is good especially during island mode operation due to the MMC technology. The most prominent feature is that bi-directional power transfer is feasible due to the IGBT's capability. On the negative side, the control system is complex and the cost of the system is more due to a large number of submodules. This also requires a considerable amount of footprint at the offshore substation.

Test system 2, i.e., DRU-HVDC system also demonstrated robust performance with the integration of the OWF during island mode operation and LVFRT conditions. A small STATCOM equipped with GFM-PSC at the offshore side provides the necessary voltage support during these conditions. The STATCOM being a dynamic RPC device regulates the reactive power exchange between the grid and the converter. Later in this thesis, it was also demonstrated that if GFM-PSC is directly integrated into the offshore type 4 WTGs, the STATCOM could be removed as the WTG's could form and control the voltage and frequency of the offshore grid. Thus, making the system more compact and cost-effective. This also eliminates the sophisticated controls at the offshore side unlike test system 1.

One negative aspect of this topology is that the diode rectifiers being non-linear, distorts the line current inducing harmonics in the frequency range of $12n\pm1$ and hence, tuned filters are required to compensate for the same. The major drawback compared to test system 1 is that bi-directional power transfer is not possible due to the uni-directional feature of the power diodes. Hence, passive mode operation is not viable. Typically in large-scale offshore wind projects, the generated power from the OWF is completely transmitted to the onshore grid and then utilized/distributed. In such scenarios, there is no need to have bi-directional power transfer capability so this topology can be effective as the overall cost of the system is less compared to test system 1. Furthermore, as the components count is very less with the DRU as compared to the MMC, the footprint of the offshore substation is reduced. As per Siemens Energy, the volume and transmission losses are reduced by 80% and 20% respectively, while the total cost can be reduced by 30% [58], [59].

Test system 3, i.e., STATCOM-HVAC system which is a complete AC solution also exhibited robust performance with the integration of the OWF during island mode operation and LVFRT situations. The reactive power compensation of the STATCOMs is better utilized by placing one each at the offshore and onshore station rather than placing a big STATCOM at the mid-point of the HVAC transmission line which also results in significant cost in building a substation at the center of the sea. The STATCOMs and the offshore wind turbines equipped with GFM-PSC demonstrated very good results in smooth grid operation where the WTs were capable to form and control the offshore voltage and frequency of the grid. The biggest setback of this topology is due to the HVAC cables as it generates a significant amount of reactive power resulting in huge sizes of STATCOMs. Moreover, the losses from the HVAC cables are also significant. Therefore, even though the performance of the overall system is robust due to the dynamic STATCOMs and grid-forming strategy, this topology is not feasible to integrate long-distance OWFs. This also proves that HVDC transmission is the ultimate solution for integrating large-scale RES effectively.

While the existing synchronous machines are being decommissioned/removed from the AC grid, the voltage and frequency stability is lost, and this performance can only be replicated with grid-forming converters. Therefore, GFM converters are the ultimate solution to effectively inter-connect large-scale RES and to also realize green energy through 100% RES in the future as they can independently form and control the voltage and frequency of a weak grid and can handle disturbances from the grid. The STATCOM's will definitely play a vital role in the integration of RES due to their dynamic performance that can provide the necessary voltage support by injecting or absorbing reactive power for effective grid resilience.

To conclude, the back-to-back MMC-HVDC system and the DRU-HVDC system are the most effective ways to interconnect offshore wind farms. The selection of the topology depends upon the project specification and requirements. If bi-directional power transfer is not required and also to be more cost-effective, the DRU-HVDC system will be an excellent choice!

8.2 Future Work

This thesis has investigated the state-of-the-art OWF interconnection topologies with grid-forming control. Offshore wind generation and grid-forming control strategies are currently the hot topics being discussed in research and development to accelerate the carbon-neutral 2050 goal. Hence, plenty of further research work can be stipulated from this thesis. The following is a list of some possible future work:

- This thesis has used type 4 WTGs for all analyses. Type 3 WTGs could be investigated with grid-forming control to see how the overall system coordinates and whether it could reach close to the performance of type 4 WTGs. This can reduce the overall cost of the WTGs as the power electronic converters are rated for only 25-30% of the machine.

- An interesting research area would be to analyze the grid-forming capability in an Enhanced STATCOM (E-STATCOM) with supercapacitors. Supercapacitors have an extremely high energy density that can store and release energy instantly. Hence, active power can be exchanged with the grid which could further enhance the efficiency and stability of the power system. This technology could be very beneficial especially for integrating large-scale RES into a weak AC grid.

- Detailed modeling on the stability of the systems is not considered in this thesis. It would be interesting to analyze the subsynchronous torsional interactions (SSTI) and small-signal stability studies of the implemented systems.

- Half-bridge MMC configuration cannot ride through DC short-circuit faults. To overcome this issue full-bridge MMC can be implemented.

- A study on integrating the OWF with hydrogen storage would also be a hot topic to investigate as hydrogen storage is gaining attention these days to accelerate the green transition.

9

Ethics and Sustainability

This chapter discusses the ethical and sustainability aspects of the project.

9.1 Code of Ethics

The IEEE (Institute of Electrical and Electronics Engineers) Board of Directors adopted a set of ten codes called the IEEE Code of Ethics in 2020, with amendments, to ensure a safe working environment for everyone in any workplace by upholding the highest standards of integrity, responsible behavior and ethical conduct in professional activities [60]. Throughout this thesis work, the IEEE code of ethics as per [60] was applied to ensure that all aspects of the project were carried out ethically. Three out of ten codes are discussed as follows.

9.1.1 Code 1

Code 1 is "To hold paramount the safety, health, and welfare of the public, to strive to comply with ethical design and sustainable development practices, to protect the privacy of others, and to disclose promptly factors that might endanger the public or the environment" [60]. This thesis has depicted ethical designs and sustainable development practices by combining the OWF technology with the HVDC transmission using grid-connected VSCs with GFM control. It is worth stressing that by applying GFM control, the reliability and security of the power system are enhanced ensuring that the contingencies like faults and other disturbances from the grid will not cause any adverse effects to humans and the environment in the vicinity.

9.1.2 Code 5

Code 5 is "To seek, accept, and offer honest criticism of technical work, to acknowledge and correct errors, to be honest and realistic in stating claims or estimates based on available data, and to credit properly the contributions of others" [60]. The design of the entire system in this project has been carried out ethically. The source of contributions has been referenced and credited with respect. Honest criticism of technical work has been accepted from the supervisors and opponents which further improved the quality of the thesis. Similarly, honest criticism was offered during the opposition of another thesis work.

9.1.3 Code 7

Code 7 is "To treat all persons fairly and with respect, and to not engage in discrimination based on characteristics such as race, religion, gender, disability, age, national origin, sexual orientation, gender identity, or gender expression" [60]. This thesis was carried out in Hitachi ABB Power Grids Research, where all persons are treated equally with respect without any discrimination.

9.2 Sustainability

The United Nations General Assembly established 17 Sustainable Development Goals (SDGs) in 2015, intending to achieve them by 2030. The main purpose of these goals is to achieve a better and more sustainable future for all. From a sustainable standpoint, this research project can induce numerous benefits.

9.2.1 Goal 7

Goal 7 is to ensure access to affordable, reliable, sustainable and modern energy. This goal is strongly related to the project as it provides state-of-the-art topologies (MMC-HVDC and DRU-HVDC systems) to effectively transmit the generated power from the offshore wind farm to the onshore ac grid. By harnessing the available power from the wind, clean and sustainable energy is produced. The share of OWFs will play a crucial role to meet the energy requirements in the upcoming years. The EU strategy on offshore renewable energy strategy targets to increase Europe's offshore wind capacity from its current level of 12 GW to 60 GW by 2030 [1]. When green energy is generated with the least amount of power losses in the transmission system, the prices of the energy will also reduce making it affordable. HVDC transmission is the key to interconnect large-scale OWFs with minimum losses. When it comes to reliability, GFM control is the only solution for grid resiliency. When GFM control is employed in grid-connected VSCs, it can form and control the voltage and frequency of the grid and effectively ride through ac system faults and blackouts. Furthermore, it is important to integrate FACTS devices in the ac transmission lines for reactive power compensation and enhancement of active power flow.

9.2.2 Goal 13

Goal 13 is to take urgent action to combat climate change and its impacts. The increase in global warming due to the emission of greenhouse gases especially CO_2 has brought drastic changes in the earth's atmosphere (eg. depletion of the ozone layer) and climate. This has increased the average global temperature by about 1.2°C since 1900 [61]. The goal is to stay at or below 1.5°C as per the 'Paris Agreement' [1]. The ultimate solution to combat this major problem is to realize 100% RES in the future to achieve net-zero emissions. This ambitious goal can only be achieved with large-scale penetration of RES into the generation mix and at the same time decommissioning the existing fossil-fuel-based power plants. This thesis has demonstrated how OWFs can be effectively interconnected to the main ac grid with the HVDC transmission system and most importantly the effect of equipping GFM control such that the GFM converters can mimic the behavior of a synchronous machine.

9.2.3 Goal 15

Goal 15 is to preserve life on land by protecting and restoring nature. This thesis also contributes to this goal, by utilizing OWF to generate power, the footprint of the converter station is reduced as only one station will be built on the land. This is a big advantage as compared to the long overhead HVAC lines running on the land which requires a significant amount of land area. Moreover, the advancement of semiconductor technologies and other electrical components used in the converter station do not pollute or cause damage to the environment/land.

Bibliography

[1] *2050 Long-term strategy*, Feb. 2017. [Online]. Available: https://ec.europa.eu/clima/policies/strategies/2050_en.

[2] Y. Jiang-Häfner and P. Lundberg, "VSC HVDC Transmission Supporting Variable Electricity Generation", *CIGRE*, 2016.

[3] J. Rocabert, A. Luna, F. Blaabjerg, and P. Rodríguez, "Control of Power Converters in AC Microgrids", *IEEE Transactions on Power Electronics*, vol. 27, no. 11, pp. 4734–4749, 2012. DOI: 10.1109/TPEL.2012.2199334.

[4] Y. Jiang-Häfner and R. Ottersten, "HVDC with Voltage Source Converters. A desirable solution for connecting Renewable Energies", 2009.

[5] L. Kirschner, D. Retzmann, and G. Thumm, "Benefits of Facts for Power System Enhancement", in *2005 IEEE/PES Transmission Distribution Conference Exposition: Asia and Pacific*, 2005, pp. 1–7. DOI: 10.1109/TDC.2005.1547153.

[6] E. Callavik, P. Lundberg, M. Bahrman, and R. Rosenqvist, "HVDC Technologies for the Future Onshore and Offshore Grid", in *Cigré Symposium on Grid of the Future*, 2012.

[7] G. Shi, S. Peng, X. Cai, Z. Chen, and W. He, "Grid Integration of Offshore Wind Farms and Offshore oil/gas platforms", in *Proceedings of The 7th International Power Electronics and Motion Control Conference*, vol. 2, 2012, pp. 1301–1305. DOI: 10.1109/IPEMC.2012.6259039.

[8] *War of the Currents*, Aug. 2021. [Online]. Available: https://en.wikipedia.org/wiki/War_of_the_currents.

[9] *Nikola Tesla*, Aug. 2021. [Online]. Available: https://en.wikipedia.org/wiki/Nikola_Tesla#The_Nikola_Tesla_Company.

[10] M. Barnes, D. Van Hertem, S. P. Teeuwsen, and M. Callavik, "HVDC Systems in Smart Grids", *Proceedings of the IEEE*, vol. 105, no. 11, pp. 2082–2098, 2017. DOI: 10.1109/JPROC.2017.2672879.

[11] R. Singh and K. Shenai, "DC Microgrids and the virtues of local Electricity", *IEEE Spectrum*, vol. 6, 2014.

[12] D. Jovcic, *High Voltage Direct Current Transmission: Converters, Systems and DC Grids*. John Wiley & Sons, 2019.

[13] E. W. Kimbark, *Direct Current Transmission, Volume 1*. John Wiley, 1971.

[14] C.-K. Kim, V. K. Sood, G.-S. Jang, S.-J. Lim, and S.-J. Lee, *HVDC Transmission: Power Conversion Applications in Power Systems*. John Wiley & Sons, 2009.

[15] V. K. Sood, *HVDC and FACTS controllers: Applications of Static Converters in Power Systems*. Springer Science & Business Media, 2006.

[16] G. Andersson, P. Donalek, R. Farmer, N. Hatziargyriou, I. Kamwa, P. Kundur, N. Martins, J. Paserba, P. Pourbeik, J. Sanchez-Gasca, R. Schulz, A. Stankovic, C. Taylor, and V. Vittal, "Causes of the 2003 major grid blackouts in North America and Europe, and recommended means to improve system dynamic performance", *IEEE Transactions on Power Systems*, vol. 20, no. 4, pp. 1922–1928, 2005. DOI: 10.1109/TPWRS.2005.857942.

[17] M. P. Bahrman and B. K. Johnson, "The ABCs of HVDC Transmission Technologies", *IEEE Power and Energy Magazine*, vol. 5, no. 2, pp. 32–44, 2007. DOI: 10.1109/MPAE.2007.329194.

[18] *HVDC Light*. [Online]. Available: https://search.abb.com/library/Download.aspx?DocumentID=POW-0038&LanguageCode=en&DocumentPartId=&Action=Launch.

[19] B. Wu and M. Narimani, *High-Power Converters and AC Drives*. John Wiley & Sons, 2017.

[20] P. Kundur, *Power System Stability*. CRC Press New York, NY, USA, 2007, pp. 7–1.

[21] N. Mohan, T. M. Undeland, and W. P. Robbins, *Power Electronics: Converters, Applications, and Design*. John wiley & sons, 2003.

[22] *HVDC Links in System Operations*. [Online]. Available: https://eepublicdownloads.entsoe.eu/clean-documents/SOC%20documents/20191203_HVDC%20links%20in%20system%20operations.pdf.

[23] "IEEE guide for planning DC links terminating at AC locations having low short-circuit capacities", *IEEE Std 1204-1997*, pp. 1–216, 1997. DOI: 10.1109/IEEESTD.1997.85949.

[24] C. Thio, J. Davies, and K. Kent, "Commutation failures in HVDC Transmission Systems", *IEEE Transactions on Power Delivery*, vol. 11, no. 2, pp. 946–957, 1996. DOI: 10.1109/61.489356.

[25] L. Zhang and M. Bollen, "Characteristic of Voltage Dips (sags) in Power Systems", in *8th International Conference on Harmonics and Quality of Power. Proceedings (Cat. No.98EX227)*, vol. 1, 1998, 555–560 vol.1. DOI: 10.1109/ICHQP.1998.759969.

[26] L. Zhang, "Modeling and Control of VSC-HVDC links connected to Weak AC Systems", Ph.D. dissertation, KTH, 2010.

[27] L. Zhang and L. Dofnas, "A novel method to mitigate commutation failures in HVDC systems", in *Proceedings. International Conference on Power System Technology*, vol. 1, 2002, 51–56 vol.1. DOI: 10.1109/ICPST.2002.1053503.

[28] K. Sharifabadi, L. Harnefors, H.-P. Nee, S. Norrga, and R. Teodorescu, *Design, Control, and Application of Modular Multilevel Converters for HVDC Transmission Systems*. John Wiley & Sons, 2016.

[29] N. Flourentzou, V. G. Agelidis, and G. D. Demetriades, "VSC-based HVDC Power Transmission Systems: An overview", *IEEE Transactions on Power Electronics*, vol. 24, no. 3, pp. 592–602, 2009. DOI: 10.1109/TPEL.2008.2008441.

[30] R. Marquardt, A. Lesnicar, J. Hildinger, *et al.*, "Modulares stromrichterkonzept für netzkupplungsanwendung bei hohen spannungen", *ETG-Fachtagung, Bad Nauheim, Germany*, vol. 114, 2002.

[31] A. Lesnicar and R. Marquardt, "An innovative Modular Multilevel Converter topology suitable for a wide power range", in *2003 IEEE Bologna Power Tech Conference Proceedings,*, vol. 3, 2003, 6 pp. Vol.3-. DOI: 10.1109/PTC.2003.1304403.

[32] A. Nami, J. Liang, F. Dijkhuizen, and G. D. Demetriades, "Modular Multilevel Converters for HVDC Applications: Review on Converter Cells and Functionalities", *IEEE Transactions on Power Electronics*, vol. 30, no. 1, pp. 18–36, 2015. DOI: 10.1109/TPEL.2014.2327641.

[33] S. Allebrod, R. Hamerski, and R. Marquardt, "New transformerless, scalable Modular Multilevel Converters for HVDC-transmission", in *2008 IEEE Power Electronics Specialists Conference*, 2008, pp. 174–179. DOI: 10.1109/PESC.2008.4591920.

[34] B. Westman, K. Eriksson, G. Persson, and A. Maeland, "HVDC Power from Shore", *CIGRE*, 2016.

[35] *Global rise of HVDC and its background*. [Online]. Available: https://www.hitachi.com/rev/archive/2020/r2020_04/pdf/gir.pdf.

[36] B. Jacobson, P. Karlsson, G. Asplund, L. Harnefors, and T. Jonsson, "VSC-HVDC Transmission with Cascaded two-level Converters", in *Cigré session*, 2010, B4–B110.

[37] N. G. Hingorani and L. Gyugyi, *Understanding FACTS: Concepts and Technology of Flexible AC Transmission Systems*. Wiley-IEEE Press, 2000.

[38] M. Eremia, C.-C. Liu, and A.-A. Edris, *Advanced Solutions in Power Systems: HVDC, FACTS, and Artificial Intelligence*. John Wiley & Sons, 2016.

[39] H. Li and Z. Chen, "Overview of different Wind Generator Systems and their comparisons", *IET Renewable Power Generation*, vol. 2, no. 2, pp. 123–138, 2008.

[40] Q. Wu and Y. Sun, *Modeling and Modern Control of Wind Power*. John Wiley & Sons, 2018.

[41] *Offshore Transmission Technology*. [Online]. Available: https://entsoe.eu/fileadmin/user_upload/_library/publications/entsoe/SDC/European_offshore_grid_-_Offshore_Technology_-_FINALversion.pdf.

[42] D. Pan, X. Wang, F. Liu, and R. Shi, "Transient Stability of Voltage-Source Converters with Grid-Forming Control: A design-oriented study", *IEEE Journal of Emerging and Selected Topics in Power Electronics*, vol. 8, no. 2, pp. 1019–1033, 2020. DOI: 10.1109/JESTPE.2019.2946310.

[43] A. Jain, J. N. Sakamuri, and N. A. Cutululis, "Grid-Forming Control strategies for Black Start by Offshore Wind Power Plants", *Wind Energy Science*, vol. 5, no. 4, pp. 1297–1313, 2020.

[44] X. Wang, M. G. Taul, H. Wu, Y. Liao, F. Blaabjerg, and L. Harnefors, "Grid-Synchronization Stability of Converter-based resources—An overview", *IEEE Open Journal of Industry Applications*, vol. 1, pp. 115–134, 2020. DOI: 10.1109/OJIA.2020.3020392.

[45] P. Fischer de Toledo, "Modelling and Control of a Line-Commutated HVDC Transmission System interacting with a VSC STATCOM", Ph.D. dissertation, KTH, 2007.

[46] L. Harnefors, M. Bongiorno, and S. Lundberg, "Input-Admittance Calculation and Shaping for Controlled Voltage-Source Converters", *IEEE Transactions on Industrial Electronics*, vol. 54, no. 6, pp. 3323–3334, 2007. DOI: 10.1109/TIE.2007.904022.

[47] M. Durrant, H. Werner, and K. Abbott, "Model of a VSC HVDC terminal attached to a weak AC system", in *Proceedings of 2003 IEEE Conference on Control Applications, 2003. CCA 2003.*, vol. 1, 2003, 178–182 vol.1. DOI: 10.1109/CCA.2003.1223288.

[48] D. Jovcic, L. Lamont, and L. Xu, "VSC Transmission model for analytical studies", in *2003 IEEE Power Engineering Society General Meeting (IEEE Cat. No.03CH37491)*, vol. 3, 2003, 1737–1742 Vol. 3. DOI: 10.1109/PES.2003.1267418.

[49] L. Zhang, L. Harnefors, and H.-P. Nee, "Power-Synchronization Control of Grid-Connected Voltage-Source Converters", *IEEE Transactions on Power Systems*, vol. 25, no. 2, pp. 809–820, 2010. DOI: 10.1109/TPWRS.2009.2032231.

[50] R. Ottersten, *On Control of Back-to-Back Converters and Sensorless Induction Machine Drives*. Chalmers University of Technology, 2003.

[51] B4.57, *Guide for the Development of Models for HVDC Converters in a HVDC Grid*. CIGRE, 2014.

[52] Q. Tu, Z. Xu, and J. Zhang, "Circulating Current Suppressing Controller in Modular Multilevel Converter", in *IECON 2010 - 36th Annual Conference on IEEE Industrial Electronics Society*, 2010, pp. 3198–3202. DOI: 10.1109/IECON.2010.5675048.

[53] N. Ahmed, L. Ängquist, A. Antonopoulos, L. Harnefors, S. Norrga, and H.-P. Nee, "Performance of the Modular Multilevel Converter with Redundant Submodules", in *IECON 2015 - 41st Annual Conference of the IEEE Industrial Electronics Society*, 2015, pp. 003 922–003 927. DOI: 10.1109/IECON.2015.7392712.

[54] K. Ilves, S. Norrga, L. Harnefors, and H.-P. Nee, “On Energy Storage Requirements in Modular Multilevel Converters”, *IEEE Transactions on Power Electronics*, vol. 29, no. 1, pp. 77–88, 2014. DOI: 10.1109/TPEL.2013.2254129.

[55] G. Tsolaridis, H. A. Pereira, A. F. Cupertino, R. Teodorescu, and M. Bongiorno, “Losses and cost comparison of DS-HB and D-FB MMC based large utility grade STATCOM”, in *2016 IEEE 16th International Conference on Environment and Electrical Engineering (EEEIC)*, 2016, pp. 1–6. DOI: 10.1109/EEEIC.2016.7555715.

[56] L. Harnefors, M. Hinkkanen, U. Riaz, F. M. M. Rahman, and L. Zhang, “Robust Analytic Design of Power-Synchronization Control”, *IEEE Transactions on Industrial Electronics*, vol. 66, no. 8, pp. 5810–5819, 2019. DOI: 10.1109/TIE.2018.2874584.

[57] S. Bernal-Perez, S. Añó-Villalba, R. Blasco-Gimenez, and J. Rodríguez-D’Derlée, “Off-shore Wind Farm grid connection using a novel Diode-Rectifier and VSC-inverter based HVDC transmission link”, in *IECON 2011 - 37th Annual Conference of the IEEE Industrial Electronics Society*, 2011, pp. 3186–3191. DOI: 10.1109/IECON.2011.6119820.

[58] O. Kuhn, P. Menke, R. Zurowski, T. Christ, S. Seman, G. Giering, *et al.*, “2nd Generation DC grid access for Offshore Wind Farms: HVDC in an AC fashion”, *CIGRE, Paris*, pp. 1–7, 2016.

[59] *Siemens reveals DRU solution for connecting Offshore Wind Plants*, Sep. 2019. [Online]. Available: https://www.ebmag.com/siemens-reveals-dru-solution-for-connecting-offshore-wind-plants-17919/.

[60] *IEEE Code of Ethics*. [Online]. Available: https://www.ieee.org/about/corporate/governance/p7-8.html.

[61] *The 17 goals | Sustainable Development*. [Online]. Available: https://sdgs.un.org/goals.

A

Appendix 1

A.1 Implementation of $\alpha\beta$ and dq transformations

In this section, the mathematical expressions for abc-$\alpha\beta$ and $\alpha\beta$-dq transformations are described.

A.1.1 abc-$\alpha\beta$ transformation

The abc-$\alpha\beta$ transformation is called Clarke transformation. The three-phase voltages in a symmetric and balanced three-phase system can be described as

$$
\begin{aligned}
v_a(t) &= \hat{v}cos(wt) \\
v_b(t) &= \hat{v}cos(wt - \frac{2\pi}{3}) \\
v_c(t) &= \hat{v}cos(wt - \frac{4\pi}{3})
\end{aligned} \tag{A.1}
$$

where $\hat{v}$ is the voltage amplitude and ω the angular frequency. Since the zero-sequence quantities in the three-phase system are neglected,

$$
v_a(t) + v_b(t) + v_c(t) = 0 \tag{A.2}
$$

As shown in fig. A.1(a), the complex vector $\mathbf{v}$ is defined as

$$
\mathbf{v}^s(t) = \frac{2}{3}\left(v_a(t) + v_b(t)e^{j\frac{2\pi}{3}} + v_c(t)e^{j\frac{4\pi}{3}}\right) \tag{A.3}
$$

where superscript s denotes the stationary $\alpha\beta$ reference frame. $\mathbf{v}^s$(t) can be decomposed into its real and imaginary parts as

$$
\mathbf{v}^s(t) = v_\alpha(t) + jv_\beta(t) \tag{A.4}
$$

where α and β are the real and imaginary components respectively of the rotating vector. Equating the real and complex parts of A.3 and A.4 results in the following transformation

$$
\begin{aligned}
v_a(t) &= v_\alpha(t) \\
v_b(t) &= -\frac{1}{2}v_\alpha(t) + \frac{\sqrt{3}}{2}v_\beta(t) \\
v_c(t) &= -\frac{1}{2}v_\alpha(t) - \frac{\sqrt{3}}{2}v_\beta(t)
\end{aligned} \tag{A.5}
$$

Therefore, as long as the three-phase system is symmetric, $\alpha\beta$ perfectly represents abc frame.

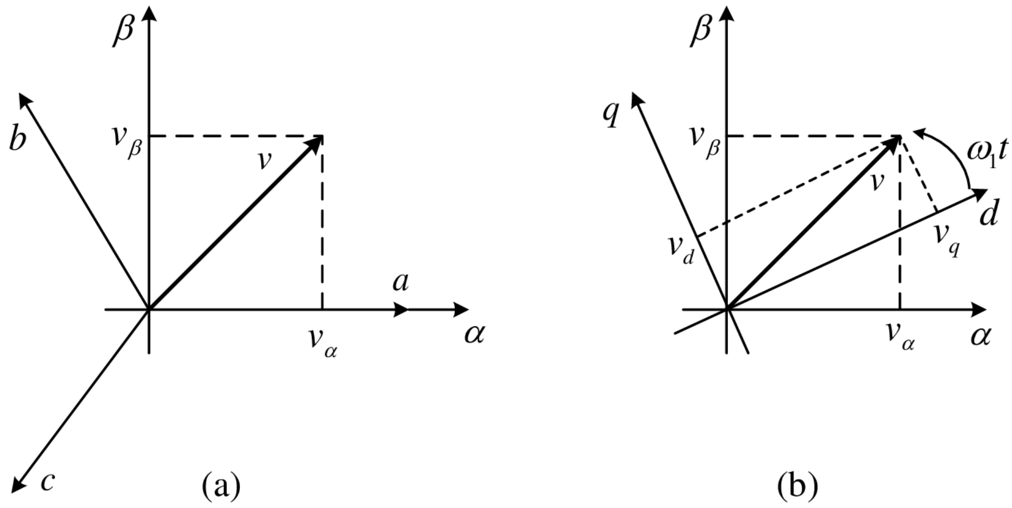

Figure A.1: Reference frame transformations. (a) abc frame to a rotating vector in the stationary $\alpha\beta$ frame. (b) Stationary $\alpha\beta$ frame to synchronous dq frame.

A.1.2 $\alpha\beta$-dq transformation

The $\alpha\beta$-dq transformation is called Park transformation. By using Park's transformation, it becomes easier to analyze and control the oscillating signals (from the system) in the DC system than the AC quantities. When a system is controlled with its DC quantities, the gain of the integral controller grows infinitely resulting in a zero steady state error. This can be realized by rotating the $\alpha\beta$ reference frame to a fixed one, a rotating dq reference frame is introduced, as shown in fig. A.1(b) The dq frame rotates in the same direction as $\mathbf{v}^s$(t) at the same speed as the ac system's angular frequency ω_1. Hence, the vector $\mathbf{v}$(t) in the dq frame is related to $\mathbf{v}^s$(t) in the stationary frame by $\mathbf{v}^s(t) = \mathbf{v}e^{j\omega_1 t}(t)$ and can be mathematically formulated as

$$\mathbf{v}^s(t) = v_d(t) + jv_q(t) = (v_\alpha + jv_\beta)e^{-j\omega_1 t} \tag{A.6}$$

where ωt is the synchronization angle from the PSL or PLL of the VSC. $\mathbf{v}^s$(t) can be decomposed into its component form as

$$\begin{aligned} v_d(t) &= v_\alpha(t)\cos\omega t + v_\beta(t)\sin\omega t \\ v_q(t) &= -v_\alpha(t)\sin\omega t + v_\beta(t)\cos\omega t \end{aligned} \tag{A.7}$$

Similarly, the vector $\mathbf{v}^s(t)$ in the stationary $\alpha\beta$ frame is related to $\mathbf{v}(t)$ in the synchronous dq frame by $\mathbf{v}^s(t) = \mathbf{v}e^{j\omega t}(t)$ which can also be decomposed in its component form as

$$\begin{aligned} v_\alpha(t) &= v_d(t)\cos\omega t - v_q(t)\sin\omega t \\ v_\beta(t) &= v_d(t)\sin\omega t + v_q(t)\cos\omega t \end{aligned} \tag{A.8}$$

B

Appendix 2

B.1 Technical Data of the MMC-HVDC system

OWF Rated power P_{owf}	2 x 80 WT= 160 MW
OWF collection transformer rating	200 MVA, 33/400kV, $X_t = 12\%$
MMC Rated power P_{dc}	200 MVA
Rated AC Voltage (L-L) V_{ac}	183 kV
Nominal AC system frequency f_1	50 Hz
Arm inductance L_{arm}	0.28 p.u.
Phase-reactor resistance R_c	0.01 p.u.
Number of SMs per arm N_{sm}	111, 10% redundancy
SM capacitance C_{sm}	3456 uF
IGBT rating V_c	3.3 kV
Nominal energy storage per arm E_{nom}	42 kJ/MVA
Switching frequency f_{sw}	150 Hz
Maximum valve current I_{max}	1.08 p.u.
Rated direct voltage V_{dc}	±150 kV
DC capacitance C_{dc}	0.0226 p.u.
Converter transformer rating	220 MVA, 183/400 kV, $X_t = 12\%$

Table B.1: Technical data of the MMC-HVDC system. AC: per unit based on 200 MVA and 183 kV. DC: per unit based on 200 MW and 150 kV.

B.2 Technical Data of the DRU-HVDC system

OWF Rated power P_{owf}	2 x 80 WT= 160 MW
OWF collection transformer rating	200 MVA, 33/150 kV, $X_t = 12\%$
Onshore MMC rating	
MMC Rated power P_{dc}	200 MVA
Rated AC Voltage (L-L) V_{ac}	183 kV
Nominal AC system frequency f_1	50 Hz
Arm inductance L_{arm}	0.28 p.u.
Phase-reactor resistance R_c	0.01 p.u.
Number of SMs per arm N_{sm}	111 , 10% redundancy
SM capacitance C_{sm}	3456 uF
IGBT rating V_c	3.3 kV
Nominal energy storage per arm E_{nom}	42 kJ/MVA
Switching frequency f_{sw}	150 Hz
Maximum valve current I_{max}	1.08 p.u.
Rated direct voltage V_{dc}	$\pm$150 kV
DC capacitance C_{dc}	0.0226 p.u.
Converter transformer rating	220 MVA, 183/400 kV, $X_t = 12\%$
DRU rating	
12- pulse Transformer (Y-Y-Δ)	220 MVA, 150/114 kV, $X_t = 12\%$
Smoothing inductor L_{smo}	0.2 H
Filters- Reactive Power Compensation	12n$\pm$1, 28 MVAr
STATCOM rating	
MMC Rated power P_{dc}	100 MVA
Rated AC Voltage (L-L) V_{ac}	75 kV
Nominal AC system frequency f_1	50 Hz
Arm inductance L_{arm}	0.28 p.u.
Phase-reactor resistance R_c	0.01 p.u.
Number of SMs per arm N_{sm}	80, 10% redundancy
SM capacitance C_{sm}	7439 uF
IGBT rating V_c	1.7 kV
Nominal energy storage per arm E_{nom}	42 kJ/MVA
Switching frequency f_{sw}	150 Hz
Maximum valve current I_{max}	1.08 p.u.
DC capacitance C_{dc}	0.01 p.u.
Converter transformer rating	120 MVA, 75/150 kV, $X_t = 12\%$

Table B.2: Technical data of the DRU-HVDC system.

B.3 Technical Data of the STATCOM (1200 MVA)-HVAC system

AC Grid Voltage (L-L) E	400 kV
OWF Rated power P_{owf}	2 x 80 WT= 160 MW
OWF collection transformer rating	200 MVA, 33/400kV, $X_t = 12\%$
STATCOM (MMC) rated power P_{dc}	1200 MVA
Rated AC Voltage (L-L) V_{ac}	300 kV
Nominal AC system frequency f_1	50 Hz
Arm inductance L_{arm}	0.28 p.u.
Phase-reactor resistance R_c	0.01 p.u.
Number of SMs per arm N_{sm}	121, 10% redundancy
SM capacitance C_{sm}	8434 uF
IGBT rating V_c	4.5 kV
Nominal energy storage per arm E_{nom}	42 kJ/MVA
Switching frequency f_{sw}	150 Hz
Maximum valve current I_{max}	1.08 p.u.
DC capacitance C_{dc}	0.01 p.u.
Converter transformer rating	1333 MVA, 300/400 kV, $X_t = 15\%$
HVAC cable data (100 km length)	R = 0.0149 Ω/km, L = 0.369 mH/km, C = 0.207 μF/km

Table B.3: Technical data of the STATCOM (1200 MVA)-HVAC system.

B.4 Technical Data of the STATCOM (600 MVA)-HVAC system

AC Grid Voltage (L-L) E	400 kV
OWF Rated power P_{owf}	2 x 80 WT= 160 MW
OWF collection transformer rating	200 MVA, 33/400kV, X_t = 12%
STATCOM (MMC) rated power P_{dc}	600 MVA
Rated AC Voltage (L-L) V_{ac}	200 kV
Nominal AC system frequency f_1	50 Hz
Arm inductance L_{arm}	0.28 p.u.
Phase-reactor resistance R_c	0.01 p.u.
Number of SMs per arm N_{sm}	91, 10% redundancy
SM capacitance C_{sm}	7116 uF
IGBT rating V_c	4.5 kV
Nominal energy storage per arm E_{nom}	42 kJ/MVA
Switching frequency f_{sw}	150 Hz
Maximum valve current I_{max}	1.08 p.u.
DC capacitance C_{dc}	0.01 p.u.
Converter transformer rating	666 MVA, 200/400 kV, X_t = 15%
HVAC cable data (100 km length)	R = 0.0149 Ω/km, L = 0.369 mH/km, C = 0.207 μF/km

Table B.4: Technical data of the STATCOM (600 MVA)-HVAC system.

DEPARTMENT OF SOME SUBJECT OR TECHNOLOGY
CHALMERS UNIVERSITY OF TECHNOLOGY
Gothenburg, Sweden
www.chalmers.se

AVANCEZ
1829

CHALMERS
UNIVERSITY OF TECHNOLOGY